International
WOCE
Newsletter

Number 26 April 1997

IN THIS ISSUE

❒ **News from the SSG**

Where has WOCE got to? *John A. Church* 2

❒ **Atmospheric-Ocean Coupled Models**

Some Oceanographic Inferences from Coarse-Resolution Ocean and Climate Models *Peter G. Baines* 3

Predictability of North Atlantic Climate on Decadal Times Scales Estimated Using a Coupled Ocean-Atmosphere Model *Kirk Bryan and Stephen M. Griffies* 5

The Ocean Simulation in the Hadley Centre Coupled Climate Model *Chris Gordon, et al.* 9

The OPA/ARPEGE and OPA/LMD Global Ocean-Atmosphere Coupled Model *Gurvan Madec and Pascale Delecluse* 12

The NCAR Climate System Model *Peter R. Gent and Frank O. Bryan* 15

Dynamics of Interdecadal Variability in Coupled Ocean-Atmosphere Models *Mojib Latif* 17

Ocean Models for Climate Forecasting *Stuart Godfrey and Andreas Schiller* 25

A New Eddy Mixing Parametrization and Ocean General Circulation Model *David K. Wright* 27

❒ **Other Science**

Decadal Variability of the North Atlantic Overflows *Sheldon Bacon* 29

Observing Opposing Temperature Changes in the Upper and Intermediate Layers of the North Atlantic Ocean *Alexander Sy, et al.* 30

Evidence of Secular Change in the Northeast Pacific Ocean *Howard J. Freeland and Frank A. Whitney* 34

The Antarctic Margin Experiment, 80° to 150°E *Nathaniel L. Bindoff* 36

Comparison of Bottom-Tracking and Profiling LADCP Data in a Section Across the ACC at Drake Passage *Stuart A. Cunningham, et al.* 39

Recent Speeding Up of the Pacific Subarctic Circulation *Costa Rogachov* 40

The Ashtech GG24 as an Alternative to P-Code GPS *Brian A. King, et al.* 42

❒ **Meetings**

Meetings Timetable 1997/1998 20

Ocean Data Symposium, 15–18 October 1997 43

"Monitoring the Oceans in the 2000s: an Integrated Approach", 15–17 October 1997 43

❒ **Miscellaneous**

Data Guide 33

Published by WOCE International Project Office at Southampton Oceanography Centre, UK

Where has WOCE got to?

John A. Church, WOCE SSG co-Chair. john.church@marine.csiro.au

WOCE is rapidly approaching the end of its intensive observations but the project will not end then. A continuing effort is essential to ensure that the observations are fully exploited to achieve the WOCE goals of improving ocean models for predicting climate and determining the representativeness of the WOCE data sets.

The WOCE Synthesis and Modelling Working Group, has recently completed a draft "Analysis, Interpretation, Modelling and Synthesis Strategy" for the project to go through 2002. This plan will be circulated for comment this summer and finalised in the fall. Progress in implementing elements of the AIMS phase strategy are highlighted below.

Ocean Model Data Intercomparison Project

A joint WOCE-CLIVAR Ocean Model Data Intercomparison Project has been proposed following the well-known Atmospheric Model Intercomparison Project. A modelling workshop will be held (probably in early 1998) to plan how the project might run. It will need to take account of the current status of ocean model development and of the computer and human resources available.

WOCE Conference

Preliminary registration for the WOCE Conference, "Ocean Circulation and Climate", Halifax, Canada, 24-29 May 1998, will start shortly (http://www.soc.soton.ac.uk/OTHERS/woceipo/wconf/). The Science Organising Committee (chaired by Gerold Siedler) has designed an exciting programme that will directly address the WOCE goals. Each morning will have plenary overview talks by prominent oceanographers. These will be followed by Poster sessions in the afternoon. Many of the invited speakers have already enthusiastically accepted invitations to make presentations.

JSC Meeting

Each year WOCE reports to its parent body the Joint Scientific Committee for the World Climate Research Programme. At its 18th session in Toronto (17–22 March 1997) John Gould, Breck Owens and I reported on WOCE and its plans for the AIMS phase. The JSC is pleased with the continuing efforts WOCE makes to meet its goals and contribute effectively to the overall WCRP strategy. Of particular importance is the need to produce products (*e.g.* global data sets, improved understanding of the oceans' role in the climate system and improved ocean models) that are of value to other WCRP projects, and to ensure a smooth transition from WOCE to CLIVAR. The JSC remains concerned about the challenges (particularly the personnel and computing resources required for the assimilation of the WOCE data sets) posed by WOCE AIMS.

A WCRP Conference is planned for Geneva (August 1997). Its purpose is to inform senior decision makers of the contribution that the WCRP is making to the understanding of major societal issues such as climate variability and change, and to convince them of the value of further investment in WCRP and its component projects. As a mature project, WOCE will be an important example of the success of the WCRP and we need to adequately document the WOCE achievements.

The future

The AIMS phase will be implemented through national contributions. Recent publication of a US plan (and budget estimates) for synthesis of WOCE observations and for the further development of ocean models is a significant step forward. US WOCE, with other ocean programmes, is also defining the most appropriate form for an Ocean Data Assimilation Centre. Such a Centre with wide community involvement would ensure continued improvement in the ocean models necessary for predicting climate variability and change.

The decision to build a US/French follow-on satellite (JASON), to the successful TOPEX/POSEIDON altimeter mission is another very positive development as is the go-ahead for a dedicated gravity mission (GRACE).

The failure to fund the bid for a UK AIMS phase is a significant setback. While some limited synthesis activities will undoubtedly occur in the UK, this decision will prevent UK scientists from exploiting the major investment already made and hinder further improvement in ocean models (through data assimilation) essential for predicting the timing and regional impact of climate change. The full implications are still being assessed. On the positive side, the UK will continue to support the WOCE International Project Office.

As a project of the WCRP, WOCE is directly aimed at improving ocean models needed for predicting climate change. WOCE results are already having a significant impact on coupled ocean/atmosphere models but WOCE needs to continue to develop closer links to the broader climate modelling community. As part of this process, this Newsletter focuses on developments in coupled models.

Finally, the IPO and the SSG need your help to document significant achievements of the WOCE. These achievements/deliverables are valuable in ensuring the continued funding of large scale oceanography that addresses the role of the ocean in the climate system. In the next Newsletter we will itemise our view of WOCE's achievements. I encourage all of you to consider the impact of the science you are conducting and to e-mail suggestions for inclusion in this list to the IPO (using the headings Achievement, Significance, References).

Some Oceanographic Inferences from Coarse-Resolution Ocean and Climate Models

Peter G. Baines, CSIRO Division of Atmospheric Research, Aspendale 3195, Australia. pgb@dar.csiro.au

Coarse resolution ocean models have been with us since the pioneering work of Kirk Bryan and Michael Cox, and their virtues and shortcomings are well-known. Modern-day models have a typical resolution of 3.5° latitude by 5.6° longitude, 12 vertical levels, with corresponding continental boundaries and ocean bathymetry. When compared with the real ocean their most conspicuous deficiencies include: viscously dominated western boundary currents that are much too wide and inadequately described, coarse representation of high latitude convection, inadequate resolution of equatorial phenomena, and dubious representation of sub-grid-scale effects on the large scale motions.

In spite of these shortcomings, however, these models do describe large-scale mid-ocean processes in a reasonably realistic manner, and they are useful tools to examine possible modes of oceanic behaviour. Suitably forced, they reproduce the main large-scale features of the wind-driven circulation, the thermocline structure, and the deep circulations driven by sinking at high latitudes in the North Atlantic and near Antarctica. They may be run for long periods of time (up to thousands of years) on modern computers, all variables may be retrieved at each time step, and they may be modified to carry out "what-if" experiments, such as the effect of modifying the topography or changing the surface forcing. Coupled ocean-atmosphere climate models will depend on such models for their ocean component for the next few years, at least. There has recently been an explosion of the literature on this subject. Here I describe some results about the ocean and ocean-atmosphere system that have been recently learnt from these models, concentrating on the work of the Ocean Modelling Group at Aspendale.

Ocean Models

The response of ocean-only models to various forms of atmospheric forcing has been investigated. These include temperature (SST) and salinity (SSS) restoring (which means that ocean surface values may vary, but they have a continual tendency toward climatological values, with a chosen decay constant – a boundary condition known as Haney relaxation (Haney, 1971)) with and without restored wind forcing. One result from these studies is that the Antarctic Circumpolar Current (ACC) is partly driven by the sinking of Antarctic Bottom Water (AABW), which drives the southern thermohaline circulation. When this circulation crosses the latitudes of the ACC, the northward-moving lower part is constrained by the bottom topography, whereas the southward-moving upper part is accelerated eastwards by the Coriolis force, or equivalently, conservation of angular momentum (Cai and Baines, 1996). This effect was first noticed by Gill and Bryan (1971). The magnitude of this driving is approximately fQD, where f is the Coriolis parameter, Q the northward transport of AABW, and D is the width of the Drake Passage. This is comparable with, but generally less than, the net eastward wind stress on the ACC. This suggests, among other things, that a measure of AABW formation may be inferred from observations of the ACC transport. Variations in ACC transport also occur with variations in AABW formation in coupled model runs.

With the above restoring boundary conditions, constant forcing tends to produce a steady solution. From these solutions, fluxes of heat and freshwater at the surface may be diagnosed, and these maybe used to provide new flux boundary conditions, on either heat or freshwater or both. Some of these combinations (in particular, "mixed boundary conditions" – restored temperature, imposed flux on salinity) give oscillatory solutions (Weaver *et al*., 1993). A more realistic variation on the heat flux boundary condition has been given by Schopf (1983), which assumes a zero heat-content atmosphere in its derivation (Cai *et al*., 1995; Cai, 1996a, 1996b).

Oscillations in the thermohaline circulation may arise for other reasons. For example, in a simple rectangular basin representative of the Atlantic Ocean, with sinking in the northeast corner, and using the Schopf surface condition on heat flux, baroclinic Rossby waves are generated at high latitudes, giving oscillations in overturning that have the period of the time taken for the waves to cross the basin from east to west (Cai, 1996c). A change in the decay constant for restored temperature can produce similar effects (Cai and Chu, 1997).

Hirst and Godfrey (1994) have assessed the effect of the Indonesian throughflow on the Indian and Pacific Oceans, in a series of experiments where the model throughflow was varied in profile and magnitude, and in one case, cut off altogether. Changes in the throughflow induced substantial changes in the subsurface densities across both oceans, in a pattern that may be explained in terms of baroclinic wave response modified somewhat by advection by the background wind-driven Sverdrup circulation. A significant surface temperature response (of up to 4°C for the total cut-off case) occurred in particular regions; these regions may be more extensive if the Schopf boundary condition (or similar) were used, instead of the restoring conditions mentioned above. Gent and McWilliams (1990), Gent *et al*. (1995) introduced a parametrisation scheme for the lateral transport of heat due to sub-grid-scale baroclinic eddies, which removes the need for a large lateral thermal eddy diffusivity in the ocean model. It involves the addition of an eddy-induced transport velocity along isopycnals, and a diffusivity, that both depend on the local baroclinicity. The appropriate form of

this GM scheme is still the subject of debate (McDougall and McIntosh, 1996), but its inclusion improves considerably the similarity between model and real ocean in many respects (Danabasoglu *et al*., 1994; McDougall *et al*., 1996; Hirst and McDougall, 1997). It also brings added benefits in coupled models, as described below.

Coupled Models

The results described here are based on the CSIRO coupled model (Gordon and O'Farrell, 1997),which may be regarded as representative of the current generation of flux-corrected models, although it has a sophisticated ice model and a land biosphere. Two important variables that may be used to characterise the flow state in the ocean component are the magnitudes of the overturning in each of the North Atlantic-driven and Antarctic-driven thermohaline convection circulations. If zonal averages are taken, these may be visualised as one-dimensional loops, and their magnitudes are given in terms of Sverdrups of meridional circulation. A number of possible feedbacks have been identified in these loops, and we consider the North Atlantic-driven circulation for definiteness. If we imagine a perturbation (spontaneous or imposed) at high latitudes that causes an increased deep water formation and stronger circulation in this loop, the following feedback mechanisms may occur.

(i) A negative feedback between overturning and high latitude SST (where the sinking occurs) (Rahmstorf and Willebrand, 1995). Strengthening circulation increases northward heat transport, raising high latitude SST and decreasing surface density there. This weakens convective activity, and hence also the thermohaline circulation.

(ii) A positive feedback between overturning and SSS (Stommel, 1961).

(iii) A positive feedback between overturning and evaporation (Cai *et al.*, 1997).

(iv) A negative feedback between overturning and ice melting/formation (Cai *et al.*, 1997).

(v) A positive feedback between albedo and sea ice (Cai *et al*., 1997).

Feedbacks (ii) to (v) work in a similar way to (i), and positive feedbacks tend to produce a new steady state. In the CSIRO coupled model, these processes operate simultaneously and the net effect is a negative feedback, implying a dominant role for feedbacks (i) and (iv). In consequence, when the coupled model Atlantic is subjected to an imposed freshening (a "great salinity anomaly "perturbation), the North Atlantic deep water formation and the associated conveyor belt circulation recover, after an initial weakening (Cai *et al.*, 1997). Studies with ocean-only models and imposed surface forcing generally contain a limited number of these feedbacks, and the results may not be representative of the coupled atmosphere-ocean system.

A combined effect of feedbacks (i), (ii) and (iii) is that in polar/high-latitude regions, the vertical structure of temperature and salinity is such that both have a maximum at subsurface, rather than at the surface (Cai and Gordon, 1997a). This is because precipitation is greater than evaporation, giving cool fresh surface water. Under "greenhouse" conditions in the CSIRO coupled model, this tendency is increased in mid to high southern latitudes, because the hydrological cycle is stronger and overcomes the expected radiative increase in SST. This leads to a maximum warming below the surface (see Fig. 1 (upper panel) page 22). This pattern is consistent with some field observations (Bindoff and Church, 1992). On the other hand, under the same conditions in the northern North Atlantic the hydrological cycle is weaker and maximum heating occurs at the surface (see Fig. 1 (lower panel) page 22), although surface cooling does take place in the regions where convective activity is concentrated.

In flux-corrected coupled models, surface conditions are imposed to maintain a mean climatology. In the CSIRO model, there is some incompatibility between the imposed climatology and the model dynamics, and this can result in a secular drift in the mean state (*e.g*. temperature) of the model. Mechanisms of this drift have been identified (Cai and Gordon, 1997b). However, inclusion of the GM mixing scheme has the effect of reducing the drift (Hirst *et al.*, 1996, see Fig. 2, page 22), in addition to its other beneficial effects. Hence, eliminating drift in climate models requires both good climatology and improved model dynamics.

Acknowledgement

In preparing this brief review I am grateful for the input from other members of the Aspendale Ocean Modelling group, particularly Wenju Cai and Tony Hirst.

References

Bindoff, N.L., and J. Church, 1992: Warming of the water column in the southwest Pacific Ocean. Nature, 357, 59-62.

Cai, W., 1996a: The stability of NADWF under mixed boundary conditions with an improved diagnosed freshwater flux field. J. Phys. Oceanogr., 26, 1081-1087.

Cai, W., 1996b: Surface thermohaline forcing conditions and the response of the present-day global ocean climate to global warming. J. Geophys. Res., 101, 1079–1093.

Cai, W., 1996c: Generation of thermal ocscillation in an ocean model. Quart. J. Roy. Met. Soc., 122, 1721–1738.

Cai, W., and P.G. Baines, 1996: Interactions between thermohaline- and wind-driven circulations and their relevance to the dynamics of the Antarctic Circumpolar Current, in a coarse-resolution global ocean general circulation model. J. Geophys. Res., 101, 14073–14093.

Cai, W., and P.C. Chu, 1997: A thermal oscillation under a restorative forcing. Quart. J. Roy. Met. Soc., to be submitted.

Cai, W., and H.B. Gordon, 1997a: Ocean responses of the CSIRO climate model to two CO_2 warming scenarios and the inferences from an imposed high latitude freshening episode. J. Climate, submitted.

Cai, W., and H.B. Gordon, 1997b: Southern high latitude ocean climate drift in the CSIRO coupled model. J. Climate, to be submitted.

Cai, W., J. Syktus, H.B. Gordon, and S.P. O'Farrell, 1997: Response of a global coupled ocean-atmosphere-sea ice climate model to an imposed North Atlantic high latitude freshening. J. Climate, to appear.

Cai, W., R. Greatbatch, and S. Zhang, 1995: Interdecadal variability in an ocean model driven by a small, zonal redistribution of the surface buoyancy flux. J. Phys. Oceanogr., 25, 1998–

2100.
Danabasoglu, G., J.C. McWilliams, and P.R. Gent, 1994: The role of meso-scale tracer transports in the global ocean circulation. Science, 264, 1123–1126.
Gent, P.R., and J. McWilliams, 1990: Isopycnal mixing in ocean circulation models. J. Phys. Oceanogr., 20, 150–155.
Gent, P.R., J. Willebrand, T.J. McDougall, and J.C. McWilliams, 1995: Parameterising eddy-induced tracer transports in ocean circulation models. J. Phys. Oceanogr., 25, 463–474.
Gill, A.E., and K. Bryan, 1971: Effects of geometry on the circulation of a three-dimensional Southern-Hemisphere ocean model. Deep-Sea Res., 18, 685–721.
Gordon, H.B., and S.P. O'Farrell, 1997: Transient climate change in the CSIRO coupled model with dynamical sea ice. Mon. Wea. Rev., to appear.
Haney, R.L., 1971: Surface boundary condition for ocean circulation models. J. Phys. Oceanogr., 1, 241-248.
Hirst, A.C., and J.S. Godfrey, 1994: The response to a sudden change in Indonesian throughflow in a global ocean GCM. J. Phys. Oceanogr., 24, 1895–1910.
Hirst, A.C., and T. McDougall, 1997: Meridional overturning and dianeutral motion in a z-coordinate model including eddy-induced advection. J. Phys. Oceanogr., submitted.
Hirst, A.C., H.B. Gordon, and S.P. O'Farrell, 1996: Global warming in a coupled climate model including oceanic eddy-induced advection. Geophys. Res. Let., 23, 3361–3364.
McDougall, T.J., A.C. Hirst, M.H. England, and P.C. McIntosh, 1996: Implications for a new eddy parametrisation for ocean models. Geophys. Res. Let., 23, 2085–2088.
McDougall, T.J., and P.C. McIntosh, 1996: The temporal-residual-mean velocity. Part I: derivation and the scalar conservation equations. J. Phys. Oceanogr., 26, 2653–2665.
Rahmstorf, S., and J. Willebrand, 1995: The role of temperature feedback in stabilising the thermohaline circulation. J. Phys. Oceanogr., 25, 787–805.
Schopf, P.S., 1983: On equatorial waves and El Nino. II: effects of air-sea thermal coupling. J. Phys. Oceanogr., 13, 1878–1893.
Stommel, H., 1961: Thermohaline convection with two stable regimes of flow. Tellus, 13, 224–230.
Weaver, A.J., J. Marotzke, P.F. Cummins, and E.S. Sarachik, 1993: Stability and variability of the thermohaline circulation. J. Phys. Oceanogr., 23, 39–60.

Predictability of North Atlantic Climate on Decadal Times Scales Estimated Using a Coupled Ocean-Atmosphere Model

Kirk Bryan, Program in Atmospheric and Oceanic Sciences, Princeton University, USA, and Stephen M. Griffies, Geophysical Fluid Dynamics Laboratory, Princeton, USA. kbryan@splash.princeton.edu

The northern North Atlantic has pronounced climate variability on the time scale of several decades. The evidence for this long-term variability is chiefly in the historical record of surface temperature over the ocean and adjacent land areas. However, pioneering work by Talley and McCartney (1982) pointed out that changes on decadal time scales are also taking place in the water mass properties of the North Atlantic. As an example of the analysis of sea surface temperature records, Hansen and Bezdek (1996) have recently shown the slow drift of anomalies in the direction of the North Atlantic drift and the Norwegian current, with other anomalies drifting southwestward along the eastern and southern flank of the subtropical gyre. These anomalies drift at a slower rate than the surface currents and have a time scale of many years. Because of the close proximity to the Norwegian Current, Northern Norway is particularly sensitive to such long-term climate variability and confirmation of this is found in tree ring records.

In the late 1980s the Atlantic Climate Change Program (ACCP) was formed in the US. The programme was largely based on earlier work in the UK by Folland *et al*. (1986) and Palmer and Sun (1985). Of particular importance was a seminal paper by J. Bjerknes (1964) in which it was pointed out that there might be a connection between decadal climate shifts and changes in northward heat transport by the North Atlantic Ocean. One of the key goals of this programme was to determine the predictability of North Atlantic climate variations. Even a cursory analysis of the few time series that exist for the North Atlantic suggest predictability. The aim of the present study (Griffies and Bryan, 1997a, b) is to put this question into a quantitative framework.

It is well known that weather is only predictable for a week at most, and the predictability of atmospheric planetary waves for time scales greater than seasons variations is more closely tied to the predictability of the ocean. This is not the first time that a coupled ocean atmospheric model has been used to investigate predictability. Coupled models have been used to determine the predictability of El Niño in the Equatorial Pacific. Without having a long time series of three-dimensional ocean data for the North Atlantic, it is impossible to make a direct test of predictability through trial predictions of multidecadal climate changes in this region. Our approach is to undertake ensemble experiments as originally suggested by Lorenz (1969), but using a coupled ocean-atmosphere model. At the time this study commenced, the most appropriate model for this purpose appeared to be the climate model at the Geophysical Fluid Dynamics Laboratory (Manabe *et al.*, 1991). The GFDL model has been used in many studies and has been run for as long as 2000 years with only a small amount of climate drift. Delworth *et al.* (1993) have shown that the GFDL model contains a multidecadal variability associated with 5–10% swings in the amplitude of the Atlantic thermohaline circulation (THC). Although the model has a relatively low resolution, the long term sea surface temperature (SST) variations in the North Atlantic correspond roughly to those found for decadal variability by Kushnir (1994).

Since the atmosphere is unpredictable for more than

a week, the atmospheric component is the main factor in causing a loss of predictability in the coupled model. For this reason the predictability experiments are designed in the following way: a set, or ensemble, of numerical integrations of the model are carried out which have the same initial conditions in the ocean component, but different initial conditions for the atmospheric component. To make sure that the atmospheric initial conditions are compatible with the model, they are chosen randomly (different years, same day of the year) from the 1000 year control run. One way to interpret this design is that the experiments assume an observational system which provides perfect data for the ocean. The experiment is testing the loss of predictability in the ocean component of the model which is solely due to coupling with a nearly unpredictable atmosphere. Essentially the ensemble experiments are designed to determine the upper limit of predictability for the case of a perfect ocean model and perfect ocean initial data.

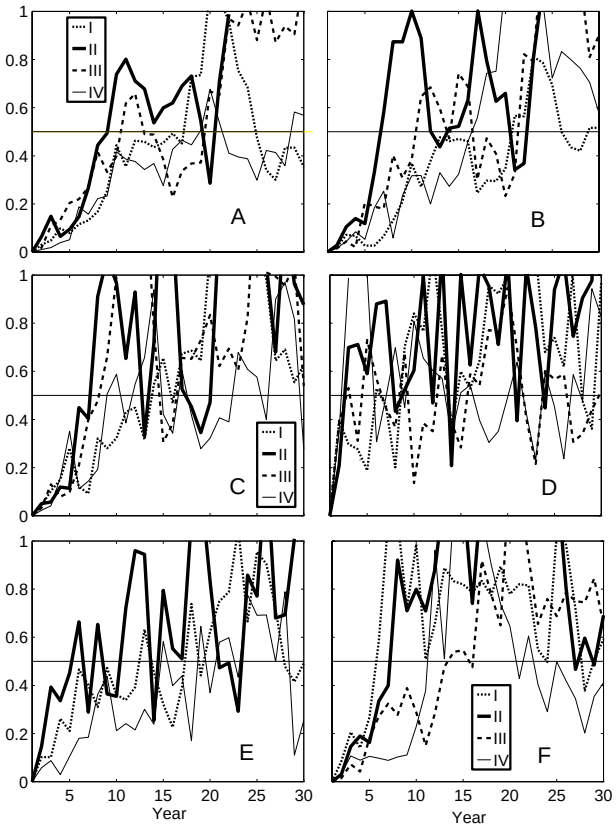

Figure 1. Normalized ensemble variances for selected principle component time series as a function of time from four ensemble experiments. The ensembles used to generate these statistics represent a total of 1200 years of integration from the coupled model. Ensemble I contains 12 members, was initialized with the ocean at year 130 from the control experiment, and employed the linear detrended climatology from years 1–200 for defining its associated climatology patterns and statistics. Ensemble II has 12 members, was initialized with ocean at year 500, and used climatology from years 401-600. Ensembles III and IV have 8 members each, were initialized with ocean at years 941 and 951, respectively, and used climatology from years 801–1000. The full 1000 year experiment contains a nonlinear drift which motivated our choice for 200 year climatologies, each of which showed only a modest linear drift. Given here are results for the North Atlantic (0–70°N and 0–90°W) (A) dynamic topography EOF1, (B) temperature at 170 metres EOF-1 (this field is indicative of the very clean subsurface signals associated with the multidecadal variability), (C) SSS EOF-1, (D) SST EOF-1, (E) EOF-2 for the meridional streamfunction of the zonally integrated Atlantic (50°S–90°N) velocity (streamfunction EOF-1 represents a basin-wide drift and is not of interest here), and (F) SST averaged over 15°–25°W at 70°N in the East Greenland Sea.

The different atmospheric states quickly interact with the upper layers of the ocean component of the model, and the ocean components in the different members of the ensemble slowly drift apart from one another. Loss of predictability as a function of time is estimated by the growth of variance of ocean variables in different members of the ensemble. An excellent feature in the calculations is the very realistic level of "weather noise" in the Delworth *et al*. (1993) model. The time required for the variance to reach 50% is considered to be the limit of useful predictability. When the variance between different members of the ensemble becomes equal to that expected from climatology, all predictability is considered lost.

After analyzing the results it became clear that the most predictable variables in the ocean component of the model were large scale averages of water mass properties in the upper thermocline. Therefore leading order EOFs (empirical orthogonal functions) of SST, temperature at lower levels and dynamic topography turned out to be convenient and efficient representations of the state of the ocean. The model is global, but the EOF patterns are calculated from the covariance matrix for an area which included just the North Atlantic, excluding the Nordic Seas. Four ensemble calculations were carried out and the increase in variance over time is shown in Fig. 1. The first panel in Fig. 1 shows the increase in variance of the amplitude of the first EOF for dynamic topography. The amplitude of the variance in the diagram is normalized by the climatological variance. In the first few years of the ensemble run, the growth of the variance is nearly monotonic. After reaching the 0.5 level the ensemble variance begins to fluctuate. Fig. 1a shows that the first EOF of dynamic topography has a useful predictability ranging from 8–20 years. This is an encouraging result. The Bermuda record shows that dynamic topography and low frequency changes in sea level (Levitus, 1990) are closely related, and sea level is already being monitored by satellites.

Panel (B) in Fig. 1 shows the equivalent results for the horizontal field of temperature at a level of 170 m in the ocean model. The variances show a predictability which is equivalent to that of the dynamic topography. From this result we conclude that the predictability of dynamic topography does not arise through a reduction of noise by vertical averaging, but simply because it samples subsurface water mass properties like the temperature at 170 m, which

are much less noisy than the sea surface salinity (SSS) and the sea surface temperature. The growth in variance of the first EOF of those fields is shown in panels (C) and (D). It is clear that sea surface salinity is much more predictable than sea surface temperature. This result supports the importance of long-term monitoring of surface salinity.

The lower two panels in Fig. 1 correspond to the growth in variance for the leading EOFs of the North Atlantic meridional transport stream function and the SST for a limited region in the East Greenland Sea. The ensemble results show the meridional stream function, and hence the amplitude of the THC "conveyor belt" is predictable. While it is important for understanding the basis of predictability in other variables, the predictability of the meridional circulation is not of direct usefulness, since no practical way has been developed to monitor the "conveyor belt" by direct measurements. On the other hand, the predictability of SST in the Greenland Sea is very important because anomalies in this region appear to be linked to downstream temperatures over land in Eurasia in the coupled model.

The results shown in Fig. 1 are summarized schematically in Fig. 2. The ocean predictability is from 10–20 years in the upper thermocline of the North Atlantic. This region is shielded from the loss of predictability caused by the nearly random perturbations of the synoptic systems of the mid latitude atmosphere. Near the surface the temperature and salinity are much less predictable. As expected the feedbacks of the heat balance at the ocean surface make the sea surface temperature much less predictable than sea surface salinity and the model shows this difference.

Why is the predictability indicated by different ensembles so different? Some insight on this question is indicated by the analysis of a single ensemble experiment shown in Fig. 3. Panels (A) and (B) of Fig. 3 show the auto correlation function and the power spectrum of the first EOF of dynamic topography. The equivalent information is displayed in two different ways. Along with the power spectrum an envelope of dashed lines indicates the 95% null hypothesis for a simple red noise model fit. At frequencies of one cycle per decade, or greater, the spectrum is well within the red noise envelope. However, as noted by Delworth *et al.* (1993) there is a spectral peak at lower frequencies which clearly emerges above the 95% null line. The auto correlation is dominated by this peak frequency and shows a clearly oscillatory behaviour with the first zero crossing at 15 years. Panel (C) shows the trajectories of the amplitude of the first EOF of dynamic topography for the ensemble experiment. Note that the trajectories are tightly packed together for the first five years and then gradually split apart as signals from the atmospheric component of the model slowly penetrate down into the thermocline in such a way as to alter the large scale pattern of dynamic topography.

Hasselmann (1976) has suggested a much simpler model for an ocean interacting with an overlying atmosphere. In Hasselmann's model the ocean is taken to be a well mixed thermal reservoir with two sources of heating at its upper surface. One source is simple random impulses due to passing weather systems, and the other is a slow damping towards an equilibrium temperature determined by radiation and other climate factors. The model has no dynamics and responds in a random walk of temperature around the equilibrium point. The spectrum expected from the Hasselmann model is red noise with a flattening of the spectrum at low frequencies.

The auto correlation curve shown in Fig. 3A is very different from what would expect from Hasselmann's model. It appears to be more like the auto correlation one would expect from a damped linear oscillator. A physical analogue would be a pendulum driven by random impulses, but submerged in a tank of water. Swings of the pendulum would be repeated, but they could not be predicted for an extended period of time. In panel (D) of Fig. 3 the growth in ensemble variance of the amplitude of the first EOF of dynamic topography is plotted as a function of time as in Fig. 1A. For comparison the smooth curve in the same panel is the theoretical increase in variance for an ensemble of infinite size for an idealized noise-driven, damped oscillator. For the first 10 years of the ensemble experiment the correspondence between the two curves is excellent.

The oscillatory behaviour of the first EOF of dynamic topography suggests that the ocean circulation is playing an important role, with a preferred natural period of 40–60 years in this model. While the red noise behaviour will provide a limited amount of predictability just due to damped persistence, the model results indicate that the North Atlantic may have a much greater predictability due to an intrinsic frequency connected with the dynamics of the thermohaline circulation. The differences in the predictability indicated by the different ensemble experiments are partly the random differences one would expect from a small statistical sample. A more important factor appears to be the difference in amplitude of

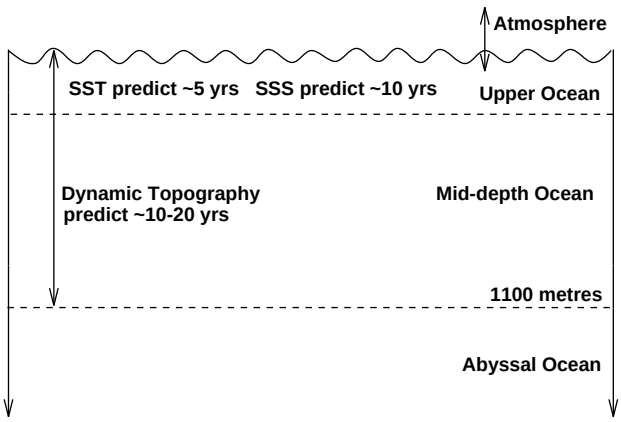

Figure 2. Schematic diagram illustrating the oceanic predictability seen in the coupled model. The surface ocean serves as the interface between the noisy synoptic atmosphere and the more coherent mid-depth ocean. When the mid-depth ocean is oscillating, the surface properties and those at mid-depth contain multi-year to multi-decadal predictability. The oscillation is seen most distinctly in the dynamic topography.

thermohaline circulation variations in various parts of the 1000 year control run of the model. When the thermohaline circulation variations are large, the predictability is high and vice-versa. The model appears to have a high predictability in extreme events, which tend to excite the oscillations shown in Fig. 3.

It is also possible to use the results of the ensemble experiments to determine the geographical regions which have the highest predictability. This information might be useful in designing climate monitoring systems. Fig. 4 (page 23) shows synoptic maps of the normalized variance of dynamic topography in one ensemble for four different periods spaced 2 years apart. The maps show that the early growth of variance is along the eastern boundary of the ocean. The growth appears to be strongly associated with areas of strong winter ocean convection in the model in the Irminger and Labrador Sea. In this region the influence of the atmosphere can penetrate into the deep ocean most easily. Thus chaotic signals from the atmosphere will tend to cause an early splitting of the ensemble solutions in these northern areas. Propagation parallel to the coast spreads these signals in a north-south direction. Spread of variance into the mid-ocean interior takes place by advection along the eastward drift. In other areas the beta effect tends to trap high variance towards the western boundary, thus enhancing predictability over the eastern part of the North Atlantic.

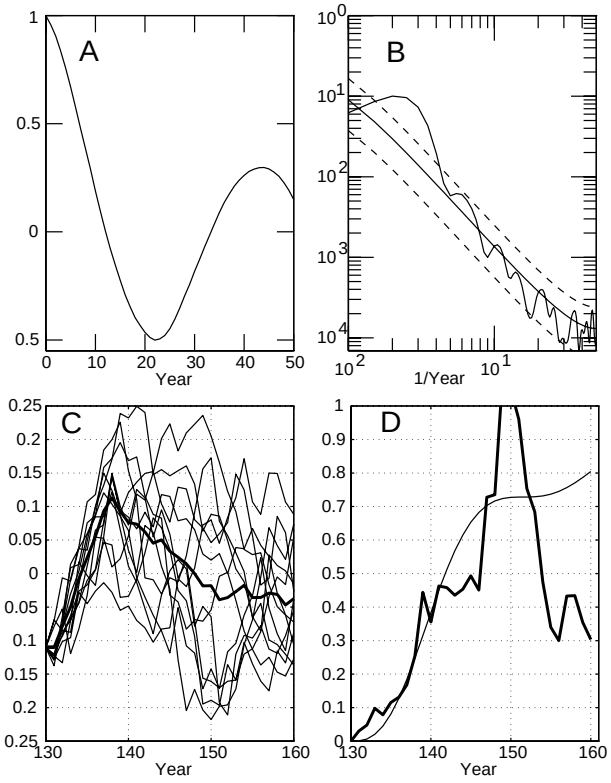

Figure 3. (A) Auto-correlation function for the first North Atlantic dynamic topography principle component defined from yearly mean fields over model years 1–200. The ordinate is the auto-correlation and the abscissa is the lag in years. The time series were linearly detrended prior to computing the eigenfunctions (EOF patterns) of the zero lag covariance matrix. The damped sine-wave behavior is characteristic of oscillatory variability. This sample auto-correlation function can be fit to that from a damped harmonic oscillator driven by white noise, where the oscillator period and damping time are roughly 40 years each. (B) Power spectrum (ordinate) corresponding to the previous auto-correlation function. The abscissa is the frequency in cycles/year. The power rises well above the 95% red noise null hypothesis bounds (the dashed lines) in the 40–60 year time scale. (C) The principle component trajectories from Ensemble I for dynamic topography EOF-1. The dark solid line indicates the ensemble mean. Units are dynamic meters. (D) The normalized ensemble variance (ordinate), with the thin smooth line being the variance predicted from an infinite sized ensemble of the noise driven damped harmonic oscillator.

From the standpoint of the design of monitoring networks Fig. 4 suggests that observations are most needed in regions of low predictability along the western boundary of the North Atlantic. Through the WOCE programme important progress is being made in developing *in situ* monitoring. Tests on both roving and stationary platforms show great promise. Judgements will soon have to be made on what mix of platforms will be most efficient for monitoring the North Atlantic. Similar predictability calculations with a higher resolution coupled model could be of use to produce specific observational requirements.

Several important questions arise in connection with this study, but have not been addressed. One is the question of what governs the apparent frequency of the thermohaline oscillations which are so important to the predictability found in this model. This question is being pursued with simple models. The second unanswered question concerns the link between ocean predictability and predictability of atmospheric climate in the North Atlantic area. It is known that there are low frequency changes of winds over the North Atlantic and the Nordic Seas. The North Atlantic Oscillation (NAO) has been studied by meteorologists for many decades. The relation between sea surface temperature and the NAO is a very complex question for which our model is not really suited. The atmospheric component of the coupled model produces highly realistic "weather" at the surface of the ocean model, and it exhibit climate variability on all time scales, but it is still a very low resolution representation of the atmosphere. We conclude that our model shows definite predictability on multidecadal time scales for the ocean and to a lesser extent for sea surface temperature, but the question whether this results in predictability for the climate of the atmosphere is left to future studies.

References

Bjerknes, J., 1964: Atlantic air-sea interaction. Advances in Geophysics, 10, 1–82.

Delworth, T., S. Manabe, and R.J. Stouffer, 1993: Multidecadal variations of the thermohaline circulation in a coupled ocean-atmosphere model. J. Climate, 12, 1993–2011.

Folland, C. K., T.N. Palmer, and D.E. Parker, 1986: Sahel rainfall

and worldwide sea temperature. Nature, 320, 602–606.
Griffies, S.M., and K. Bryan, 1997: Ensemble predictability of simulated North Atlantic multidecadal climate variability. Submitted to Climate Dynamics, Sept. 1996.
Griffies, S.M., and K. Bryan, 1997: Predictability of North Atlantic multidecadal climate variability. Science, 275,181–184.
Hansen., D.V., and H.F. Bezdec, 1996: On the nature of decadal in North Atlantic anomalies in sea surface temperature. J. Geophys. Res., 101, 8749–8758.
Hasselmann, K., 1976: Stochastic climate models, part 1 – theory. Tellus, 18, 473–484.
Kushnir, Y., 1994: Multidecadal variations in North Atlantic sea surface temperature and associated atmospheric conditions. J. Climate, 7, 141–157.
Levitus, S., 1990: Multipentadal variability of steric sea level and geopotential thickness of the North Atlantic Ocean, 1970-1974 versus 1955–1959. J. Geophys. Res., 95, 5233–5238.
Lorenz, E., 1969: Three approaches to atmospheric predictability. Bulletin of the American Meteorological Society, 50, 345–349.
Manabe, S., R.J. Stouffer, M.J. Spelman, and K. Bryan, 1991: Transient response of a coupled ocean-atmosphere model to gradual changes of atmospheric: Part I: Annual mean response. J. Climate, 4, 785–818.
Palmer, T.N., and Z. Sun, 1985: A modelling and observational study of the relationship between sea surface temperatures in the north-west Atlantic and the atmospheric general circulation. Q.J.R. Met. Soc., 111, 947–975.
Talley, L.D., and M.S. McCartney, 1982: Distribution and Circulation of Labrador Sea Water. J. Phys. Oceanogr., 12, 1189–1205.

The Ocean Simulation in the Hadley Centre Coupled Climate Model

Chris Gordon, Claire Cooper, Richard Wood, and Helene Banks, Hadley Centre for Climate Prediction and Research, Meteorological Office, UK.
cgordon@meto.gov.uk

Over the past few years a number of developments have been made to the Hadley Centre global coupled model that is used in the investigation of anthropogenic climate change. As with other global coupled models, previous versions produced severe drifts in the simulated climate which had to be alleviated by the use of artificial flux adjustments (Johns *et al*., 1997). Recent developments to both the atmosphere and ocean models have gone a long way towards reducing the model climate drift, and thereby the need for flux adjustment. This article describes some of the early results from a short simulation of current climate using the latest version of the Hadley Centre coupled model (HADCM3).

One of the critical elements in the climate system is the heat transported by the oceans. The resolution of ocean models used in climate modelling is limited by computing time constraints, since multi-century coupled 'control' runs and ensemble integrations are needed to establish natural climate variability and allow significant climate changes to be identified. In an earlier version of the coupled model with a coarse resolution ocean model ($2.5° \times 3.75°$ latitude-longitude) the ocean meridional heat transports were typically underestimated by a factor of two. The understanding and improvement of the heat transport mechanisms in the ocean component of the coupled model continues to be a high priority for model development. The use of analysis based on WOCE observations will be crucial to this process.

The HADCM3 model

The atmospheric component of the model is the latest version of the 19-level Hadley Centre atmospheric general circulation model (GCM). It is similar to the model described in Johns *et al*. (1997) but with a number of refinements to the physical parametrizations incorporated. In particular it contains a revised radiation scheme and other enhancements not discussed in detail here.

The ocean model is a 20 level version of the Cox (1984) model on a $1.25° \times 1.25°$ latitude-longitude grid. There are six ocean grid boxes to each atmosphere model grid box and each high latitude ocean grid box can have partial sea ice cover. The vertical levels are distributed to provide enhanced resolution near the ocean surface. Horizontal mixing of tracers uses a version of the Gent and McWilliams adiabatic diffusion in which the thickness diffusion coefficient is determined locally (see Wright, this issue). The near surface vertical mixing is parametrized by a hybrid approach in which the mixing of tracers is carried out via a Kraus-Turner mixed layer sub-model and momentum via a K-theory scheme. There is also a simple representation of sill overflows across the Denmark Straits and Iceland-Scotland Ridge and a parametrization of the outflow of water from the Mediterranean. The sea ice model uses a simple thermodynamic scheme and contains parametrizations of ice drift and leads (Cattle and Crossley, 1995).

Some preliminary results from a 30 year simulation of the model are discussed below. Ocean currents were initially set to zero and the initial temperature and salinity were taken from the Levitus (1994) climatology. The ocean-atmosphere coupling period was one day and there is no flux adjustment. Although 30 years is a relatively short simulation, there is little temperature drift in the near surface layers between years 20 and 30 (see Fig. 1), and gives sufficient time for all the major surface climate drifts to develop.

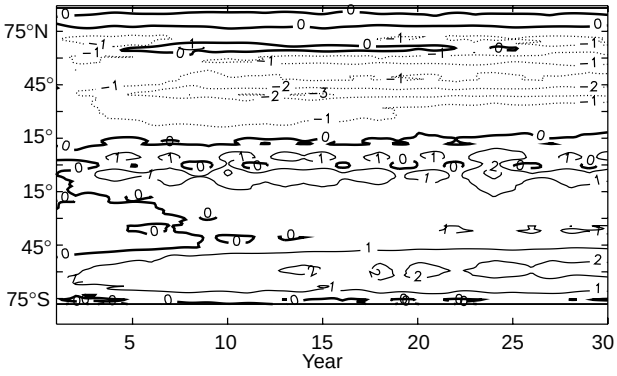

Figure 1. The time evolution of the annual zonal mean SST difference from the GISST climatology throughout the 30 years of the coupled simulation (°C).

Simulated sea surface temperature

The most important ocean variables in the coupled model are the simulated sea surface temperatures (SSTs) and the sea ice extents, as these determine the interaction with the atmosphere. The HADCM3 year 21 to year 30 mean simulated SST minus the GISST climatology (Rayner *et al*., 1996) is shown in Fig. 2. Over much of the ocean the SST is simulated to within 2°C of climatology, although there are a number of regions where the model drift is considerably larger.

The North Pacific is too cold and this is associated with deficiencies in both the atmosphere and ocean model simulations. In the ocean model the Kuroshio separates too far south and the large SST differences are associated with the positioning of the high SST gradients accompanying this current. In addition, the atmosphere model underestimates the short wave heating at the ocean surface, especially in summer, and combined with the shallow summer North Pacific mixed layer depths, this leads to significant errors in SST. In the North Atlantic the differences are, in part, associated with the positioning of the North Atlantic Current which tends to be too zonal in the region of the Grand Banks. This feature is specific to the Cox-type model and is not present in isopycnal models (Roberts *et al*., 1996). The warming in the marine stratocumulus regions of the tropics is a feature common to many coupled models and is largely associated with the under-prediction of cloud in these regions. The warming off the Antarctic ice edge arises because the warmer water from a few hundred meters depth rises to the surface. In reality this does not happen because there is a cold and fresh layer overlying the deeper water. In the model the fresh layer is unable to cap the deeper water and this points to an underestimation of the fresh water flux in this region. There are also significant differences in the region of the Agulhas Current where eddy transports are known to be important. Despite these differences from climatology the simulation is a considerable improvement on earlier versions of the model. The sea ice simulation is also considerably more realistic than in earlier versions of the model as are the rates of deep water formation. The understanding and reduction of the remaining systematic errors, which arise from deficiencies in the ocean, atmosphere and sea ice models, is a continuing area of active current research.

Ocean heat transports

The ocean heat transport across 24°N (Pacific and Atlantic basins) has been calculated directly (*i.e*. the small implied eddy heat flux in the model is ignored) for years 20–30. Fig. 3 shows the time series of the annual mean heat transport across this latitude for the two basins. In the Atlantic at 24°N, the annual mean northward heat transport varies between 1.15 PW and 1.29 PW (compared with the observational estimate of 1.22 PW by Hall and Bryden (1982) (hereafter HB)), while in the Pacific at 24°N there is a much stronger signal of interannual variability with the annual mean varying between 0.50 PW and 0.76 PW (compared with 0.75 PW estimated by Bryden, Roemmich and Church (1991) (hereafter BRC)). The enhanced and regular variability in the Pacific is probably related to the rather regular ENSO signal in the tropics during this period of the simulation.

The components of the ten year mean heat transport have been calculated in the manner of HB. In Table 1 the Ekman, interior and western boundary current contributions are summarised for the two sections along with the observed

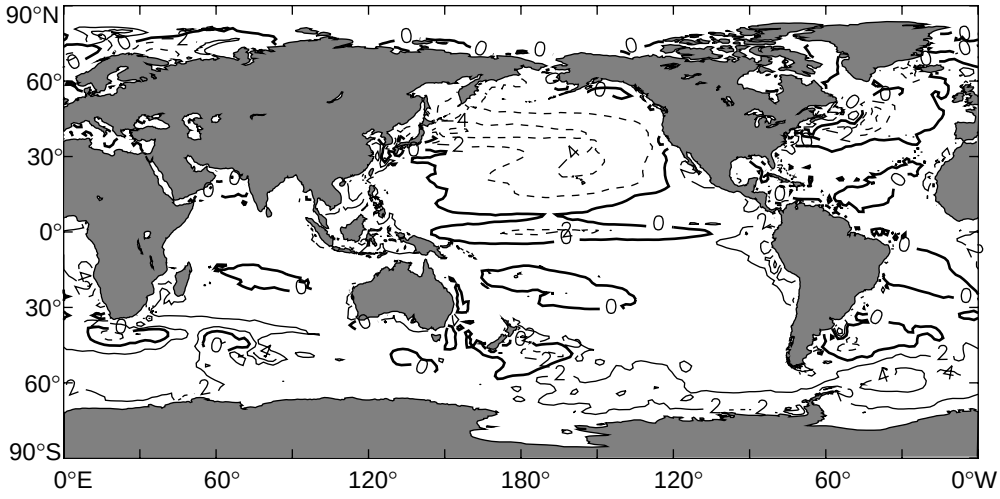

Figure 2. The coupled model years 21–30 mean simulated SST minus GISST climatology (°C).

values from HB and BRC for the Atlantic and Pacific sections respectively. Similar differences can be seen for both sections; an overestimate of the heat transported northward by the western boundary current and an underestimate of the heat transported northward by the Ekman component. The Pacific Ekman layer shows the largest discrepancy in the heat transport budget (0.35 PW). From the model windstresses we estimate an Ekman transport of 4.4 Sv in the Atlantic (HB estimate 5.0 Sv) and only 7.5 Sv in the Pacific (BRC estimate 12.0 Sv).

In the Atlantic, the heat transport can be explained entirely by a vertical-meridional overturning cell (in agreement with HB), while in the Pacific, the overturning cell contributes only 0.1 PW and most of the heat is transported via a horizontal circulation cell (BRC estimate an equal contribution from each cell). Overall the magnitude and mechanisms for heat transport in the model appear to be in reasonable agreement with estimates from observations.

These results show that climate models have developed to a state where there is useful understanding to be gained by a detailed comparison of modelled and observed heat transport processes. In earlier models the usefulness of this was limited by coarse resolution, which made it difficult to disentangle different flow regimes (*e.g.* western boundary current and interior), and required an over-viscous flow for reasons of numerical stability. Although not all important ocean processes are adequately resolved at 1.25° resolution (*e.g.* eddies, boundary currents, sill flows), there is hope that many of the important processes for climate can be identified and if necessary parametrized. At the Hadley Centre the programme of ocean model validation has recently been expanded, with the aim of strengthening links with the WOCE community and so bringing on board the results of WOCE analysis. Testing the climate models against the emerging understanding of the global ocean circulation will help us to quantify the uncertainty in climate change predictions due to particular model errorsand so to drive future model development.

Table 1. Components of the northward heat transport (PW) for the Atlantic 24°N section and the Pacific 24°N section. The model results derive from the 10 year mean (years 21–30) and the observations are taken from HB (Atlantic) and BRC (Pacific).

	Atlantic 24°N		Pacific 24°N	
Component	Model	Observed	Model	Observed
WBC	1.81	1.73	1.94	1.73
Ekman	0.35	0.42	0.58	0.93
Interior	-0.93	-0.93	-1.86	-1.91
Total	1.23	1.22	0.66	0.75

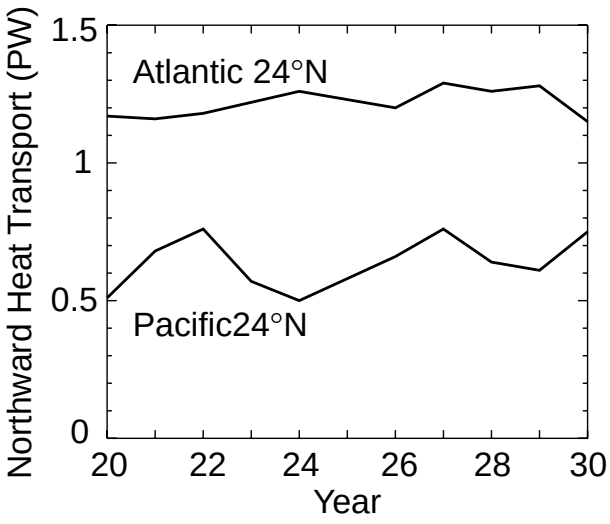

Figure 3. The year 20-30 time series of the simulated annual mean heat transport across 24°N in the Atlantic and Pacific basins.

References

Bryden, H.L., D.H. Roemmich, and J.A. Church, 1991: Ocean heat transport across 24°N in the Pacific. Deep-Sea Res., 38, 297–324.

Cattle, H., and J. Crossley, 1995: Modelling Arctic Climate Change. Phil. Trans. R. Soc. Lond., A352, 201–213.

Cox, M.D., 1984: A primitive equation, three dimensional model of the ocean. GFDL Ocean Group Technical Report No.1, Princeton, NJ, USA. 143pp.

Gent, P., and J. McWilliams, 1990: Isopycnal mixing in ocean circulation models. J. Phys. Oceanogr., 20, 150–155.

Hall, M.M., and H.L. Bryden, 1982: Direct estimates and mechanisms of ocean heat transport. Deep-Sea Res., 29, 339–359.

Johns, T.C., R.E. Carnell, J.F. Crossley, J.M. Gregory, J.F.B. Mitchell, C.A. Senior, S.F.B. Tett, and R.A. Wood, 1997: The second Hadley Centre coupled ocean-atmosphere GCM: model description, spinup and validation. Climate Dynamics (in press).

Levitus, S., R. Burgett, and T.P. Boyer, 1994: World Ocean Atlas 1994, Volume 3: Salinity. NOAA Atlas NESDIS 3, US Dept. Commerce, Washington, DC.

Levitus, S., and T.P. Boyer, 1994: World Ocean Atlas 1994, Volume 4: Temperature. NOAA Atlas NESDIS 4, US Dept. Commerce, Washington, DC.

Rayner, N.A., E.B. Horton, D.E. Parker, C.K. Folland, and P.B. Hackett, 1996: Version 2.2 of the Global sea-Ice and Sea Surface Temperature (GISST) data set, 1903-1994. CRTN 74. Hadley Centre, Meteorological Office, Bracknell, UK.

Roberts, M.J., R. Marsh, A.L. New, and R.A. Wood, 1996: An intercomparison of a Bryan-Cox type ocean model and an isopycnic ocean model. Part I: The subpolar gyre and high latitude processes. J. Phys. Oceanog., 26, 1495–1527.

The OPA/ARPEGE and OPA/LMD Global Ocean-Atmosphere Coupled Model

Gurvan Madec and Pascale Delecluse, Laboratoire d'Océanographie Dynamique et de Climatologie (LODYC), Université Pierre et Marie Curie, Paris, France.
gm@lodyc.jussieu.fr

When studying the general circulation of the ocean, it is natural to move from forced ocean models to coupled ocean-atmosphere models which provide air-sea fluxes through the atmosphere dynamics. It is indeed much more satisfying to calculate the interactive fluxes than to use specified values. A forced ocean model is never truly forced: there is usually a feedback term in the heat flux formulation which implies a coupling with a diagnostic atmosphere:

$$Q = \left(\frac{dQ}{dT}\right)_o \left(SST_{mod} - T^*\right) \qquad (1a)$$

or equivalently,

$$Q = Q_o + \left(\frac{dQ}{dT}\right)_o \left(SST_{mod} - SST_{obs}\right) \qquad (1b)$$

where T^* is an equivalent surface air temperature, Q_o and $(dQ/dT)_o$ are the heat flux and its associated sensitivity to SST given by an atmospheric model or computed from observations, and SST_{mod} and SST_{obs} are the ocean model and observed sea-surface temperature, respectively.

The feedback term in (1) mimics the air-sea interactions (from linearized bulk formulae). This is only a local negative feedback which damps SST_{mod} anomalies. This parameterization neglects the role of the atmospheric circulation and has no integral constraint. It specifies the spatial structure of the SST through the shape of the SST_{obs} independently of what the ocean model would like to represent. A shift of model SST structure generates strong unrealistic air-sea fluxes which result in new water mass formation that has no physical variability. This is particularly true in western boundary regions where currents are associated with permanent and vigorous fronts. Furthermore, a similar feedback term is usually used to prescribe the effect of fresh water fluxes on Sea Surface Salinity (SSS). There is no physical argument to support this parameterization. SSS does not influence the overlying atmosphere except indirectly and nonlocally through changes in the ocean stratification and circulation. Finally, it is awkward to try to determine the ocean circulation by specifying the most reactive medium (the atmosphere).

For all the above reasons, our interest in understanding the ocean variability has motivated the participation in a research group, called GASTON. This group combines the efforts of the French climate community for building a comprehensive set of models of the Earth's climate system. GASTON involves several laboratories, namely: CERFACS (Centre Européen de Recherche et de Formation Avancées en Calcul Scientifique), CNRM (Centre de Recherche Météorologiques, Météo France), LMCE (Laboratoire de Météorologie Dynamique, CNRS-IPSL) and LODYC (Laboratoire d'Océanographie Dynamique et de Climatologie, CNRS/UPMC/ORSTOM).

The general strategy of GASTON can be summarised as follows. The aim is to assess present-day climate variability and to study the role of each component in that variability using several global ocean-atmosphere coupled General Circulation Models (GCMs). Each model is developed on its own grid (best suited to its physical and numerical requirements) and a coupler permits the exchanges between the different grids involved. The initial oceanic state is chosen as close as possible to observations and no flux correction technique is used at the air-sea interface. The departure from the observed climate is very useful to illustrate the mechanisms working to modify the coupled system equilibrium. In particular, the resulting climate drift points out the deficiencies of the coupled model physical parameterizations and suggests refinements for further development in model formulation and modelling assumptions.

Within GASTON, two atmospheric GCMs (ARPEGE-climate and LMD) and one oceanic GCM (OPA) are used at various spatial resolutions and with various physics. They are coupled together through the same coupling tool (OASIS). The ARPEGE GCM is the climate version of ARPEGE/IFS forecast model, developed jointly by Météo-France and the European Centre for Medium-range Weather Forecasts (ECMWF). The model and its validation are described by Déqué *et al.* (1994). Three triangular spectral truncations (T21, T31, and T42) have been used for horizontal resolution corresponding to a 5.6°, 3.8° and 2.8° grid size. All versions have 30 vertical levels and can be used with different parameterizations. The LMD GCM is a C-grid atmospheric model described in Sadourny and Laval (1984) and Le Treut *et al.* (1994). The model horizontal resolution is 96×72 (standard) or 64×50 (coarse) points equally spaced in longitude and sine of latitude which provides a comparatively higher resolution in the tropics. The number of vertical levels is 15 or 11.

The global ocean is based on OPA, the GCM developed at LODYC (Delecluse *et al.*, 1993). It is a C-grid primitive equation model written in orthogonal curvilinear coordinates. Its horizontal mesh is stretched so that the mesh North Pole is moved onto Asia while its southern hemisphere has a geographical configuration (Madec and Imbard, 1996). Its standard space resolution is roughly equivalent to a geographical mesh of 2° by 1.5° (with a meridional resolution of 0.5° near the Equator). 31 levels are used with 10 levels in the top 100 metres. A coarse resolution (roughly 4° by 3°) is also used (Braconnot *et al.*,

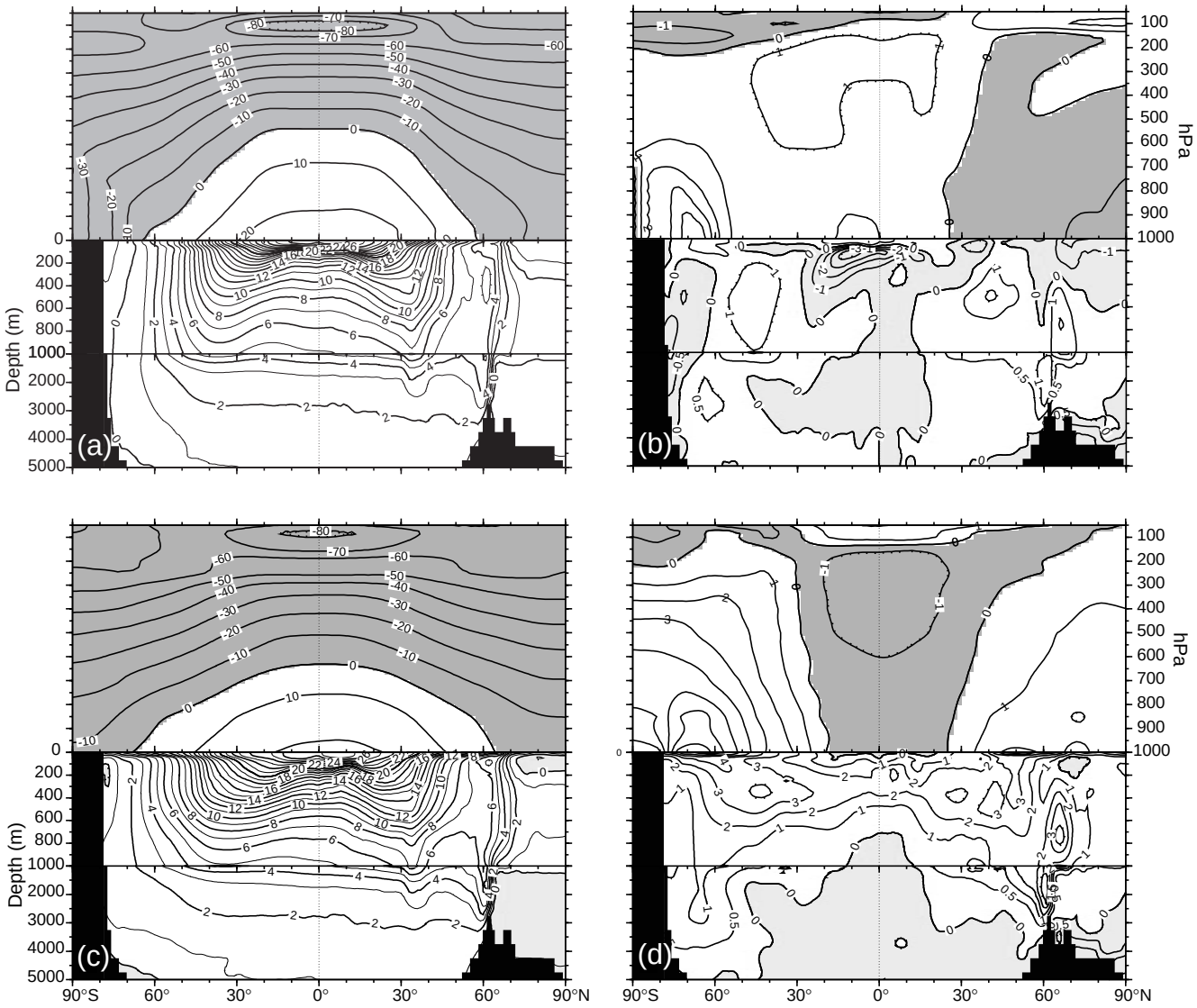

Figure 1. Zonal mean of annual-mean temperature (°C) in the atmosphere and the ocean, and the difference with uncoupled atmosphere simulation and initial oceanic state. (a) and (b) ARPEGE T21/OPA experiment, (c) and (d) LMD/OPA experiment. Contour interval is 10°C for atmosphere, 1°C in ocean and 1°C in the difference figure (0.5°C below 1,000 m).

1997). Different physical parameterizations can be used: lateral diffusive operator acting along geopotential or neutral surfaces, or including eddy induced velocity (Gent and McWilliams, 1990), vertical physics computed from a 1.5 turbulent closure scheme (Blanke and Delecluse, 1993). In addition, the ocean GCM hosts a sea-ice model also developed at LODYC (M.-N. Houssais, M.-A. Filiberti, and J.-L. Dufresne, personal communication 1996). Successful coupled ocean/ice simulations have been performed, and the extension to coupling with atmospheric components is underway.

The OASIS coupler has been developed at CERFACS (Terray, 1994). It ensures the time synchronization between the two GCMs and does the spatial interpolations from one grid to another. It respects the GCMs structure and very few changes have to be implemented to achieve the coupling. The coupler offers multiple options regarding interpolation schemes, I/O formatting and type of models being coupled. It also allows distributed coupled simulations (Cassou *et al.* 1997) as well as the coupling of parallel models on Massively Parallel Processor (MPP) machines (a useful property as ARPEGE and OPA can also run on such computers). Note that another coupling technique has been developed in GASTON: the delocalized physics method (Vintzileos and Sadourny, 1997) in which the whole vertical atmospheric physics is computed on the horizontal ocean mesh. This method allows a direct coupling between the ocean and the physical parameterizations of the atmospheric model and thus provides a better representation of non-linear effects. Nevertheless, it requires major modifications within the atmospheric model and increases the CPU time required. It has been validated for a regional coupled model (global LMD/Pacific Ocean OPA) (Vintzileos *et al.*, 1997).

Several coupled experiments have been performed

using different components and resolutions (ARPEGE T21, T31, T42, standard or coarse LMD and OPA). Here, we illustrate the results obtained by the first two high resolution experiments. These 30 year long coupled experiments use the same standard global oceanic GCM and two atmospheric GCMs (ARPEGE T42 and standard LMD). All the components have been coupled without specific tuning for coupled mode (uncoupled standard values of physical parameterizations are used). Fig. 1 shows the last 10 year zonal mean temperature in both components and the difference with the initial state *(i.e.* Levitus in the ocean and an uncoupled simulation in the atmosphere).

Atmospheric responses to the same ocean are quite contrasted; a huge warming occurs at high and mid-latitudes in the LMD/OPA experiment whereas ARPEGE/OPA exhibits smaller differences with a warming in the south and a cooling in the north. The lower tropical troposphere response is also different; warming for the ARPEGE/OPA experiment and cooling for the LMD/OPA experiment. A parameter adjustment in the LMD model (mainly the size of droplets) leads to a significant improvement in terms of magnitude of the difference but does not change its structure. A contrasted response is also found in the ocean. ARPEGE/OPA maintains the main thermocline. It is even tighter than the observed equatorial thermocline and has a marked 'W' structure, yet its shape becomes symmetrical with respect to the equator; its north-south tilt is flattened and even slightly reversed (see in Fig. 1b the strong cold anomaly at a depth of 200 m south of the equator). This results from the symmetrization of the atmospheric tropical response in this experiment and the formation of a second convergence zone south of the equator in both the Atlantic and the Pacific Oceans. The LMD/OPA experiment maintains the north-south tilt of the thermocline due to the ability of the LMD model to simulate an asymmetrical circulation in the tropics. Nevertheless, the thermocline becomes thicker with a 2° warming in between depths of 200 and 400 m (Fig. 1d). The time evolution of this warming shows that it results from the heating in mid-latitudes: warmer water masses are formed; they subduct in the main thermocline and invade the equator.

The response of the ARPEGE T42/OPA in both the atmosphere and the ocean is remarkably similar to the one obtained in the T21 ARPEGE/OPA experiment described in Guilyardi *et al.* (1995) and Guilyardi and Madec (1997). The latter experiment only differs by the atmospheric GCM resolution. The biases are weaker when the resolution is increased but their structure is unchanged.

Fig. 2 shows the SST of the ARPEGE T42/OPA experiment after 30 years and its difference with the annual mean SST from Levitus data and with a 10 year mean SST obtained in a forced simulation using equation (1) as heat flux parameterization with the AMIP ARPEGE T42 model outputs. The front displacements of western boundary currents are marked by strong dipole anomalies in SST. In the coupled model, these anomalies widen offshore. The large scale patterns (eastern equatorial warming, mid-latitude cooling) present in both forced and coupled

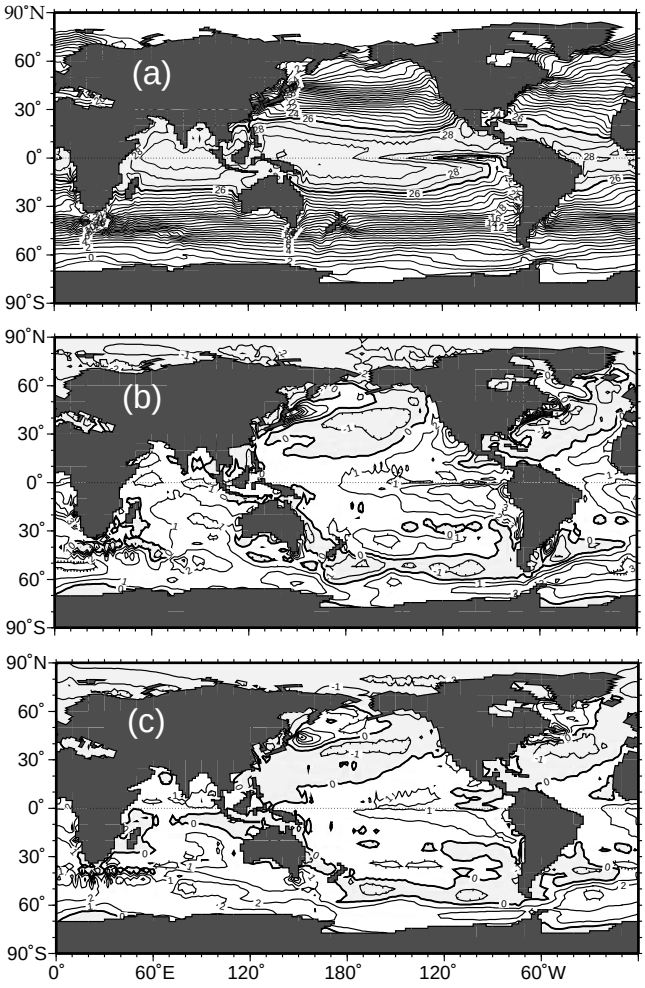

Figure 2. Sea surface temperature (°C). (a) coupled ARPEGE T42/OPA experiment, (b) its difference with Levitus data, and (c) its difference with an uncoupled ocean experiment forced with AMIP ARPEGE T42 model outputs. Contour interval is 1°C.

simulations suggest that most biases in the SST patterns are driven by systematic errors in each model component.

Whereas we still have many things to learn from "forced" ocean experiments, the use of more physical surface boundary conditions allows the ocean model to better express its physical processes and/or its limitations. Of course, the system becomes more complex and expensive, and errors can arise that are not only related to the ocean but also to the atmosphere. Fortunately, significant progess has been made in atmospheric modelling over the past decades as a result of a huge observational data set and pressure exerted by the need to improve weather forecasts. Nowadays, without flux correction techniques at the air-sea interface, ocean-atmosphere coupled simulations provide a consistent representation of the climate system. They do not drift too far from the real system so that process studies can provide useful information on the role of the ocean in the Earth climate system. In this perspective a sensitivity study to the ocean physics is underway.

References

Blanke, B., and P. Delecluse, 1993: Variability of the tropical Atlantic ocean simulated by a general circulation model with two different mixed layer physics. J. Phys. Oceanogr., 23, 1363–1388.

Braconnot, P., O. Marti, and S. Joussaume, 1997: Adjustment and feedbacks in a global coupled ocean-atmosphere model. Clim. Dyn., in press.

Cassou, C.P. Noyret, E. Sevault, O. Thual, L. Terray, D. Beaucourt, and M. Imbard, 1997: Distributed Ocean-Atmosphere modelling and sensitivity to the coupling flux precision: the CATHODe project. Submitted to Mon. Wea. Rev.

Delecluse, P., G. Madec, M. Imbard, and C. Lévy, 1993: OPA version 7 Ocean General Circulation Model reference manual. LODYC, France, Internal Report, 93/05, 111pp.

Déqué, M., C. Dreveton, A. Braun, and D. Cariolle, 1994: The climate version of Arpège/IFS: a contribution to the French community climate modelling. Clim. Dyn., 10, 249–266.

Gent, P.R., and J. C. McWilliams, 1990: Isopycnal mixing in ocean circulation models. J. Phys. Oceanogr., 20, 150–155.

Guilyardi, E., G. Madec, L. Terray, M. Déqué, M. Pontaud, M. Imbard, D. Stephenson, M.-A. Filiberti, D. Cariolle, P. Delecluse, and O. Thual, 1995: Simulation couplée océan-atmosphère de la variabilité du climat, C. R. Acad. Sci Paris, t. 320, série IIa, 683–690.

Guilyardi, E., and G. Madec, 1997: Performance of the OPA/ARPEGE T21 global ocean-atmosphere coupled model. Clim. Dyn., in press.

Le Treut, H., Z.X. Li, and M. Forichon, 1994: Sensitivity of the LMD General Circulation Model to greenhouse forcing associated with two different cloud water parameterizations. J. Clim., 7, 1827–1841.

Madec, G., and M. Imbard, 1996: A global ocean mesh to overcome the North Pole singularity. Clim. Dyn., 12, 381–388.

Sadourny, R., and K. Laval, 1984: January and July performances of the LMD General Circulation Model. New perspective in Climate Modelling, A. Berger and C. Nicolis Eds, Elsevier, 173–198.

Terray, L., 1994: The OASIS coupled user guide version 1.0. CERFACS Tech. Rep. TR/CMGC/94–33.

Vintzileos, A., and R. Sadourny, 1997: A general interface between an atmospheric general circulation model and underlying ocean and land surface models: delocalized physics scheme. Mon. Wea. Rev., in press.

Vintzileos, A., P. Delecluse, and R. Sadourny, 1997: On the mechanisms in a tropical ocean-global atmosphere coupled general circulation model. Part I: mean state and seasonal cycle. Submitted to Climate Dynamics.

The NCAR Climate System Model

Peter R. Gent and Frank O. Bryan, Climate and Global Dynamics Division, NCAR, Boulder, USA. gent@ra.cgd.ucar.edu

The NCAR Climate System Model, version 1 (CSM1) is a step towards the development of a comprehensive model of the climate system, including chemical and biogeochemical processes. The modelling system is made freely available to the general scientific community through the World Wide Web. The initial version is really a physical climate model similar to other coupled climate models. It contains a global atmospheric model (CCM3, with resolution of about 2.9° and 18 vertical layers), a global ocean model (NCAR CSM Ocean Model, 2.4° longitude resolution, 1.2°–2.4° variable in latitude and 45 vertical layers), a land surface biophysics and basic soil hydrology model (LSM), and a sea-ice dynamics and thermodynamics model (NCAR CSM Ice Model). These models communicate using message passing with a driver program called the Flux Coupler which controls the time coordination of the integration. The component models are driven primarily by fluxes at the earth's surface. Those interfacial fluxes which directly depend on the state of more than one component model, *e.g.*, turbulent fluxes of latent and sensible heat, are computed within the Flux Coupler. The Flux Coupler is also responsible for interpolating and averaging between the different grids of the component models while conserving local and integral properties. The atmospheric fields are interpolated to the finer grid of the ocean model and the fluxes are calculated on the ocean model grid. The fluxes are then averaged back onto the coarser atmospheric model grid. This becomes more important if the ocean model has higher resolution.

Spin-up procedure

In order to perform relatively drift-free coupled simulations, a careful spin-up of the ocean and ice models is required. The flexible nature of the modelling system is exploited to easily carry out several integrations during the spin-up phase.

1. Equilibrium solutions are obtained for the atmosphere and ocean models separately by using observed forcing for the other: climatological SSTs for the atmosphere, National Centers for Environmental Prediction (NCEP) reanalyses for the ocean.
2. Daily CCM3 data from the climatological SST experiment are used to drive the ocean and ice models for 50 years using standard acceleration techniques for the ocean. The deep ocean tracer fields experience an effective spin-up time of 500 years. A 14 day running mean is applied to the fluxes into the ocean because of the acceleration.
3. During the first 25 years of the spin-up, the ice albedo feedback is turned off by specifying the absorbed solar radiation at the surface.
4. During the second 25 years of the spin-up, the ice albedo feedback is turned on by specifying the downward solar radiation at the surface and letting the ice distribution determine the surface albedo.
5. During years 50 to 60, the ocean acceleration is turned off and daily fluxes are given to the ocean for 10 years to allow the mass and momentum fields to readjust.

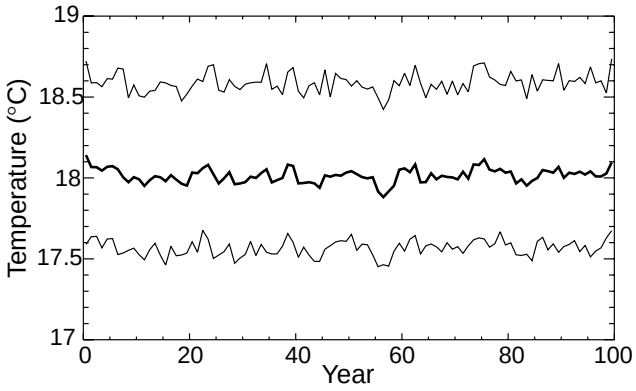

Figure 1. Time series of annual mean (thick line), and annual range (thin lines) of globally averaged ocean sea surface temperature in the CSM coupled integration.

The 60 year spin-up integration has no local flux corrections in momentum, heat or fresh water. However, one global correction is made to the fresh water budget because the CSM, at present, does not have a river run-off model. Thus, the precipitation over the active ocean and ice is multiplied by a constant factor so that it balances evaporation at every one day coupling interval. This ensures fresh water balance in the ocean and ice models, and will be removed when a river run-off model is incorporated. The fully coupled run is integrated in the same way with no local flux corrections, and only two code changes were made during the run. A minor bug in the ocean to ice fresh water exchange was corrected at year 10, and the coupling interval to the CCM3 was changed from 20 minutes to an hour at year 50. A 10 year duplicate run showed this second change did not affect the coupled run statistics.

Coupled simulation

The global mean ocean sea surface temperature from the first 100 years of the coupled run is shown in Fig. 1. There is some initial adjustment over the first five to ten years of the simulation, but it is remarkably stable afterwards. There is interannual variability on multi-year timescales but no discernible trend after year 10. There is a rapid adjustment of the ocean temperatures in the first few months of the simulation, which can be seen in the monthly average ocean and ice temperature. The initial month is about 0.2 K warmer than any subsequent month, but this is difficult to see in the 12 month running means.

The decadal average SST from years 91 to 100 from the coupled model (Fig. 2, page 21) is quite similar in distribution to the climatological SST. Over much of the globe, SST errors are less than 1 K. The marine stratus regions off the western coasts of North and South America and off Africa are too warm by 2 to 3 K, resulting from a bias in cloud simulation in CCM3. In higher northern latitudes, a shift in the Gulf Stream is apparent, with a warm bias off Labrador, while the SSTs are too cold near Norway and in the North Pacific. These biases are accompanied by shifts in the ice distribution. The high latitude Southern Ocean is slightly too warm, although the largest differences with climatology are associated with deviations of the Antarctic Circumpolar Current over large ridges in bottom topography.

The northward ocean heat transport (Fig. 3) from the uncoupled ocean model spun-up using NCEP atmospheric state variables is quite similar to the implied ocean heat transport from CCM3 driven by climatological SSTs. This is a major reason for the lack of drift of the coupled model following a relatively short spin-up experiment. The main difference in the ocean heat transports in the uncoupled models is in low latitudes of the Northern Hemisphere. The ocean and sea ice spin-up experiment driven by CCM3 fluxes gives an ocean heat transport which lies generally between the ocean heat transports in the uncoupled experiments and is almost identical to the ocean heat transport in the coupled simulation (Fig. 3). In the coupled model, the actual and implied ocean heat transports agree almost exactly. They do not agree exactly because CCM3 only conserves heat to within $0.4\,\mathrm{Wm}^{-2}$, so that the CSM is losing heat at this rate during the coupled integration. The top of the atmosphere heat balance in the coupled run is less than $0.1\,\mathrm{Wm}^{-2}$. This very small heat loss can be contrasted with flux corrected models where the flux correction is typically responsible for much of the ocean heat transport, so that the atmosphere and ocean heat transport mismatch is far greater than in the CSM.

Although the coupled integration is thermally stable, there are small, but persistent, trends in the ocean salinity field. The upper ocean is gradually getting fresher and the deep ocean saltier. There are no fast, local feedbacks on the atmosphere due to the ocean surface salinity, so that these trends can continue for several hundred years. However, the global ocean circulation will eventually change because

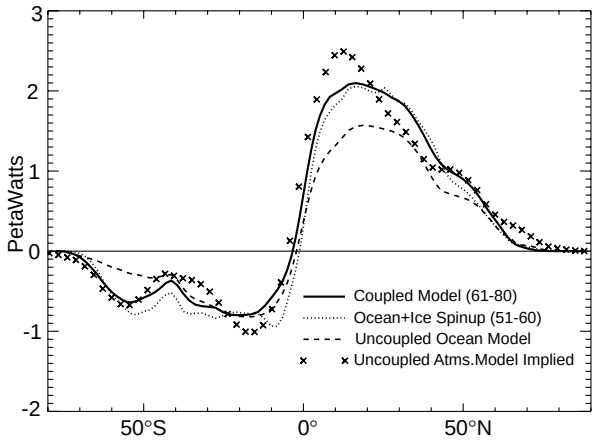

Figure 3. Annual mean northward ocean heat transport for years 61–80 of the coupled integration (solid line), years 51–60 of the ocean-ice model spin-up (dotted line), the equilibrium state of the uncoupled ocean model forced with observed atmospheric conditions (dashed line), and the implied transport from the uncoupled atmospheric model (CCM3) forced with observed SST (crosses).

a continual surface freshening will result in shutting off the conveyor belt circulation in the North Atlantic Ocean. It is not clear when this would happen in the present coupled run, but probably after a few hundred years. Thus, a small correction to the fresh water forcing of the ocean would be needed to make the equilibrium solution of the NCAR CSM version 1 like the present earth's climate.

As far as we are aware, this is the first global coupled simulation which includes sea-ice, is thermally stable over a century, and does not use any flux corrections. We believe there are two main reasons for this. The first is that the CSM component models are state of the art, high quality components whose heat transports are compatible with each other and representative of the earth's climate. The second is that the spin-up procedure produced an ocean and sea ice simulation that is compatible with the atmospheric simulation, which leads to a very small shock to the model simulation when it is started in fully coupled mode.

Dynamics of Interdecadal Variability in Coupled Ocean-Atmosphere Models

Mojib Latif, Max-Planck-Institut für Meteorologie, D-20146 Hamburg, Germany.
latif@dkrz.de

This a short version of the review article by Latif (1997) describing the interdecadal variability as simulated by coupled ocean-atmosphere models. The interdecadal variability simulated can be divided roughly into four classes: tropical interdecadal variability, interdecadal variability that involves both the tropics and the extra-tropics as active regions, mid-latitudinal interdecadal variability involving the wind-driven ocean gyres, and midlatitudinal interdecadal variability involving the thermohaline circulation. Several coupled models predict the existence of different interdecadal climate cycles, with periods ranging from approximately 10–50 years. This implies some inherent predictability at decadal time scales, provided that these interdecadal cycles exist in the real climate system.

The causes of interdecadal climate variability can be quite different, including external and internal forcing mechanisms. On the one hand, external forcing mechanisms have been discussed for a long time. Variations in the incoming solar radiation, for instance, were proposed as one of the major sources of interdecadal variability (*e.g.* Lean *et al.* (1995)). However, it is fairly controversial at present how strong the fluctuations in the solar insolation actually are. The forcing of interdecadal climate variability by volcanoes is well established and therefore less controversial, and major volcanic eruptions can be easily seen in regional and globally averaged temperature records (*e.g.* Robock and Mao (1995)).

On the other hand, interdecadal variability arises from interactions within and between the different climate sub-systems. The two most important climate sub-systems are the ocean and the atmosphere. Non-linear interactions between different space and time scales can produce interdecadal variability in both the ocean (*e.g.* Spall (1996)) and the atmosphere (*e.g.* James and James (1989)) as shown by many modelling studies. More important, however, seem to be the interactions between the two systems. The stochastic climate model scenario proposed by Hasselmann (1976) is a "one-way" interaction: the atmospheric "noise" (the high-frequency weather fluctuations) drives low-frequency changes in the ocean, leading to a red spectrum in the ocean's sea surface temperature (SST), for instance, in analogy to Brownian motion. It has been shown that the interannual variability in the midlatitudinal upper oceans is consistent with Hasselmann's stochastic climate model. This concept has been generalised recently by Frankignoul *et al.* (1996) who incorporated the wind-driven ocean gyres into the stochastic climate model concept, which extends the applicability of the stochastic climate model to interdecadal time scales. The atmospheric noise can excite also damped eigenmodes of the ocean circulation on interdecadal to centennial time scales, as shown, for instance, by the model study of Mikolajewicz and Maier Reimer (1990).

"Two-way" interactions between the ocean and the atmosphere in the form of unstable ocean-atmosphere interactions were also proposed to cause interdecadal climate variability (*e.g.* Latif and Barnett (1994)). Ocean and atmosphere reinforce each other, so that perturbations can grow to climatological importance. The memory of the coupled system (which resides generally in the ocean) provides delayed negative feedbacks which enable continuous, but probably damped, oscillations that are forced by the internal noise within the coupled ocean-atmosphere system.

This note does not attempt to provide a complete overview of all mechanisms that can lead to interdecadal variability. Emphasis is given to those modes which were either identified in coupled ocean-atmosphere models, or for which ocean-atmosphere interactions are crucial. Several "ocean-only" modes (*e.g.* Weaver and Sarachik (1991)), for instance, identified in uncoupled ocean model simulations are not described. Furthermore, this note does not aim to provide a complete overview of the observational work documenting interdecadal variability. A fairly comprehensive overview of the different aspects of interdecadal variability (including theoretical, modelling and observational studies) can be found in the recent book published by Anderson and Willebrand (1996).

The tropical Pacific Ocean has a prominent role in forcing global climate anomalies. This is due to the existence of the El Niño/Southern Oscillation (ENSO) phenomenon, the strongest interannual climate fluctuation (see, for instance, Philander (1990)). It is likely that interdecadal fluctuations in tropical Pacific SST will also have a significant impact on regional and global climate. The coupling between ocean and atmosphere is important in generating not only ENSO itself but also some part of the interdecadal variability in the tropical Pacific by amplifying the noise in the system (*e.g.* Eckert and Latif (1997)). This is consistent with the results obtained from the Lamont intermediate coupled model (Zebiak and Cane (1987)). The Lamont model simulates not only considerable interdecadal but also centennial variability. Since the atmospheric component of the Lamont model generates internal variability, it is likely that the occurrence of the low-frequency variability is also related, at least partly, to the stochastic forcing. Non-linear effects, however, might be also important (*e.g.* Münnich *et al.* (1991)).

Interdecadal variability in the tropical Atlantic evolves rather differently than that in the tropical Pacific, which is probably due to the different basin geometries. While the zonal wind stress/SST feedback is the dominant growth mechanism in the equatorial Pacific and the surface heat flux acts as a damping, the surface heat flux has a much more active role in the tropical Atlantic (see Chang *et al.* (1996) for a good summary and references therein). The existence of a decadal dipole mode with opposite SST anomalies north and south of the Intertropical Convergence Zone (ITCZ) has been postulated by several authors (*e.g.* Mehta and Delworth (1995), Chang *et al.* (1996)). The SST dipole influences the rainfall over parts of South America, as shown by Moura and Shukla (1981), and there is some evidence that Sahelian rainfall also is affected by the dipole (see, for instance, Lamb and Peppler (1991) for a good overview). However, it is controversial as to whether there exists a distinct time scale, and even the existence of the dipole structure itself is questioned in some studies (*e.g.* Houghton and Tourre (1992)).

Chang *et al.* (1996) derived a plausible theory which would explain physically the "dipole-oscillation" and its spatial structure by conducting a series of experiments with simplified coupled models. The mechanism for the oscillation can be summarized as follows. Suppose the system is in a state characterized by warm SST anomalies north and cold SST anomalies south of the ITCZ. The associated wind response will be such that the trade winds are weakened over the warm SST anomaly in the north and strengthened over the cold SST anomaly in the south. This will lead to surface heat flux anomalies that reinforce the initial SST anomalies in both poles of the dipole. Thus, the air-sea interactions over the tropical Atlantic are unstable. The horizontal advection of heat by the steady ocean currents will counteract the growth in SST by transporting anomalously cold (warm) water to the north (south). As pointed out by Chang *et al.* (1996), the system gives rise to self-sustained oscillations, when the positive and negative feedbacks balance properly. In this scenario, the Atlantic dipole is an inherently coupled air-sea mode which might be predictable several years ahead. Preliminary results from decadal forecast experiments with a simplified (hybrid) coupled ocean-atmosphere model support this picture (P. Chang, pers. comm., 1996).

A hypothesis for the generation of interdecadal variability based on tropics-midlatitudes interactions was proposed by Gu and Philander (1996). Their theory is based on the existence of a shallow meridional circulation which links the tropics to the extra-tropics. Certain pathways were identified in the ocean through which information can flow from the extra-tropics towards the tropics (*e.g.* Liu *et al.* (1994)). These pathways which are mainly located in the central and eastern Pacific are given by surfaces of constant densities (isopycnals). Temperature anomalies at the surface in the extra-tropics can affect the tropics by travelling along the isopycnals into the equatorial thermocline, where the anomalies are upwelled to the surface. Observational evidence for Gu and Philander's (1996) theory is provided by the work of Deser *et al.* (1996) who investigated the evolution of the subsurface temperatures in the Pacific for the period 1970–1991. Deser *et al.* (1996) show that a negative temperature anomaly propagated slowly equatorward along isopycnals during the period analyzed.

A mechanism for interdecadal climate variability that can lead to an interdecadal climate cycle in the North Pacific with a period of about 20 years was proposed by Latif and Barnett (1994) by analyzing the results of a multi-decadal integration with a coupled ocean-atmosphere general circulation model. This "gyre mode" is generated by large-scale ocean-atmosphere interactions in midlatitudes and must be regarded as an inherently coupled mode, as originally suggested by Bjerknes (1964). The memory of the coupled system resides in the ocean and is associated with slow changes in the subtropical ocean gyre. When, for instance, the subtropical ocean gyre is anomalously strong, more warm tropical waters are transported poleward by the Kuroshio and its extension, leading to a positive SST anomaly in the North Pacific. The atmospheric response to this SST anomaly is the PNA (Pacific North American) pattern which is associated with changes at the air-sea interface that reinforce the initial SST anomaly, so that ocean and atmosphere act as a positive feedback system. The atmospheric response, however, consists also of a wind stress curl anomaly which spins down the subtropical ocean gyre, thereby reducing the poleward heat transport and the initial SST anomaly. The ocean adjusts with some time lag to the change in the wind stress curl, and it is this transient ocean response that allows continuous oscillations and which can be exploited for the prediction of decadal changes in the North Pacific. In particular, the strong cooling in central North Pacific SST in the mid-seventies was highly predictable, as can be inferred from the lead-lag relationship between western North Pacific sea level and central North Pacific SST anomalies (Fig. 1).

A gyre mode may exist also in the North Atlantic. According to the theory of Latif and Barnett (1994), the

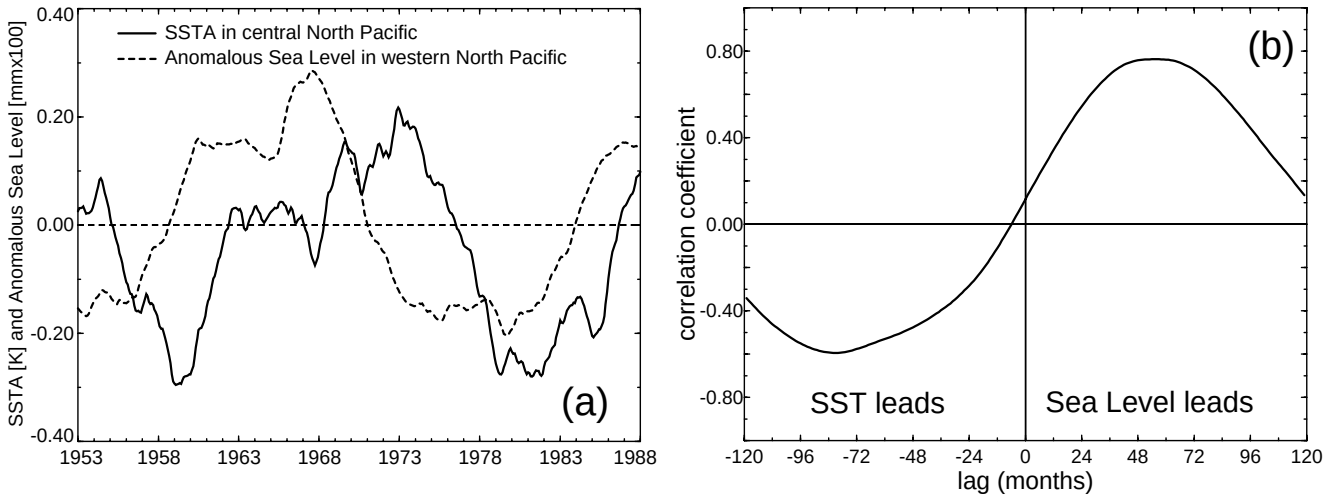

Figure 1. (a) Time series of anomalous sea level in the western North Pacific as simulated by an oceanic GCM and of observed anomalous SST in the central North Pacific. (b) Lagged cross correlations between the anomalous western Pacific sea level and the anomalous central Pacific SST. Both time series were smoothed by applying a five-year running mean filter. Figure kindly provided by S. Venzke.

period of the North Atlantic gyre mode should be shorter relative to that of the North Pacific gyre mode, and observations support this (*e.g.* Deser and Blackmon (1993)). The characteristic SST and sea level pressure (SLP) structures associated with the North Atlantic interdecadal mode as simulated by Groetzner *et al.* (1997) and as observed are shown in Fig. 2 (page 24). The main anomalies are a positive SST anomaly centred near 35°N and a negative SST anomaly to the northwest near 50°N. The atmospheric response pattern is reminiscent of the NAO (North Atlantic Oscillation), with centres of action near Iceland and the Azores. The evolution in the upper ocean heat content is very similar to that simulated in the North Pacific, with a clockwise rotation of the anomalies around the subtropical gyre.

One can separate conceptually the oceanic wind-driven from the oceanic thermohaline circulation. While the wind-driven circulation is forced by wind stress variations, the thermohaline circulation is forced by density anomalies. In reality, however, both circulations are coupled to each other, especially in the North Atlantic. Delworth *et al.* (1993) analyzed the multi-century integration with the GFDL coupled model and identified a mode with a period of approximately 50 years. The spatial SST structure of the Delworth *et al.* (1993) mode agrees favourably with observations described by Kushnir (1994). Delworth *et al.* (1993) describe their mode basically as an ocean-only mode which does not depend critically on the feedback by the atmosphere. The physics of the mode involve both the thermohaline and a horizontal (gyral) circulation. Salinity-related density anomalies in the sinking region (52°N–72°N) drive anomalies in the strength of the thermohaline circulation. The transport of the salinity anomalies into the sinking region is controlled by a horizontal (gyral) circulation which is mainly controlled by upper ocean temperature anomalies further to the south. The gyral circulation, however, is not in phase with the thermohaline circulation, and it is this phase difference between the two circulations that is important to the Delworth *et al.* (1993) oscillation. It should be noted that the Delworth *et al.* (1993) mode seems to be linked to pronounced oscillations in the Greenland Sea (Delworth *et al.* (1997)), and that these oscillations involve the atmosphere as an active component. Another interdecadal mode involving the thermohaline circulation was described by Timmermann *et al.* (1997) who analyzed a multi-century run with the ECHAM3/LSG CGCM integration. The level of the interdecadal variability simulated is similar to that in the GFDL CGCM. However, in contrast to the Delworth *et al.* (1993) mode described above, the Timmermann *et al.* (1997) mode appears to be an inherently coupled ocean-atmosphere mode.

In summary, coupled ocean-atmosphere models simulate a wide range of interdecadal variability, and many aspects of the simulations show an encouraging similarity with the interdecadal variability observed. Different competing hypotheses, however, were put forward to explain the interdecadal variability in the simulations. Some models, for instance, are largely consistent with Hasselmann's (1976) stochastic climate model scenario, exhibiting relatively featureless red spectra in some oceanographic key quantities. Other models simulate interdecadal oscillations, with statistically significant spectral peaks superimposed on the red background.

The role of large-scale air-sea interactions in causing interdecadal variability must be addressed in more detail. One key factor determining the nature of the simulated interdecadal variability appears to be the atmospheric response to midlatitudinal SST anomalies. Some atmosphere models seem to be relatively insensitive, while other atmosphere models exhibit a detectable response to extra-tropical SST anomalies. We are at a relatively early stage in the understanding of the dynamics of this atmospheric response, and further numerical experimentation with state-of-the-art AGCMs will help to advance our understanding.

Similarly, the oceanic adjustment to changes in the fluxes at the air-sea interface, especially the fresh water flux, is not well understood yet. In particular, it is not clear how well the coarse-resolution OGCMs (which are commonly used in coupled ocean-atmosphere models) simulate the "real" ocean.

There are, however, many other problems that need to be addressed in the modelling community, such as the role of flux corrections or the relative importance of salinity and temperature anomalies in the generation of interdecadal variability. Likewise, the relative roles of the tropics and the extratropics, of stochastic and deterministic processes need to be investigated in more detail. Furthermore, the dependence of the results on model parameterizations and parameters has not yet been adequately explored. The problem of decadal predictability has been addressed so far in very few studies only, and a co-ordinated international decadal prediction programme under the auspices of CLIVAR (Climate Variability and Predictability) would be desirable.

References

Anderson, D.L.T., and J. Willebrand, 1996: Decadal climate variability: Dynamics and Predictability. NATO ASI Series, Series I: Global Environmental Change, Vol. 44, Springer, 493 pp.

Bjerknes, J., 1964: Atlantic air-sea interaction. Adv. in Geophys., Academic Press, 10, pp 1–82.

Chang, P., L. Ji, and H. Li, 1996: A decadal climate variation in the tropical Atlantic Ocean from thermodynamic air-sea interactions. Nature, submitted.

Delworth, T., S. Manabe, and R.J. Stouffer, 1993: Interdecadal variations of the thermohaline circulation in a coupled ocean-atmosphere model. J. Climate, 6, 1993–2011.

Delworth, T.L., S. Manabe, and R.J. Stouffer, 1997: Multidecadal climate variability in the Greenland Sea and surrounding regions: a coupled model simulation. Geophys. Res. Letters, submitted.

Deser, C. and M.L. Blackmon, 1993: Surface climate variations over the North Atlantic ocean during winter: 1900–1989. J. Climate, 6, 1743–1753.

Deser, C., M.A. Alexander, and M.S. Timlin, 1996: Upper ocean thermal variations in the North Pacific during 1970–1991. J. Climate, in press.

Eckert, C., and M. Latif, 1997: Predictability of a stochastically forced hybrid coupled model of El Niño. J. Climate, accepted.

Frankignoul, C., P. Müller, and E. Zorita, 1996: A simple model of the decadal response of the ocean to stochastic wind forcing. J. Phys. Oceanogr., submitted.

Grotzner, A., M. Latif, and T.P. Barnett, 1997: A decadal climate cycle in the North Atlantic Ocean as simulated by the ECHO coupled GCM. J. Climate, submitted.

Gu, D., and S.G.H. Philander, 1996: A theory for decadal climate fluctuations. Nature, submitted.

Hasselmann, K., 1976: Stochastic climate models. Part I: Theory. Tellus, 28, 473–485.

Houghton, R.W. and Y.M. Tourre, 1992: Characteristics of low-frequency sea surface temperature fluctuations in the tropical Atlantic. J. Climate, 5, 765–771.

James, I.N. and P.M. James, 1989: Ultra-low-frequency variability in a simple atmospheric model. Nature, 342, 53–55.

Kushnir, Y., 1994: Interdecadal variations in the North Atlantic sea surface temperature and associates atmospheric conditions. J. Climate, 7, 141–157.

Lamb, P.J. and R.A. Peppler, 1991: Regional case studies of teleconnections: physical aspects. West Africa. In Teleconnections linking worldwide climate anomalies. Cambridge University Press, United Kingdom, pp 121–189.

Latif, M., 1997: Dynamics of interdecadal variability in coupled ocean-atmosphere models. J. Climate, submitted.

Latif, M. and T.P. Barnett, 1994: Causes of decadal climate variability over the North Pacific and North America. Science, 266, 634–637.

Lean, J., J. Beer, and R. Bradley, 1995: Reconstruction of solar irradiance since 1600: Implications for climate change. Geophys. Res. Lett., 22, 3195–3198.

Liu, Z., S.G.H. Philander, and R.C. Pacanowski, 1994: A GCM study of the tropical-subtropical upper-ocean water exchange. J. Phys. Oceanogr., 24, 2606–2623.

Mehta, V.M. and T. Delworth, 1995: Decadal variability of the tropical Atlantic ocean surface temperature in shipboard measurements and in a global ocean-atmosphere model. J. Climate, 8, 172–190.

Mikolajewicz, U. and E. Maier-Reimer, 1990: Internal secular variability in an ocean general circulation model. Climate Dynamics, 4, 145–156.

Moura, A.D. and J. Shukla, 1981: On the dynamics of drought in northeast Brazil: observations, theory, and numerical experiments with a general circulation model. J. Atmos. Sci., 38, 2653–2675.

Münnich, M., M.A. Cane, and S.E. Zebiak, 1991: A study of self-excited oscillations in a tropical ocean-atmosphere system. Part II: Nonlinear cases. J. Atmos. Sci., 48, 1238–1248.

Philander, S.G.H., 1990: El Niño, La Niña, and the Southern Oscillation. Academic Press, Inc., San Diego, 293 pp.

Robock, A.D. and J. Mao, 1995: The volcanic signal in surface temperature observations. J. Climate, 8, 1086–1103.

Spall, M.A., 1996: Dynamics of the Gulf Stream/ Deep western boundary current crossover. Part II: Low-frequency internal oscillations. J. Phys. Oceanogr., 26, 2169–2182.

Timmermann, A., M. Latif, R. Voss, and A. Grotzner, 1997: North Atlantic interdecadal variability: A coupled air-sea mode. J. Climate, submitted.

Weaver, A.J. and E.S. Sarachik, 1991: Evidence for decadal variability in an ocean general circulation model: An advective mechanism. Atmos.-Ocean, 29, 197–231.

Zebiak, S.E. and M.A. Cane, 1987: A model El Niño/Southern Oscillation. Mon. Wea. Rev., 115, 2262–2278.

MEETING TIMETABLE 1997/1998

June 16–20 1997	WOCE South Atlantic Workshop	Brest
July 1–9 1997	IAMAS/IAPSO XXII General Assembly	Melbourne
July 8–12 1997	WOCE Southern Ocean Workshop	Hobart
August 25–28 1997	WCRP Conference	Geneva
September 23–26 1997	WOCE-24	Boulder, CO
February 9–13 1998	Ocean Sciences Meeting	San Diego, CA
April 20–24 1998	XXII EGS General Assembly	Nice
May 24–29 1998	WOCE Conference	Halifax, NS

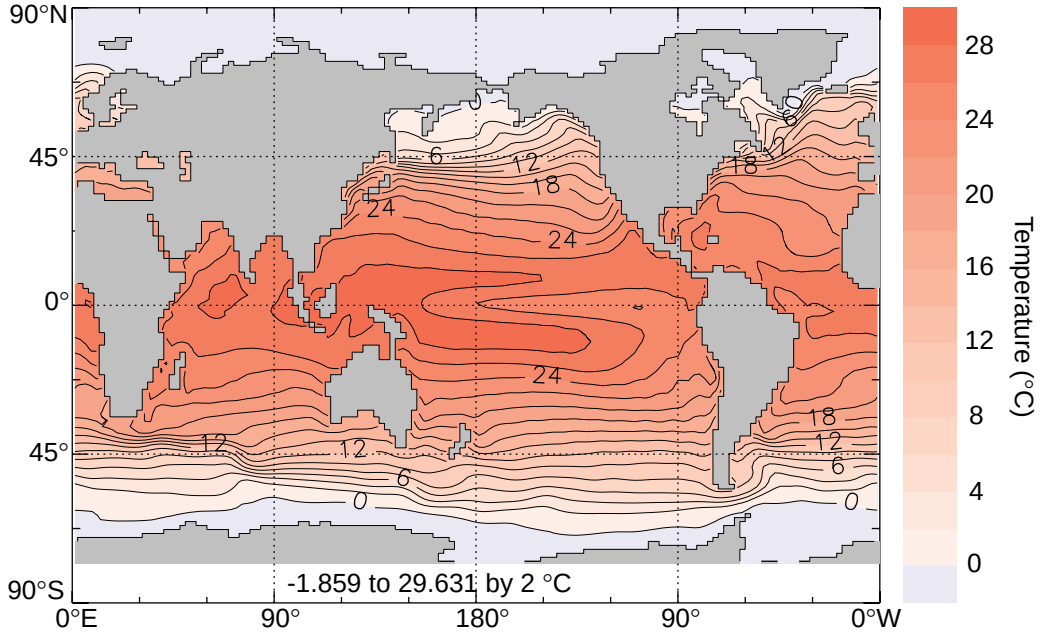

Gent and Bryan, page 16, *Figure 2. Climatological mean SST for years 91–100 of the coupled integration.*

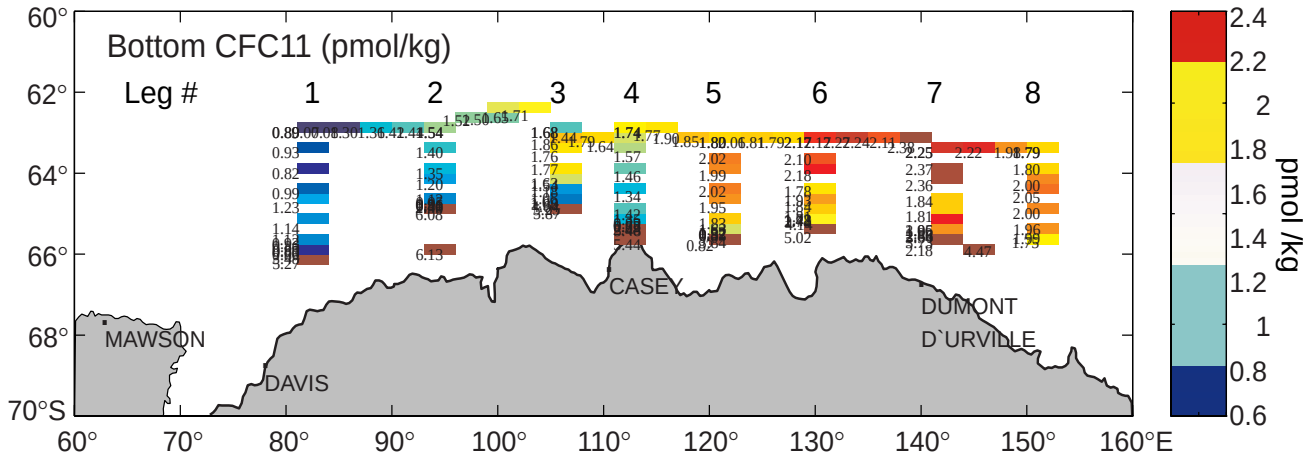

Bindoff, page 36, *Figure 1. The CFC-11 taken from the deepest Niskin Bottle for all CTD stations. The numbers are the CFC-11 values for each station and mark the location of each CTD. The colour gives the amplitude of the CFC-11 concentration.*

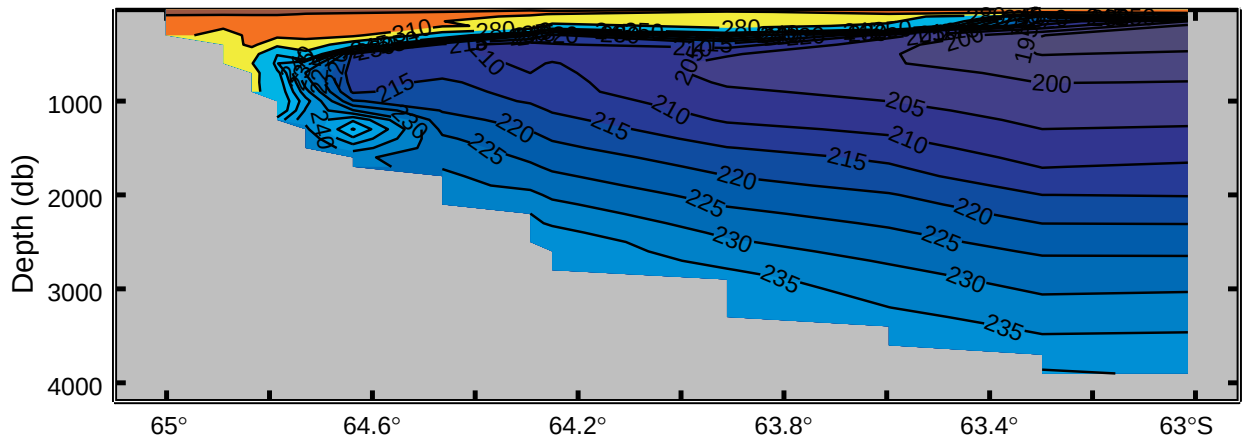

Bindoff, page 37, *Figure 2. The oxygen (μ mol kg^{-1}) section from the north-south hydrographic section along leg 3 at 104°E.*

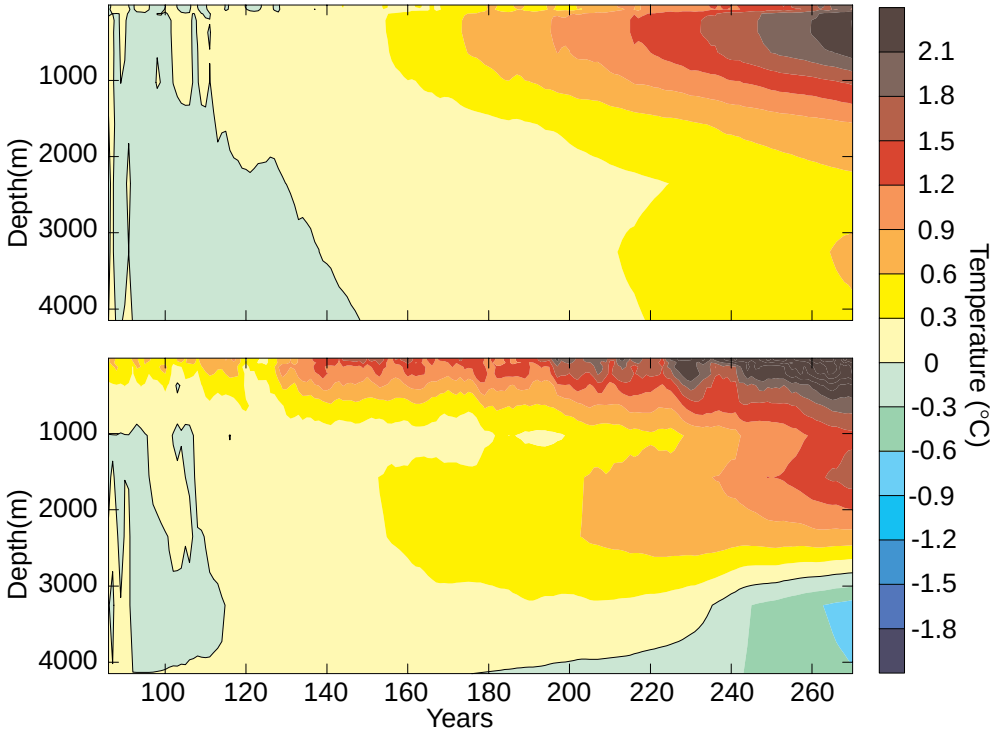

Baines, page 4, *Figure 1. Temporal response for the greenhouse gas increase scenario at each model level. In this scenario the (equivalent) atmospheric CO_2 starts to increase at year 86, and at such a rate that it reaches doubling and tripling after 128 and 180 years respectively. The response is calculated as the difference between the scenario and a control run in which CO_2 is fixed at the present level (upper panel), averaged over the ocean poleward of 45°S (lower panel). North Atlantic Ocean averaged over the region from 45°N to 65°N.*

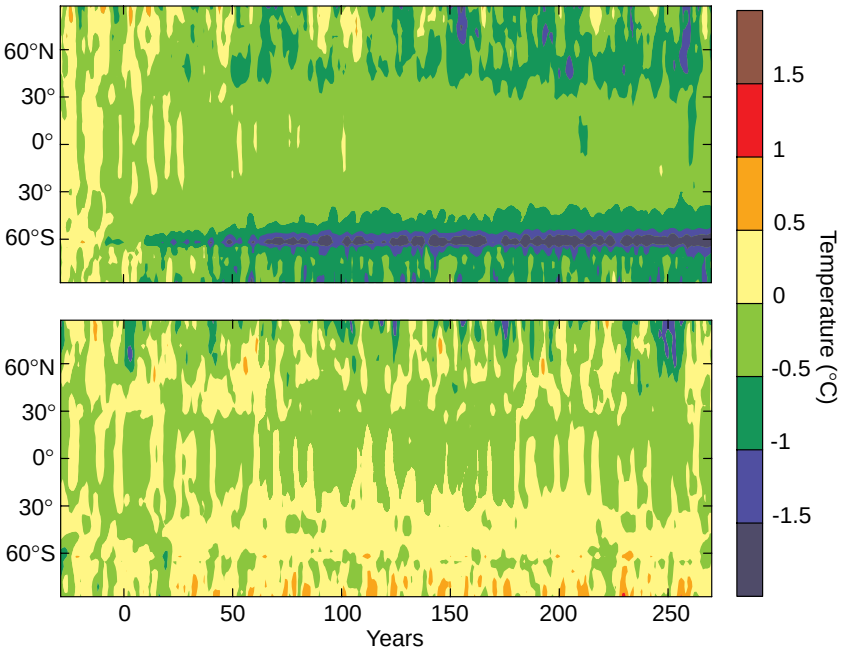

Baines, page 4, *Figure 2. The change in the zonal mean surface air temperature during the course of control (i.e. constant CO_2) integrations performed for two versions of the coupled model. (upper panel) Standard horizontal diffusion (HD) version (no eddy-induced advection included). (lower panel) GM scheme included. The integrations are plotted for 300 years, over nominal years "-30" to "270". The plots show the differences between the annual mean temperatures for each model year, and the mean temperature for the first 30 years of the coupled run. The pronounced drift in the HD control run is clearly evident, especially near the Southern Ocean sea-ice margin. The corresponding GM run contains no such drift.*

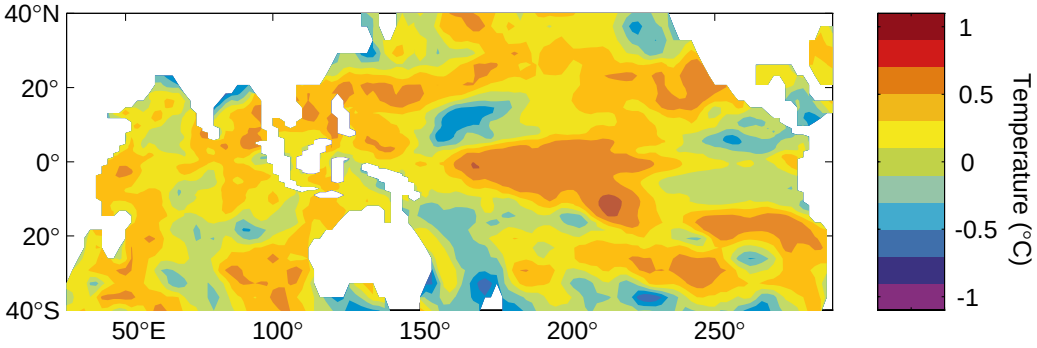

Godfrey and Schiller, page 26, *Figure 2. Correlation coefficient of anomalies of model SST from the seasonal average over 1985–1990, with the same quantity calculated from Reynolds and Smith (1994) SSTs.*

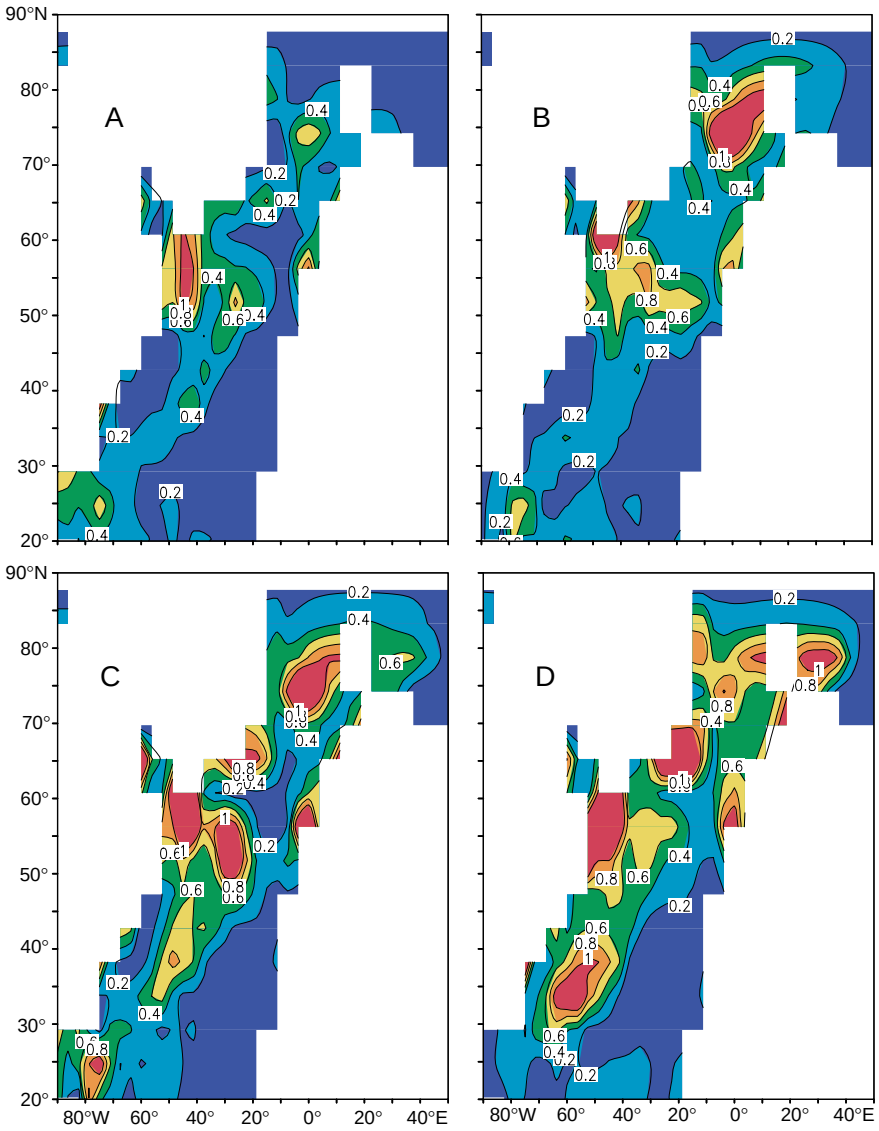

Bryan and Griffies, page 8, *Figure 4. Maps of the normalized ensemble variance for Ensemble I's North Atlantic dynamic topography shown for years 3(A), 5(B), 7(C), and 9(D). White regions represent land. Red regions indicate regions of saturated ensemble variance, and hence rapid loss of predictability. The regions of large variance in years 3 and 5 are associated with areas of strong ocean convection. The subsequent maps indicate the transfer of this variance southward along the western boundary as well as eastward across the North Atlantic drift. Once convection initiates the strong growth in ensemble variance, oceanic dynamics acts to propagate these errors southward, through the East Greenland Current and into the midlatitudes with a tendency to trap the errors along the western boundary due to the latitudinal variation of the Coriolis force (beta-effect), except in regions of strong eastward flow such as the northeastward extent of the North Atlantic Current.*

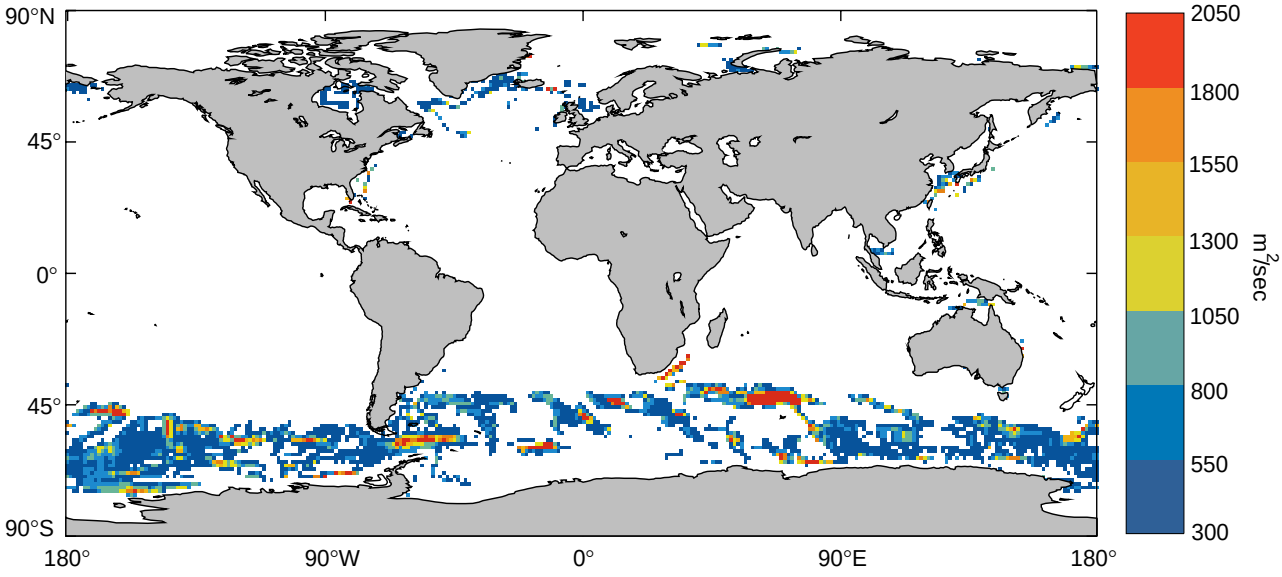

Wright, page 28, *Figure 3. Thickness diffusion coefficient, distribution after 10 years. Coloured values are over* $300\,m^2\,s^{-1}$.

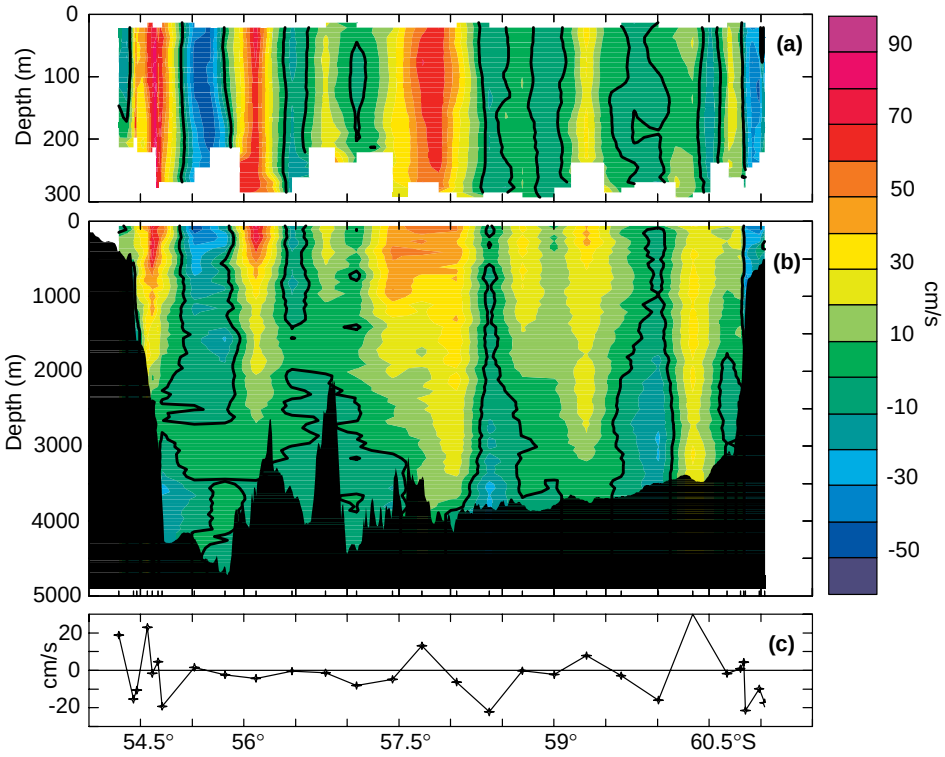

Cunningham et al., page 39, *Figure 1. Across-track velocities (cm/s, positive eastwards) on WOCE section SR1 in Drake Passage in November 1996: (a) Vessel Mounted Acoustic Doppler Current Profiler (VMADCP) velocities from 0 to 300 m; (b) full depth Lowered Acoustic Doppler Current Profiler (LADCP) velocities. Each LADCP profile has been matched to bottom-track (BT) LADCP velocites near seabed; (c) bottom velocities from BTLADCP.*

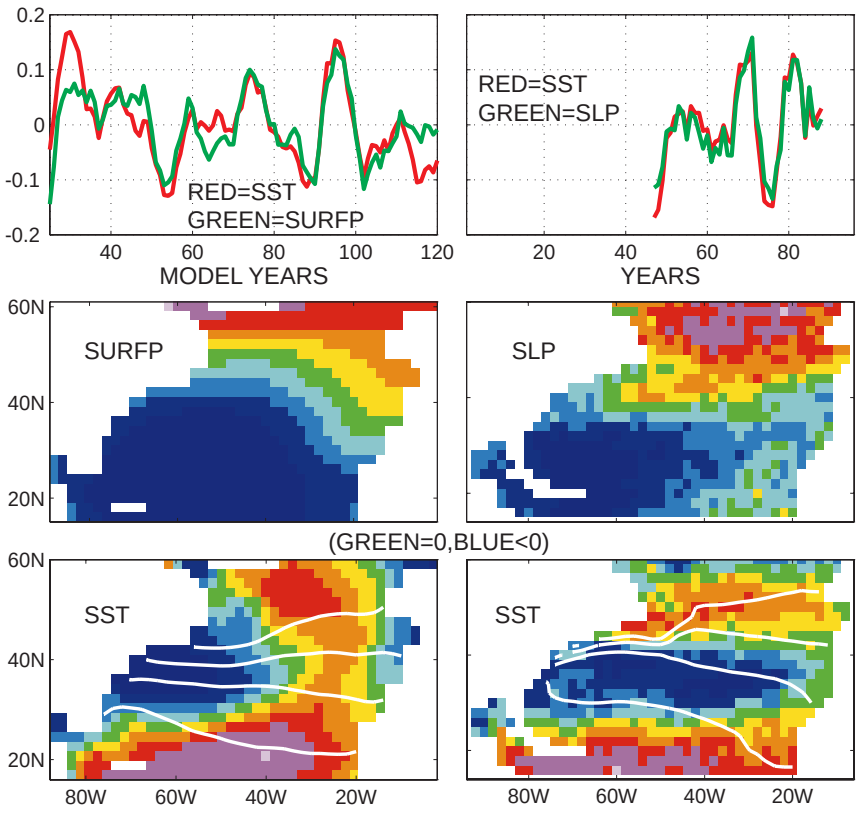

Latif, page 19, *Figure 2. Canonical Correlation Analyses (CCAs) of SST and SLP anomalies. Left: as derived from the Latif and Barnett (1994) model; right: as derived from observations. Figure kindly provided by H. Bezdek.*

Ocean Models for Climate Forecasting

Stuart Godfrey and Andreas Schiller, CSIRO Division of Marine Research, Hobart, Australia. stuart.godfrey@marine.csiro.au

Ocean models are being built at various locations around the world, which are intended to be coupled to global atmospheric models for purposes of predicting climate variations one or more seasons ahead. This type of modelling is particularly relevant for Australia, which has major year-to-year variations in climate. While these variations correlate significantly with the El Niño-Southern Oscillation (ENSO) phenomenon in much of the country, in other regions there is a stronger correlation with sea surface temperatures (SSTs) in the Indian Ocean, especially the Indonesian region. At CSIRO Division of Marine Research, we are building an ocean model designed for Australian climate forecasting. It will be tested in coupled mode at CSIRO Division of Atmospheric Research, with the aim of its eventual use by the Bureau of Meteorology to update their present climate forecasting model (Power *et al*., 1996). This project is sponsored in part by the Land and Water Resources Research and Development Corporation (LWRRDC).

Our aim is to build an ocean model which – when driven with accurate, interannually-varying fluxes of heat, momentum and fresh water – reproduces the observed interannual variations of SST accurately, especially in the tropical Pacific and Indian Ocean. The model performance in generating SSTs should be verified against observations.

Unfortunately a difficulty is encountered immediately, which is believed to be at least as serious for purposes of predicting SSTs than errors in ocean physics; so we discuss this problem first. Presently-available heat fluxes contain errors of several tens of W/m^2, even on climatological average. Furthermore, the Marine Atmospheric Boundary Layer (MABL) typically responds to a broad-scale change in SST by a similar increase in air temperature, with the same relative humidity; and this behaviour implies a rather weak negative feedback of SST on net heat flux into the water, in the range $10 - 20\,W/m^2°C$ (*e.g.* Seager *et al.* 1988). Thus an error of (say) $50\,W/m^2$ in surface heat flux will generate an unacceptable SST error of 2.5°–5°C. To usefully mimic the conditions the ocean model will experience in coupled mode, a surface heat flux boundary condition must be devised which incorporates this MABL behaviour. Luckily, experience suggests that anomalies in net heat fluxes are often of useful quality even when their long-term mean has a major error, (*e.g*. Meyers *et al*., 1986, Godfrey *et al*, 1991); so a "flux correction" approach is useful.

Having developed a model and tested its skill at generating observed SSTAs with these surface flux conditions, "real-time" subsurface ocean data from XBTs, altimeters and TAO moorings should be assimilated into it. Its SST should also be set to observed "real-time" values, so that the coupled model can benefit as much as possible from persistence of SST's when it goes into forecast mode. Work is in progress to achieve this assimilation, based on Smith's (1995) Ocean Thermal Analysis System; but we will not discuss this further here.

Surface fluxes

In the tropical region of interest, we drive our global model with Florida State University (FSU) wind pseudostresses over the period 1985-1990, with a bulk transfer coefficient of 0.0015. This period was chosen because an ISCCP satellite-based estimate of short wave radiation is available for this period (Li, 1995). Latent heat is estimated using FSU wind speeds, and an assumption that the air humidity is a variable fraction of the saturated humidity at the model SST, the fraction being determined from the observed mean seasonal cycle. The sensible heat exchange and longwave radiation were given a small temperature dependence. These heat flux parameterisations are minor modifications of those of Seager *et al*. (1988); we have not attempted to account for the scale-dependent effects found by Kleeman and Power (1995) or Murtugudde *et al*. (1996). Winds stresses are blended into the Hellerman and Rosenstein (1983) seasonal means poleward of 30° Surface salinity is relaxed to observed mean seasonal salinity, in the top (15 m) box of the model. In a typical initial run of 20 years, the seasonal mean of this surface heat flux was augmented by a strong relaxation to observed mean seasonal SST; the seasonal values of this term over the last year were retained and used as a flux correction for subsequent runs. The magnitude of this flux correction was typically of one sign and large, mainly because the shortwave radiation product was unrealistically large. The latent heat flux also contained significant errors.

Model development

The model uses the MOM-2 code (Pacanowski (1995)), with no-slip boundary conditions. Laplacian (-2) lateral friction was used, and vertical eddy diffusivity and viscosity were obtained from the Chen *et al*. (1994) mixing scheme, as modified for the MOM Code by Power *et al*. (1996) and Godfrey and Schiller (1997). The model has a zonal grid spacing of 2°, and a meridional spacing of 0.5° near the equator, expanding rapidly to higher values elsewhere. With such grid resolutions, if a gap is introduced at Lombok Strait the Indonesian Throughflow will generally all pass through this gap, with very little passing through Timor Passage. To avoid this problem we have artificially increased the horizontal eddy diffusivity in the model's Lombok Strait, near 8°S, 115°E (Fig. 1). This may be qualitatively reasonable, as a proxy for the strong tide-induced viscosity

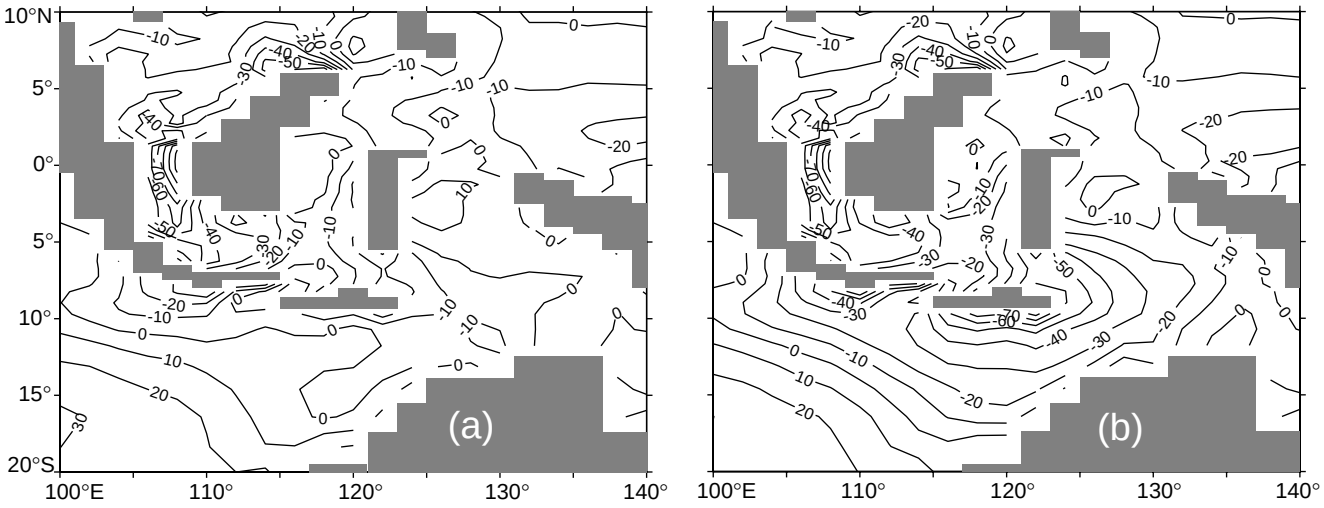

Figure 1. Annual mean net surface heat flux out of the ocean. (a) without, and (b) with enhanced "tidal mixing" in Indonesian seas.

that is likely to occur in this region. We also raise the background vertical eddy viscosity and diffusivity to $2\times10^{-4}\,\mathrm{m^2 s^{-1}}$ in a part of the Indonesian seas, to allow for the tidal mixing that is needed to account for the observed change of water mass structure in the Indonesian Throughflow as it passes from the Pacific to the Indian Ocean (Gordon 1986, Ffield and Gordon 1996). The result is to increase the heat flux into the water by up to $60\,\mathrm{W/m^2}$ (compare heat fluxes near the south side of the Indonesian "island" at 10°S, Figs. 1a, b). This improves agreement with climatologies (*e.g.* Oberhuber, 1988).

Results

We have calculated the model's seasonal mean SST for 1985-1990, and obtained SST anomalies (SSTAs) for this period in the Pacific and Indian Oceans. Fig. 2 (page 22) shows the correlation of these model SSTAs with observed SSTAs, calculated in the same way from Reynolds and Smith (1994) observed monthly mean SST field. Good correlation is found in the central Pacific, though the poorer correlation in the east Pacific is under exploration. Regions with correlation coefficients above 0.4 are fairly common in the tropical Indian Ocean. These results are far from final; they are presented simply to illustrate the style of approach to the problem that we are using. Fig. 3 shows an example of the observed and modelled SSTAs, from the central equatorial Indian Ocean. In this randomly-chosen example, we at present have no idea why the model SSTA diverged so drastically from observations in 1987. Our aim is to explore such model results, with a view to finding out the physics governing formation of SSTAs in various regions of the model – especially those regions where those SSTAs are known to correlate with Australian climatic anomalies, and where the model is reproducing the observed SSTAs reasonably well. We are also performing a run in which the interannually-varying shortwave radiation estimate is replaced with a seasonal mean; if there are large regions where SSTAs appear to be unaffected of this change, we will make longer runs, using the much longer time series of FSU winds that is available.

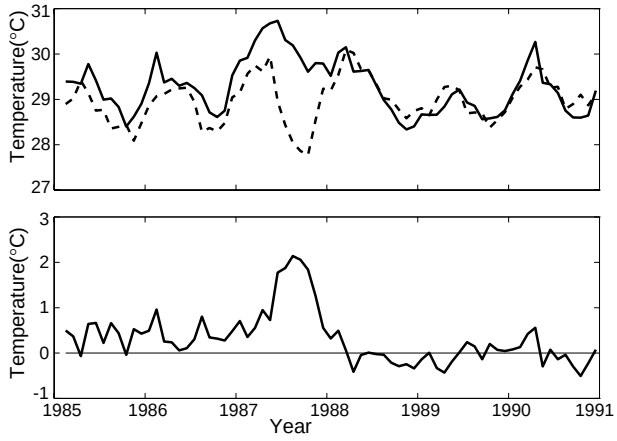

Figure 3. Top: Example of time series of SST from the model (solid) and from Reynolds and Smith (1994) observation (dashed) near the equator in the mid-Indian Ocean (90°E, 0.25°N). Bottom: Difference between the two data sets of the top figure.

References

Chen, D., L.M. Rothstein, and A.J. Busalacchi, 1994: A hybrid vertical mixing scheme and its application to tropical ocean models. J. Phys. Oceanogr., 24, 2156–2179.

Ffield, A., and A.L. Gordon, 1996: Tidal signatures in the Indonesian Seas, J. Phys. Oceanogr., 26, 1924–1937.

Godfrey, J.S., M. Nunez, E.F. Bradley, P.A. Coppin, and E.J. Lindstrom, 1991: On the net heat flux into the western equatorial Pacific. J. Geophys. Res., 96 (Suppl.), 3391–3400.

Godfrey, J.S. and A. Schiller, 1997: Tests of mixed layer schemes and surface boundary conditions in an ocean general circulation model, using an equatorial data set. CSIRO Report, in press.

Gordon, A.L., 1986: Interocean exchange of thermocline water. J. Geophys. Res., 91, 5037–5046.

Hellerman, S., and M. Rosenstein, 1983: Normal monthly wind stress over the World Ocean with error estimates. J. Phys. Oceanogr., 13, 1093–1104.
Kleeman, R., and S. Power, 1995: A simple atmospheric model of sea surface heat flux for use in ocean modeling studies. J. Phys. Oceanogr., 25, 92–105.
Li, Z., 1995: Intercomparison between two satellite-based products of net surface radiation. J. Geophys. Res., 100, 3221–3232.
Meyers, G., J.R. Donguy, and R.K. Reed, 1986: Evaporative cooling of the western equatorial Pacific Ocean by anomalous winds, Nature, 323, 523–526.
Murtugudde, R., R. Seager and A. Busalacchi, 1996: Simulation of the tropical oceans with an ocean GCM coupled to an atmospheric mixed-layer model. J. Climate, 9, 1795–1815.
Oberhuber, J.M., 1988. An atlas based on the COADS data set: The budgets of heat, buoyancy and turbulent kinetic energy at the surface of the global ocean. Max-Planck Institut für Meteorologie Report No. 15.
Pacanowski, R.C., 1995: MOM2 Documentation User's Guide and Reference Manual, Version 1.0, GFDL Technical Report No. 3.
Power, S., F. Tseitkin, R. Colman, B. McAveney, J. Fraser, R. Kleeman, and A. Sulaiman, 1996. A coupled general circulation model for seasonal prediction and climate change research. In: Proc. Symposium on Climate Prediction and Predictability, Melbourne, 12–14 November 1996.
Reynolds, R.W. and T. M. Smith, 1994. Improved global sea surface temperature analyses using optimum interpolation. J. Climate, 7, 929-948.
Seager, R., S.E. Zebiak and M.E. Cane, 1988. A model of the tropical Pacific sea surface temperature climatology. J. Climate, 7, 1943–1957.
Smith, N.R., 1995: The BMRC ocean thermal analysis system. Austr. Met. Mag., 44, 93–110.

A New Eddy Mixing Parametrization and Ocean General Circulation Model

David K. Wright, Hadley Centre for Climate Prediction and Research, Meteorological Office, UK. dkwright@meto.gov.uk

For mesoscale eddies to be resolved explicitly in an ocean general circulation experiment would require a resolution of a few tens of kilometres. As the deep ocean takes several centuries to come into equilibrium this is currently not possible in general circulation models used for climate change prediction. Thus, there is a need to parametrize eddy processes.

The Gent and McWilliams (GM) scheme attempts to parametrize sub-gridscale eddy activity by removing potential energy in an adiabatic manner. See Gent and McWilliams (1990) and Gent *et al.* (1995) for a further explanation of this scheme. The use of this scheme, however, requires an eddy transfer coefficient, κ. It is not clear what value this should take or indeed if a constant value of this coefficient is physically realistic.

In order to assess the impact of varying κ in the GCM model simulation, four experiments using the Hadley Centre Ocean Model were performed. The model is essentially the ocean component of the Hadley Centre coupled model described by Gordon *et al.* (this issue). In the present experiments the model domain is truncated at 74°N and forced by climatological surface fluxes together with a surface relaxation for temperature and salinity. Three experiments were performed which included the GM parametrization with different values of κ of 1000, 500 and $100\,\mathrm{m^2\,s^{-1}}$ against a control integration using the Redi (1982) isopycnal diffusion scheme. The results shown below are from preliminary 10-year simulations of the model. The century timescale response of the model has yet to be assessed.

Fig. 1 shows the meridional overturning stream-function from the two extreme cases, the control and $\kappa = 1000\,\mathrm{m^2\,s^{-1}}$, after 10 years of integration. Compared to the control, use of the GM scheme with this high value of κ gave a large reduction in the Deacon Cell and an improvement to the ACC frontal position but at the expense of a marked reduction in the North Atlantic gyre circulation. This is illustrated in Fig. 2, which shows the North Atlantic potential temperature at 50 m in the two runs. Whilst the control integration maintains the tight temperature gradient associated with the North Atlantic Current, the $\kappa = 1000\,\mathrm{m^2\,s^{-1}}$ run shows the horizontal temperature

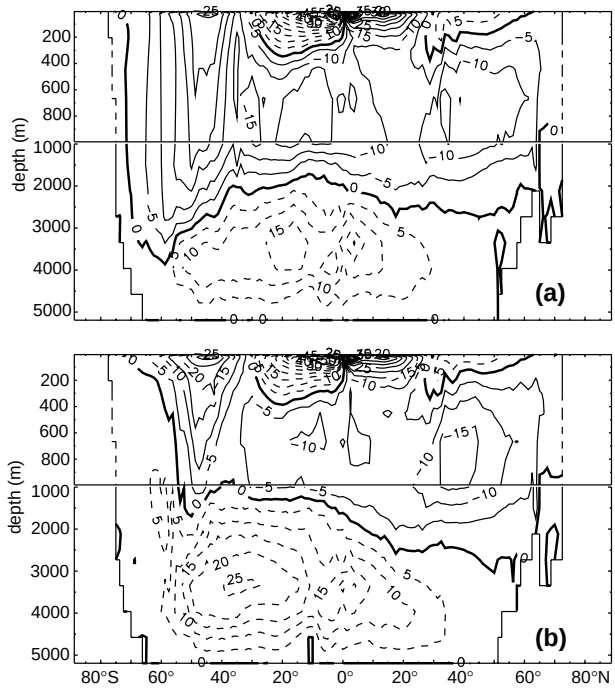

Figure 1. Global zonally integrated meridional streamfunction (Sv) for (a) the control integration. (b) the $\kappa = 1000\,m^2\,s^{-1}$ integration. The plot includes the eddy induced velocities derived from the GM scheme.

gradients have become diffuse, similar to the pattern seen in coarser resolution models. Associated with this there is a corresponding reduction in the North Atlantic Current speed. This is due to the GM scheme excessively slumping the density front associated with the North Atlantic Current. The experiments with the lower values of κ showed that the model was able to maintain the sharp fronts associated with the western boundary currents but now the improvements in the Southern Ocean were reduced.

Visbeck *et al.* (1997) highlight three cases where different values of κ might be more physically realistic. They suggest values of $2000\,\mathrm{m^2\,s^{-1}}$ in a wind driven channel (which they suggest could be thought of as the ACC), $500\,\mathrm{m^2\,s^{-1}}$ in a frontal zone (which may be indicative of that required in a western boundary current) and $300\,\mathrm{m^2\,s^{-1}}$ in a convective chimney. These values are in broad agreement with the values required by the ocean GCM experiments to maintain the climatological structure.

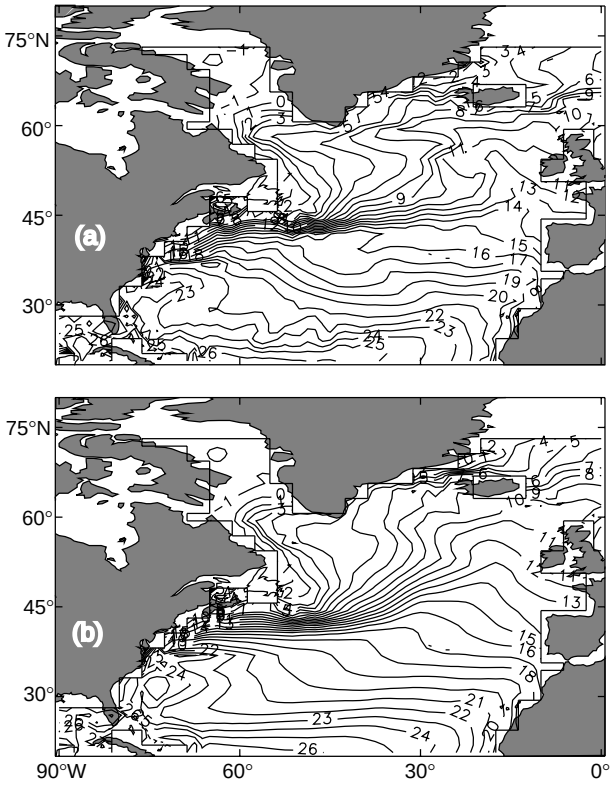

Figure 2. Potential temperature (°C) at 50 m for a) the control integration. (b) the $\kappa = 1000\,m^2\,s^{-1}$ integration.

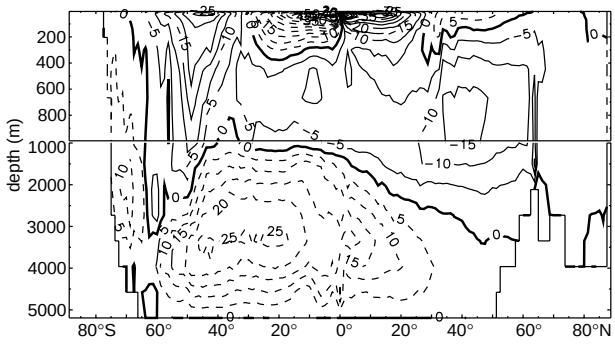

Figure 4. Global zonally integrated meridional stream-function (Sv) for the k-parametrization scheme, including the eddy induced velocities.

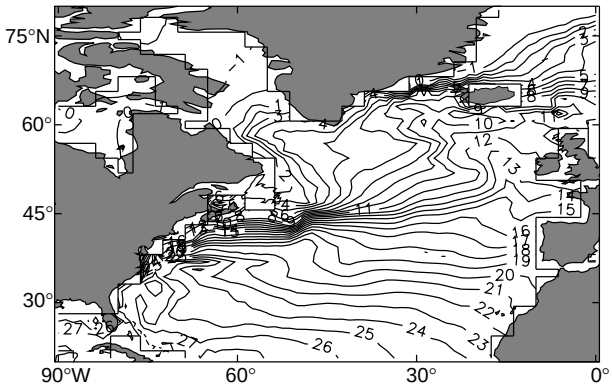

Figure 5. Potential temperature (°C) at 50 m for the k-parametrization scheme.

Visbeck *et al*. (1997) suggest a timescale for the growth of baroclinic instability of

$$T^{-2} = f\overline{Ri^{-1}}^{\upsilon}$$

where T is the timescale for the growth of eddies, *f* is the Coriolis parameter and Ri is the Richardson number. Following Treguier *et al*. (1996), a vertical average $\overline{()}^{\upsilon}$ of Ri is taken over the upper 2000 m.

Following the suggestion of Visbeck *et al.*, the eddy transfer coefficent was then defined as

$$\kappa = \alpha T^{-1} l^2$$

where α is a constant equal to 0.015 and l is a lengthscale chosen by using the width of the baroclinic zones defined by the timescale. A baroclinic zone was defined as the region where the inverse timescale is greater than $1.4\times10^{-6}\,\mathrm{s^{-1}}$, this number being determined by experiment.

This parametrization of κ was implemented in a fully global version of the model already described. A minimum of $300\,\mathrm{m^2\,s^{-1}}$ was imposed to supress noise and an upper limit of $2000\,\mathrm{m^2\,s^{-1}}$ was also set. Values of κ were calculated daily over the whole model domain as the integration progressed. The annual mean for the tenth year of integration is shown in Fig. 3 (page 28)(coloured values are greater than the minimum of $300\,\mathrm{m^2\,s^{-1}}$). This shows that over most of the ocean model the values are generally the minimum of $300\,\mathrm{m^2\,s^{-1}}$ with increased values of κ in the ACC and some increased values in the North Atlantic. The meridional streamfunction for this run (Fig. 4) shows the Deacon Cell to have been reduced to a value between the control and the $\kappa = 1000\,\mathrm{m^2\,s^{-1}}$ integrations. Also, Fig. 5 shows the temperature simulation of the North Atlantic Current now maintains a tighter density gradient than the $\kappa = 1000\,\mathrm{m^2\,s^{-1}}$ case.

The values predicted by the model are in general

agreement, both in size and position, with those suggested by both Visbeck *et al.* (1997) and Treguier *et al.* (1996) (who use TOPEX data to show the spacial inhomogeneity of oceanic eddy activity). With the spatially and time varying thickness diffusion coefficient, the GM scheme enhances mixing in regions of baroclinic instability. This also now allows the model to maintain the tight density gradients in the gyres, whilst still improving the ACC simulation. Some further work in the scheme is still required, in particular the choice of length scale may need further refining and no effort has been made to alter the vertical structure of κ, which was independent of depth in these simulations.

References

Gent, P.R., and J.C. McWilliams, 1990: Isopycnal mixing in ocean circulation models. J. Phys. Oceanogr., 20, 150–155.

Gent, P.R., J. Willebrand, T.J. McDougall, and J.C. McWilliams, 1995: Parameterizing eddy-induced tracer transports in ocean circulation models. J. Phys. Oceanogr., 25, 463–474.

Redi, M.H., 1982: Oceanic isopycnal mixing by coordinate rotation. J. Phys. Oceanogr., 12, 1154–1158.

Treguier, A.M., I.M. Held, and V.D. Larichev, 1996: On the parametrization of quasi-geostrophic eddies in primitive equation ocean models. J. Phys. Oceanogr. submitted.

Visbeck, M., J. Marshall, T. Haine, and M. Spall, 1997: On the specification of eddy transfer coefficients in coarse resolution ocean circulation models. J. Phys. Oceanogr. In press.

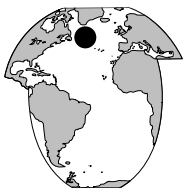

Decadal Variability of the North Atlantic Overflows

Sheldon Bacon, Southampton Oceanography Centre, Empress Dock, Southampton SO14 3ZH, UK. S.Bacon@soc.soton.ac.uk

For quite some time now, it has been the accepted wisdom that output from the Arctic to the Atlantic, in the form of the deep overflows across the ridge between Greenland, Iceland and Scotland, is invariant. The Arctic has been seen as a black box or reservoir whose relationship with the rest of the world ocean is governed solely by hydraulics. The Arctic may react to climatic changes on a longer timescale than the rest of the ocean, but it is beginning to be recognised that it is not invariant (*e.g.* MacDonald, 1996). In this note, we present further evidence for decadal variability in the Arctic in the form of rather drastic changes to the northern Atlantic overflows – it would appear that they have roughly halved in strength (volume) in the 1990s.

From measurements made during the UK WOCE CONVEX cruise in 1991 (Bacon, 1994, 1997), it was realised that the deep western boundary current (DWBC) by Cape Farewell, Greenland was unusually weak: about 6 Sv compared with the previously accepted values of about 13 Sv (Clarke, 1984; Dickson and Brown, 1994). The DWBC at Cape Farewell is a conflation of the Denmark Strait and Iceland-Scotland Overflows; the high value was calculated from hydrographic section data, merged with current meter data for the geostrophic reference level current; the recent low value was calculated by an inverse method, assisted by shipboard acoustic Doppler current profiler data. Inspection showed that the DWBC transport in both cases was approximately equally partitioned between flux due to the actual current at the ('sensible') reference level, and flux due to the intense, highly sheared deep flows (to about 500 m above the bottom). That the weak value is weak is as much due to relatively low shear as to low reference level current. Therefore it is possible to create a forty-year partial history of the strength of the DWBC by using the transport referenced to a constant zero velocity surface as an index of the strength of the DWBC, and by inspecting the archives for suitable sections to use.

Twelve such sections came to light, or were available to the present author: 1958 (IGY - Anton Dohrn), 1962 (Erika Dan), 1966 and 1978 (Hudson), 1981 (TTO - Knorr), 1983 (Atlantis), 1991 (Hudson, Tyro, Charles Darwin - CONVEX and Meteor), 1992 (Valdivia) and 1996

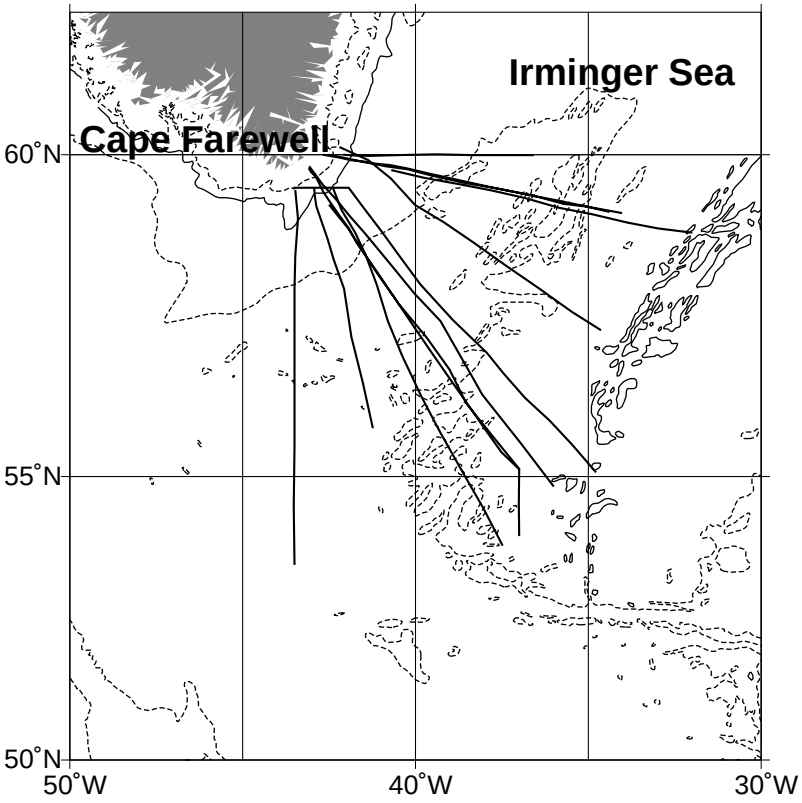

Figure 1. The twelve sections used in the analysis. Bathymetry is illustrated with the 200 m, 1000 m (solid) and 3000 m contours.

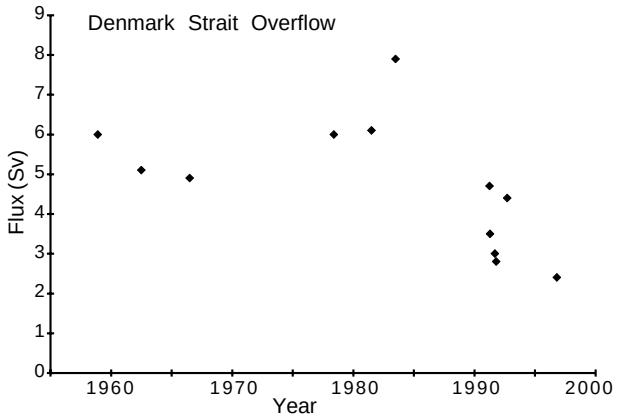

Figure 2. The DWBC referenced transport time series.

(Discovery), all between early spring and late summer. Most of the data came from the NODC CD-ROM, or the WOCE DAC at Hamburg. Fig. 1 shows their distribution; they radiate between southwards (at about 43°W) to eastwards (at about 60°N) from Cape Farewell across the Irminger Sea.

By imposing a level of zero motion at 1000 m, transports were calculated below 1500 m, although the results are not very sensitive to the two depths chosen because of the wide region of low current shear between about 800 and 1500 m. The calculation was extended from the 1500 m isobath off Greenland to roughly the centre of the Irminger Basin. There is little sensitivity to either endpoint because the high shear of the DWBC is found roughly between water depths of 1500 and 3000 m on the Greenland continental slope (between the 2000 and 3000 m isobaths). The 'bottom triangles' were filled by constant extrapolation of the last good current value (not by shear extrapolation). This means that the presented values are probably slight (~0.5 Sv) underestimates of the actual value, but we stress that these results are preliminary.

Fig. 2 shows the resulting time series of flux estimates. The six pre-1990 values average to 6.0±1.1 Sv (about half the total 13 Sv previously ascribed to the DWBC). The six post-1990 values average to 3.5±0.9 Sv. All six pre-1990 values are higher than any post-1990 one; applying a non-parametric ranking (or mean slippage) test, such as Wilcoxon's, to these data shows the chance of this being a random occurrence to be less than 0.1%. In the light of the foregoing, we believe that the DWBC has halved in strength; maybe it happened early in 1991 in the light of Dickson and Brown (1994) not seeing any significant variability up to the end of their 1986–1991 current meter measurements. This may well be a direct (but delayed?) consequence of the processes which caused the weakening of high-latitude deep convection in the 1980's (Schlosser *et al*., 1991).

One would expect to see this signal travelling downstream, and indeed it appears it may have been so observed. At the WOCE Moscow Atlantic Climate workshop in August 1996, results presented by John Lazier for the Labrador Sea and Bob Tereschenkov for 36°N provided corroboration in the form of property changes and referenced flux calculations (respectively).

I'll be tidying up this analysis in the next few months, but in the meantime, if anyone reading this note knows of any more 'southeast from Cape Farewell' sections, could they please let me know?

References

Bacon, S., 1994: Skill in an inversion solution: CONVEX-91 hydrographic results compared with ADCP measurements. J. Atmos. Oceanic. Tech., 11 (6), 1569–1591.

Bacon, S., 1997: Circulation and fluxes in the North Atlantic between Greenland and Ireland. J. Phys. Oceanogr., in press.

Clarke, R.A., 1984: Transport through the Cape Farewell-Flemish Cap section. Rapp. P.-v. Réun. Cons. int. Explor. Mer, 185, 120–130.

Dickson, R.R., and J. Brown, 1994: The production of North Atlantic Deep Water: sources, rates and pathways. J. Geophys. Res., 99 (C6), 12319–12341.

Macdonald, R., 1996: Awakenings in the Arctic. Nature, 380, 286–287.

Schlosser, P., G. Bönisch, M. Rhein, and R. Bayer, 1991: Reduction of deepwater formation in the Greenland Sea during the 1980s: evidence from tracer data. Science, 251, 1054–1056.

Observing Opposing Temperature Changes in the Upper and Intermediate Layers of the North Atlantic Ocean

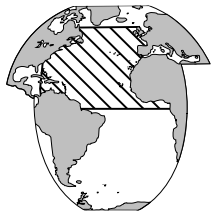

Alexander Sy, Klaus Peter Koltermann and Uwe Paul, Bundesamt far Seeschiffahrt und Hydrographie, Hamburg, Germany. Sy@BSH.d400.de

Several repetitions of transoceanic hydrographic sections in the northern North Atlantic (A1/AR7-East and A2/AR19) from 1991 through 1996 and high density XBT measurements along AX3 since 1988 reveal rapid changes of upper ocean and intermediate watermass property characteristics. We observe a warming trend in the upper ocean of the North Atlantic Current (NAC) regime and a cooling trend in the Labrador Sea Water (LSW) core of the intermediate layer below.

The northern North Atlantic Ocean plays a key role in determining long-term changes in the climate system. Warm thermocline water imported from the south by the northward flowing branch of the Meridional Overturning Cell (MOC) is transformed to cold waters by ocean-atmos-

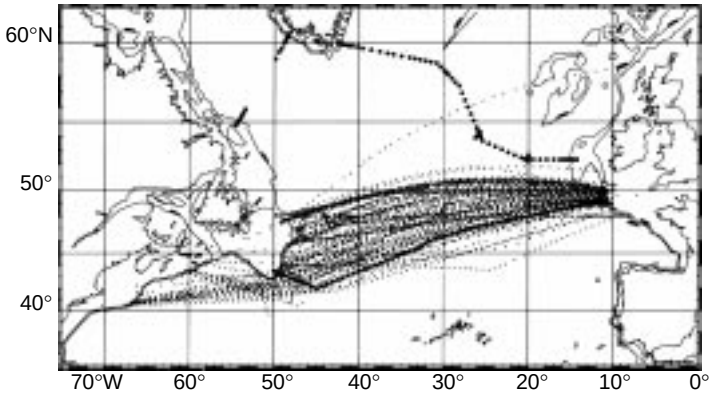

Figure 1. Area of observation with locations of stations of the WHP sections A1/AR7 and A2/AR19 (bold dots) and of XBT drops (thin dots). XBT measurements were carried out by the German container vessel Köln Express supplemented by some sections from research vessels. The data along the hydrographic sections were acquired on the following cruises:

A1/AR7-West	*RV Meteor No. 30/3*	*Nov. 1994 (incomplete)*
A1/AR7-East	*RV Meteor No. 18*	*Sept. 1991*
"	*RV Valdivia No. 129*	*Sept. 1992*
"	*RV Meteor No. 30/3*	*Nov./Dec. 1994*
"	*RV Valdivia No. 152*	*June 1995*
A2/A19	*RV Gauss No. 226/2*	*July 1993*
"	*RV Meteor No. 30/2*	*Oct./Nov. 1994*
"	*RV Gauss No. 276/2*	*May/June 1996*

phere interaction in its subpolar regime where the subsequent loss of buoyancy results in convective formation of intermediate and deep water masses.

In the Labrador Sea, convective overturning in severe winters creates the LSW with its characteristics of low salinity, high oxygen content, low potential vorticity and high anthropogenic tracer concentrations, which can be traced at depths between 1000 m and 2000 m as it spreads to other parts of the North Atlantic. Three primary pathways away from the formation region are distinguishable (Talley and McCartney, 1982; Schmitz and McCartney, 1993):

(i) northeastward into the Irminger Basin,
(ii) eastward near 50°N latitude (crossing under or parallel to the NAC) with several bifurcations east of the Mid-Atlantic Ridge (MAR), and
(iii) southward as part of the deep western boundary current system.

As the dominating fraction of the Upper North Atlantic Deep Water, LSW is one of the main water masses of the North Atlantic.

Hydrographic time series collected in the central Labrador Sea reveal that deep convection occurs discontinuously on a decadal time scale (Lazier, 1995). After a long warming phase two periods of intensified LSW production were identified, from 1972 to 1976 with θ/S characteristics in the range of 2.9°C–3.2°C and 34.83–34.85 psu and approximately from the late 1980s onward (θ=2.6°C–3.0°C, S=34.82–34.84 psu) with a dramatic impact on the temperature and the density field. It appears that the discontinuous LSW formation is controlled by the combined, remote response to the pressure systems characterized by the North Atlantic Oscillation Index (NAO) with the effect, that the evolution of convective activity in the Labrador and in the Greenland Seas during this century was in opposite phase (Dickson *et al.*, 1996). The first appearance of recently renewed LSW outside its source region was observed 1991 in the subpolar North Atlantic by comparison with historical data (Read and Gould, 1992).

Data analysis

Our observations are based on the two northernmost WHP sections and their repeats spanning the period 1991 to 1996 and high density ship-of-opportunity XBT measurements on a monthly to bi-monthly basis from the AX3 section for the period May 1988 to December 1995 (Fig. 1). For methodological reasons we used two different approaches to determine temperature changes in the upper and intermediate layers.

To trace the temporal change of LSW temperature we calculated its difference at the uniquely defined salinity minimum of the LSW core which represents the 'purest' LSW in our data. This straight-forward water-mass-following method is insensitive to depth or density variations of the LSW vintages. It clearly identifies from θ/S arguments the maximum temperature changes observed. For the upper layer the vertical temperature profile defies a similar approach. Therefore we used the integrated temperature signal of the top 750 m, the heat content. This quantity relieves us of determining a mean temperature for the layer concerned in a highly structurated region.

Due to weather-dependent ship's routes the XBT data are seasonally biased and distributed over a broad corridor of up to 400 nm width. Lying in the transition zone between the Subpolar and the Subtropical Gyre the spatial mean field is zonally correlated and the measurements could not

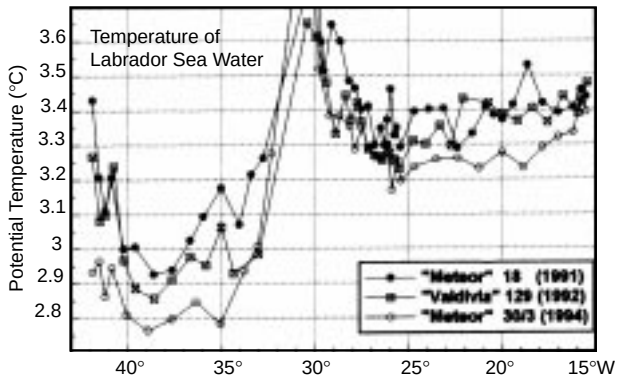

Figure 2. Change of LSW core temperature along WHP section A1/AR7-East (For better clarity only values from 1991, 1992 and 1994 are shown).

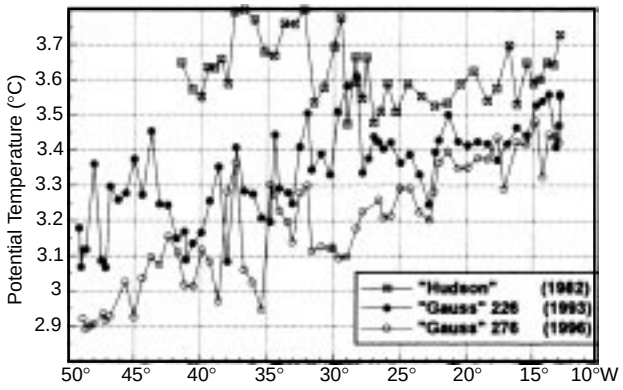

Figure 3. Change of LSW core temperature along WHP section A2/AR19 and with data from CSS Hudson from 1982 for comparison. (For better clarity values from 1994 are not shown).

be analyzed as being originated along a single section. To investigate the overall development of the upper layer and its large-scale temporal variability we calculated time series of heat content from 750 m deep XBT profiles sorted in $4° \times 4°$ boxes and averaged in monthly mean profiles for each box.

Cooling of the intermediate (LSW) layer

The comparison of LSW core temperatures along our northern section (A1/AR7-East) reveals an annual cooling in the Irminger Sea resulting in a change of -0.28°C in 4 years (Fig. 2 and Table 1), which indicates the annual arrival of a new LSW mode. Assuming 1988 as the year of the beginning of the recent period of dramatic LSW cooling we will call this multi-step event "1988-LSW cascade". Cooling in the Iceland Basin of 0.19°C and in the Rockall Trough area of 0.11°C also indicates renewed LSW. Although we find a cascade-like signal in the Iceland Basin, in the Rockall Trough area, however, the only signal of newly ventilated LSW appears in the 1994 data, indicative of a later arrival of the 1988-LSW cascade at the ocean's eastern boundary. A striking but not surprising feature is the separation of the LSW core layer by the Reykjanes Ridge (at 31°W) into two different hydrographic regimes, those of the Irminger Sea and the Iceland Basin, reflecting the effects of the longer pathway into the eastern basins and enhanced mixing over topography. Also note that the area between 25°W and 27°W is marked by the lowest LSW core temperatures observed in the eastern basins of the North Atlantic: after crossing the MAR, a branch of LSW flows at this latitude into the Iceland Basin as part of the Subpolar Gyre circulation.

Table 1. Change of mean values of LSW core potential temperatures [°C] (intermediate θ/S-Minimum) for Irminger Basin (>33°W), Iceland Basin (28°-22°W) and Rockall Trough entrance (<22°W) along section A1/AR7-East, and for Newfoundland Basin (>32°W) and West-European Basin (<32°W) along section A2/AR19.

	t [months]	Longitude [°W]		
A1/AR7-East		> 33°	< 28°-22°	< 22°
Valdivia 9/1992 – Meteor 9/1991	12	-.092	-.068	-.003
Meteor 12/1994 – Valdivia 9/1992	27	-.140	-.038	-.096
Valdivia 6/1995 – Meteor 12/1994	6	-.050	-.082	-.010
A2/AR19		> 32°	< 32°	
Gauss 7/1993 – Hudson 4/1982	135	-.450	-.154	
Meteor 10/1994 – Gauss 7/1993	15	-.057	-.096	
Gauss 5/1996 – Meteor 10/1994	18	-.103	-.042	

Besides strong cooling, the characteristic property changes of the 1988-LSW cascade are densification, deepening and only minute or no freshening. These results correspond well with observations in the central Labrador Sea. From 1988 to 1994 the LSW formation is characterized by a step-like temperature decrease of the order of 0.4°C, without significant salinity changes and accompanied by density increase (Lazier, 1996). This offset is in contrast to the properties generated during the preceding convection period (1972–1976), where strong cooling was accompanied by a substantial freshening of the order of 0.08 psu and consequently only very small densification.

These observations are supported by results from three occupations of our southern section (A2/AR19), which we supplemented by the 1982 Hudson section along 47°N as a reference for a period of 'normal' LSW production. Along the entire section we find a dramatic cooling of LSW in 1993 compared to 1982 (Fig. 3 and Table 1), with the most prominent anomalies west of the MAR amounting to 0.45°C (0.15°C east of the MAR). Associated with cooling we find a densification by $0.043\,kg/m^2$ and a deepening by more than 600 dbar for the western basin only. In contrast, salinity remains almost unchanged west of the MAR but was found to be significantly fresher (by about 0.03 psu) in the eastern basin. Similar to the northern section, the cooling continues, indicative of the arrival of the 1988-LSW cascade here as well. Between 1993 and 1996 the temperature decreased in the west by another 0.16°C and in the east by about 0.14°C: the newly formed LSW has already invaded the central West-European Basin and the renewal of the LSW layer is here currently in progress.

Estimates of circulation times derived independently by both linking single water mass property steps of the 1988-LSW cascade to equivalent counterparts in the source region and by calculations from CFC measurements lead to an unexpected short trans-Atlantic propagation time of 4 to

5.5 years from the Labrador Sea to the eastern boundary (Sy *et al*., 1996).

Warming of the upper layer of the NAC regime

The preliminary result for the period 1988 to 1995 reveals for nearly the entire area of observation (for 20 of 23 boxes) an increase of the heat content for the upper 0 to 750 m (Fig. 4a) with the largest changes in the regime of the NAC. This warming trend is not restricted to the mixed layer but evident for the whole upper 750 m. The two layers 0–100 m and 100–750 m clearly show a similar pattern (Fig. 4b,c) indicating the advection of warm water by the NAC. An inspection of single boxes reveals that the warming trend in some boxes seems to fade out after approaching peak values in 1993 and 1994. This suggests an interannual or interdecadal variability of heat content rather than a trend. A significant estimate of a probable time scale, however, is not yet possible and thus this programme will be continued.

An explanation for the interdecadal variability of LSW production is suggested by McCartney and Curry (1996, ms. in prep.). From time series of January SST anomalies prepared by Hansen and Bezdek (1996) they concluded that the large scale North Atlantic SST anomaly pattern are affecting the LSW warming and cooling periods by preconditioning the Subpolar Mode Water during its circulation around the subpolar transformation pathway. Although speculative, our observations of warming of the NAC regime lead us to assume that this pulse of warm water in the transformation pathway may have been responsible to stop the recent LSW cooling phase and to introduce the next period of LSW warming. Such a pulse of the upper branch of the MOC propagates with the subpolar circulation and warms the final transformation product LSW. First indications of the end of the recent intensified LSW period are found by Lazier (1996).

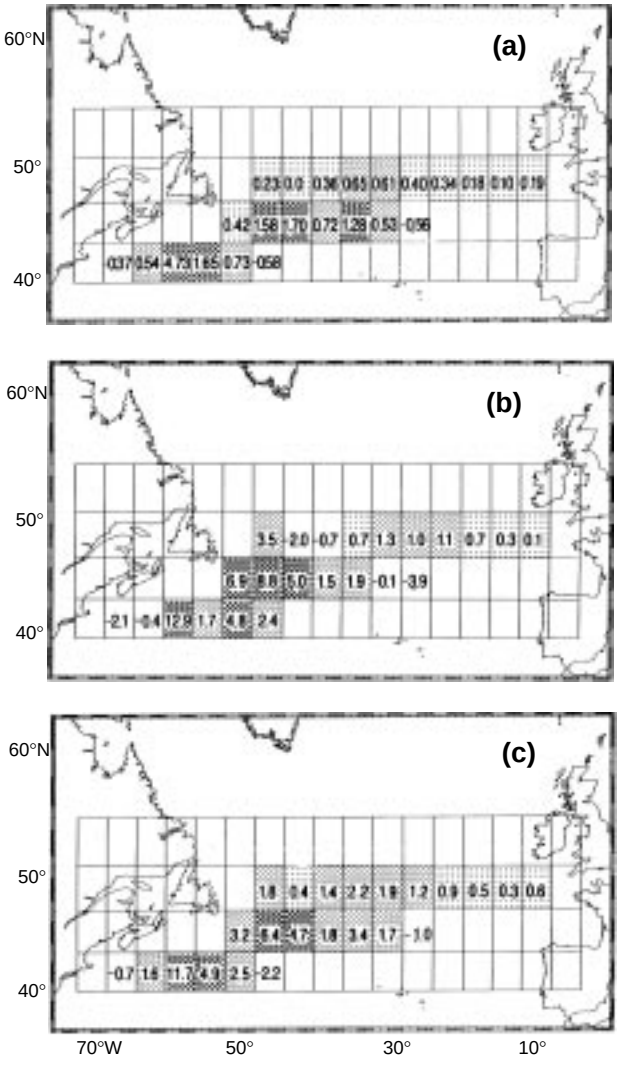

Figure 4. Preliminary results from XBT measurements along AX3, based on monthly means of 4° × 4° boxes with seasonal signal of the mixed layer (0–100 m) substracted. (a) Linear change per year (dH/dt) of the layer 0 to 750 m. (b) Relative linear change of the layer 0 to 100 m in % based on its mean heat content. (c) Relative linear change of the layer 100 to 750 m in % based on its mean heat content.

References

Dickson, R.R., J.R.N. Lazier, J. Meincke, P. Rhines and J. Swift, 1996: Long-term coordinated changes in the convective activity of the North Atlantic. Progr. Oceanogr., in press.

Hansen, D.V., and H.F. Bezdek, 1996: On the nature of decadal anomalies in the North Atlantic sea surface. J. Geophys. Res., 101, 8749–8758.

Lazier, J.R.N., 1995: The salinity decrease in the Labrador Sea over the past thirty years. In: Natural Climate Variability on Decade-to-Century Time Scales, National Research Council, Washington, D.C., 1995, 295–302.

Lazier, J.R.N., 1996: The Labrador Sea after winter convection 1990–96. J. Phys. Oceanogr., submitted.

McCartney, M.S., and R.G. Curry, 1996: The SST roots of interdecadal Labrador Sea water variability. Ms. in preparation.

Read, J.F., and W.J. Gould, 1992: Cooling and freshening of the subpolar North Atlantic Ocean since the 1960s. Nature, 360, 55–57.

Schmitz, W.J., and M.S. McCartney, 1993: On the North Atlantic Circulation. Rev. of Geophysics, 31, 29–49.

Sy, A., M. Rhein, J.R.N. Lazier, K.P. Koltermann, J. Meincke, A. Putzka, and M. Bersch, 1996: Surprisingly rapid spreading of newly-formed intermediate waters across the North Atlantic Ocean. Nature, in press.

Talley, L.D., and M.S. McCartney, 1982: Distribution and circulation of Labrador Sea Water. J. Phys. Oceanogr., 12, 1189–1205.

Data Guide 1997

The IPO with the assistance of the DIU has prepared a document describing each WOCE data stream, a summary of its inventory and how to access it on the WWW, and examples of data products. The document is now being printed and will be mailed shortly to those who received the WOCE Data Handbook. An electronic version of the document is already available at www.soc.soton.ac.uk/OTHERS/woceipo/dguide97

Evidence of Secular Change in the Northeast Pacific Ocean

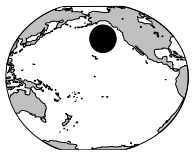

Howard J. Freeland and Frank A. Whitney, Institute of Ocean Sciences, P.O. Box 6000, Sidney, B.C. V8L 4B2, Canada. hjfree@ios.bc.ca

Temperature and salinity trends

Since 1935 sea-surface temperature and salinity have been sampled daily at about 15 shore-stations along the Pacific coast of Canada (Freeland, 1990). These data are particularly valuable for climatic studies because the sampling protocol has remained unchanged since the beginning of the programme, almost all locations still remain remote from urban centres. Fig. 1 shows a map of the Pacific coast of Canada with three of the coastal sampling locations marked. These three data sets are notable because of the unbroken length and quality of the time series, and because these three sites are well exposed to the open Pacific. Also shown

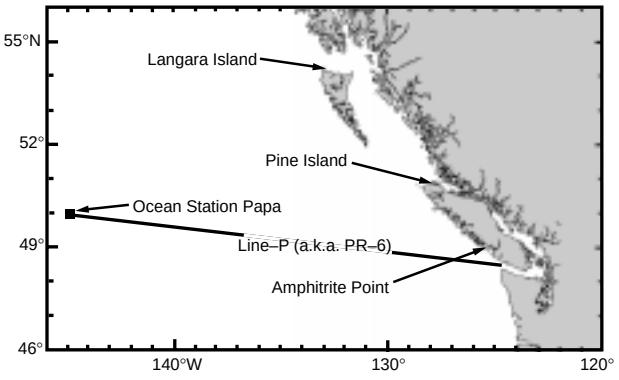

Figure 1. Location of Ocean Station Papa, three of the coastal sampling stations along the Pacific Coast of Canada and Line-P which connects Station Papa to Juan de Fuca Strait.

in Fig. 1 is the location of Ocean Station Papa – occupied by a series of weather ships from which meteorological data were obtained starting in 1950. In 1956 oceanographic observations began at Station Papa. Between 1956 and 1981 the weather ships were manned with oceanographic observers on a routine basis so securing a high quality data set of temperature and salinity observations. Since 1981 (when the weather ship program was discontinued) the time series has been maintained with 3 to 6 surveys per year. At Station Papa the techniques used to observe both temperature and salinity have changed with evolving technology.

This note will focus on Station Papa and the coastal stations, however, we do have observations along Line P (the track connecting Station Papa to the Juan de Fuca Strait, see Fig. 1), but these started much later than either the coastal time series or Station P, and sampling at some of the stations was intermittent during the early years of the Line P programme. All four stations show significant trends in surface temperature and salinity. Table 1 lists the observed trends in both these variables and the computed trend in sea-surface density anomaly.

Three of four observed temperature trends are marginally significant at the 95% confidence level, but the salinity and density trends are significant at confidence levels exceeding 99%. The density anomaly (σ_t) was computed from monthly averaged observations of temperature and salinity. For each site the average annual cycle in σ_t was computed and subtracted from the appropriate monthly observations.

Over a mixed layer of 100 metres, a temperature trend of 1.0°C/century would result from a local imbalance in the heat budget of $0.13\,\mathrm{W\,m^{-2}}$, and a salinity decline of $1\,\mathrm{century^{-1}}$ can be created by an excess of precipitation over evaporation of 3 cm of rainfall per year, in the absence of any other processes such as advection. Neither of these imbalances are measurable at sea with currently available techniques. Previous work, Ebbesmeyer and Tangborn (1993), ascribed the observed changes in salinity to a modification of the fresh water input to the N.E. Pacific occurring as the Columbia River was progressively dammed and its flow modified. However, this suggestion ignores the possible effects of advection.

Mixed layer depth at Station Papa

The data in Table 1 show that warming and freshening trends are observed over a large area of the N.E. Pacific. No similar trends have been reported below the main pycnocline and none are evident from the Station Papa data. The combined effect of the temperature trend and salinity trend is, therefore, to increase the density contrast between the surface layers of the N.E. Pacific Ocean and the deeper waters. Thus the next step is to look at trends in mixed layer properties.

Two methods were used to estimate the mixed layer depth objectively, to ensure that the trends computed were

Table 1. Temperature, salinity and density anomaly (σ_t) trends and 95% confidence levels on those trends (Bayley and Hammersley, 1946).

Site Name	Temp. Trend (95%) (°C/century)	Salt Trend (95%) (/century)	σ_t Trend (95%) (kg/m^3 / century)
Amphitrite Pt.	1.01 (±0.69)	-1.00 (±0.51)	-0.95 (±0.19)
Kains Island	0.61 (±0.77)	-0.91 (±0.61)	-0.81 (±0.24)
Langara Island	0.95 (±0.81)	-0.82 (±0.26)	-0.78 (±0.32)
Station Papa	1.96 (±1.15)	-0.43 (±0.28)	-0.47 (±0.22)

not dependent on the method chosen. The first method involves a least squares fit of a constant σ_t value (σ_1) between the surface and a depth h (the fitted mixed-layer depth) and a constant σ_t value (σ_2) between the depth h and an imposed reference depth H. Thus, three parameters result from the fit, σ_1, σ_2 and h. In the results to be presented here the calculations were all done by the first method using a reference depth of 300 metres. This method is insensitive to the choice of H between 200 to 500 metres.

The second method involves direct estimation of the mixed layer depth (h) by the equation:

$$h = \frac{\int_0^H zN^2(z)dz}{\int_0^H N^2(z)dz}$$

where $N^2(z)$ is the square of the buoyancy frequency. The integrals can be completed and the equation simplified yielding:

$$h = H\frac{(\sigma_H - \bar{\sigma})}{(\sigma_H - \sigma_0)}$$

where, σ_0 and σ_H are the values of σ_t observed at the surface and the reference depth H, respectively, and $\bar{\sigma}$ is the average value of σ_t over the depth interval 0 to the reference depth H. This method is insensitive to variations in H as long as H is relatively small. As H becomes large the two components of the difference $(\sigma_H - \sigma_0)$ are very similar and the computation of the small differences between two large numbers becomes unstable. This second method produces a sequence of mixed layers that is identical with those determined by the first method except for a displacement to slightly greater depths. Effectively this method tracks the pycnocline quite as well as method 1, but appears to select the base of the pycnocline rather than the axis.

We computed average mixed layer properties for each mid-winter period from an archive of water property observations at Ocean Station P. Some properties of the computed mixed-layers are displayed on Fig. 2 and were computed using the least squares method with a reference depth (H) of 300 m. The box symbols (■) show the observed depth of the mixed-layer, plotted as one average value for each mid-winter period. Early in the Station Papa time series many profiles were acquired in each winter period, but late in the series, with typically only 3 or 4 cruises per year each entry represents a single observation, and occasionally there are no mid-winter observations. A steady decline in mixed layer depth is evident over the 39 years of observations. If we regard each estimate as being independent of the estimate from the previous year then we compute a trend over the 39 years of observations as 63 m/century with a 95% confidence interval of ±28 m/century. With depths computed using the alternate method a shallowing trend of 58 m/century is obtained. The circle symbols (•) on Fig. 2 indicate a variable Q that is proportional to the Available Potential Energy (APE) in the mixed layer

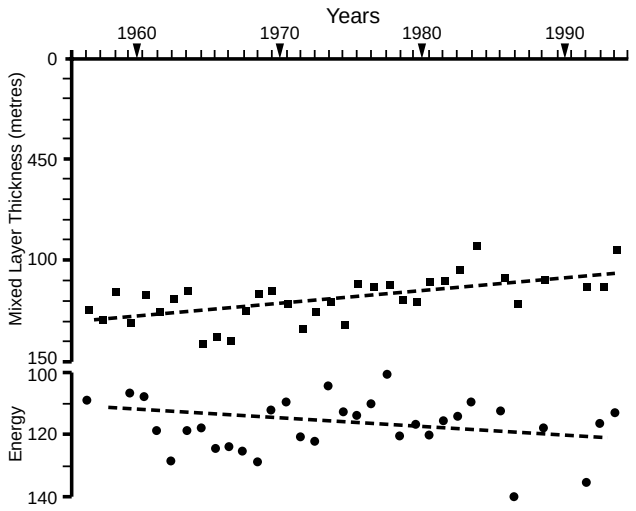

Figure 2. Squares indicate the observed depth of the mixed layer averaged over mid winter. Circles indicate a variable which is proportional to the available potential energy in the mixed layer (Peixoto and Oort, 1992).

computed following the definition of Peixoto and Oort (1992) relative to a mean state defined as the result of complete mixing to the reference depth H. A regression line on Q shows that the energy required to create the mid-winter mixed layer has increased slightly throughout this period. Thus, we cannot ascribe the apparent shoaling of the winter mixed layer to decreased windiness, if anything windiness might have increased, but rather to a change in the local density structure.

Nutrient concentrations at Station Papa

Though the nutrient levels observed in the sub-arctic Pacific are not limiting, biological activity over the summer months will tend to reduce the nutrient levels progressively. Nutrient concentrations are relatively high at depths of 100 metres or more, and so deep winter mixing tends to raise nutrients into the upper water column. If winter mixed layers are not as thick now as they were 40 years ago, then we should see a declining trend in upper mixed layer nitrate concentrations resulting from reduced winter entrainment.

Nutrient concentrations have been monitored at Station Papa since 1971. Once again, sampling was frequent in the early years, less frequent in the later years. Using all available observations we computed monthly averages of nitrate concentrations, and then computed winter averages (January through April, as for the mixed layer computations). These suggest that a declining trend is occurring. This trend is larger than the trend that would be suggested by just the shallowing of the mixed layer and perhaps a detailed model including a response in the biological system is required. The nitrate values have typical values of about $15\,\mathrm{mmols\,m^{-3}}$ and a declining trend of about $16.3\,\mathrm{mmols\,m^{-3}\,century^{-1}}$. The mid-winter nutrient concentrations are the largest values observed during the annual cycle. Biological activity guarantees that dissolved

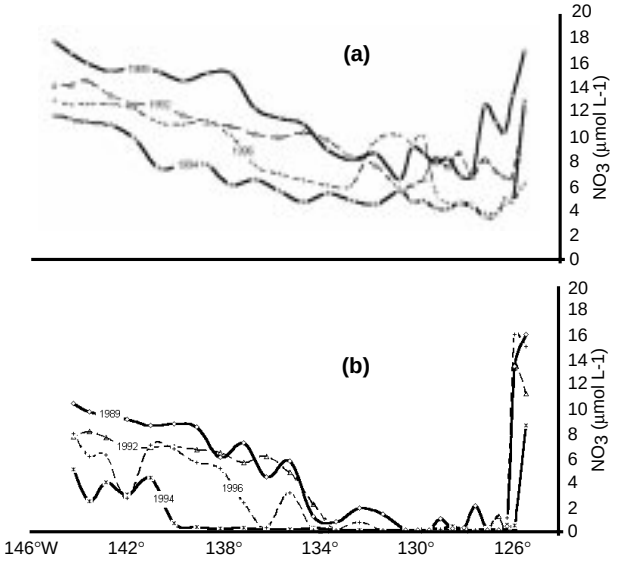

Figure 3. Near-surface dissolved nutrient concentrations along Line-P during the late winter (a) and during the late summer (b).

nutrient levels will be lower during the spring and summer. Figs. 3a and 3b show the near-surface dissolved nutrient concentrations plotted against longitude along Line-P. Fig. 3a shows conditions at the end of winter, and 3b the dissolved nitrate concentrations during the late summer. It is startling that during the last decade dissolved nitrates have declined to zero along large stretches of Line-P and we are only now beginning to assess the implications of these low nutrient concentrations.

References

Bayley G.V., and J.M. Hammersley, 1946: The "Effective" number of independent observations in an autocorrelated time series. J. Roy. Stat. Soc., B8, 184–197.

Ebbesmeyer, C.C., and W. Tangborn, 1993: Columbia River reservoir operation related to northeast Pacific sea surface salinity trends, 1930–1990. Abstract of talk presented at North Pacific Marine Science Organization (PICES) 2nd Annual Meeting, Seattle, Washington, 25–30 October 1993.

Freeland, H.J., 1990: Sea surface temperatures along the coast of British Columbia: regional evidence for a warming trend. Can. J. Fish. Aquat. Sci., 47, 346–350.

Peixoto, J.P., and A.H. Oort, 1992: Physics of Climate. American Institute of Physics, New York, N.Y., 520pp.

The Antarctic Margin Experiment, 80° to 150°E

Nathaniel L. Bindoff, Antarctic CRC, University of Tasmania, Hobart, Australia.
n.bindoff@antcrc.utas.edu.au

The main purpose of this hydrographic experiment was to study the Antarctic Bottom Water and its formation in the region 80°-150°E. Earlier results have shown the presence of two kinds of bottom water near 140°-150°E (Adelie Land, Antarctica). The first kind consisting of a warmer, saltier, and lower in oxygen water derived from the Ross Sea Bottom Water (RSBW). The second is a colder, fresher and higher in oxygen water, which formed locally (Gordon and Tchernia, 1972; Foster, 1995). From recent work the bottom water formed near 140°–150°E appears to be more important than previously thought, having a greater volume than the RSBW and possibly increasing in size (Rintoul, 1997).

The WOCE hydrographic programme has a very broad spatial scale. This makes the interpretation of the WOCE data difficult in regions of very localised bottom water formation such as the Adelie Land region because of spatial aliasing. The MARGINEX experiment was designed to overcome the problems of the large spatial scale sampling of the WHP programme by nesting a series of north-south CTD sections stations inside the earlier meridional and zonal hydrographic sections (SR3, P11, I8 and S4).

The measurements

MARGINEX was undertaken in early 1996 as part of a multi-disciplinary experiment designed to study the large scale ocean circulation along East Antarctica. This experiment is also complemented by a series of north-south sections undertaken by Prof T. Foster from the RV Nathaniel B. Palmer from 150°E to Cape Adare in April 1995. Together, these two experiments give a quasi-synoptic and fairly complete coverage of the water mass-properties along the coast of East Antarctica.

Although not formally part of the WHP, the oceanographic measurements are near to WOCE standards and consisted of 147 full-depth CTD casts including nutrients, dissolved oxygen, CFC-11, CFC-12, and CFC-113, and samples for oxygen isotope analysis.

Underway measurements included ADCP, pCO_2, SST and meteorological variables. In addition 6 ARGOS drifter buoys were deployed over the continental slope between the 1000 and 1500 m isobaths.

The experiment consisted of 8 north-south CTD sections, and one zonal section near 63°S (Fig. 1, page 21). Each north-south section is approximately 200 nm long with about 13 CTDs per section. To resolve the sharp features across the Antarctic Slope Front (ASF) the spacing between stations over the continental slope was as little as 1 nm. Combining all of these sections forms 7 closed volumes. This allows some inverse work based on these data and the earlier WOCE WHP sections to be undertaken.

Some results

Describing the distribution of bottom waters and estimating the production of bottom waters is an important aim of this experiment. The CFC-11 concentration at about 10 m

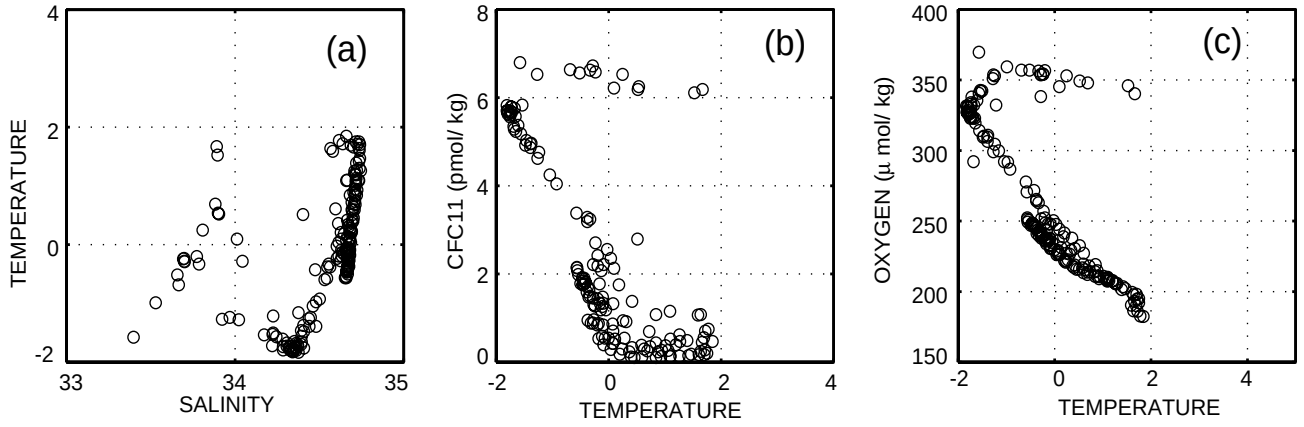

Figure 3. Property-property plots of (a) potential temperature and salinity, (b) CFC-11 (p mol/kg) and potential temperature, (c) oxygen (μ mol/kg) and potential temperature. These property-property plots are from leg 6.

above the bottom is shown in Fig. 1 (page 21). Typically each of the north-south sections (excepting leg 8 at 150°E) crosses the continental shelf break. These shelf stations have very high CFC-11 concentrations, greater than $5\,\mathrm{pmol/kg^{-1}}$. However these values decrease very rapidly down slope. The lowest deep water CFC-11 concentrations occur in the west with concentrations less than $1\,\mathrm{pmol/kg^{-1}}$. Further east the highest concentrations occur on leg 7 in waters 3–4 km deep. Leg 8 has lower concentrations than leg 7 and plots of bottom salinity show that this section is highly influenced by westward moving RSBW. From leg 7 (140°E) the bottom CFC-11 concentrations steadily decrease for legs 6, 5 and 4.

This pattern of bottom CFC concentrations suggests that between 140°E and 150°E there is a source of bottom water contributing CFC rich water. Plots of other properties show the high CFC bottom waters are colder, fresher and higher in oxygen. Curiously the highest values of the CFCs (and also the coldest freshest and highest in oxygen) occur offshore in deep water. These extrema in properties are cut-off to the south by less extreme values. This suggests that the formation of the bottom waters here is either aliased spatially or temporally. However, examination of the on-shelf properties during this experiment show that the shelf salinities are too low during the summer to form bottom waters thus suggesting that temporal aliasing is probably the more important reason for the distribution of bottom waters.

Although the main source of bottom water appears to be near 140° to 150°E it may not be the only source, west of Casey on leg 3 the CFC-11 concentrations have a local maximum. This section occurs in a large scale canyon connected to Vincennes Bay region of Antarctica (for bottom topography see Fig. 4).

All of the eight north-south sections have many shared oceanographic features. The oxygen section taken from leg 5 shows most of the expected large scale features (Fig. 2, page 21). The surface mixed layer is high in oxygen with this layer thinnest (70 m) coincident with the Antarctic Divergence near 63°S. The minimum in the mixed layer thickness here marks the southern boundary of the ACC. The strong oxygen minimum below the divergence (and further north) is the Upper Circumpolar Deep Water and is associated with a very strong temperature and salinity increase. At depths greater than 700 m (*i.e.* below the oxygen minimum) the oxygen content increases and both temperature and salinity decrease. The shoaling of the oxygen contours, isotherms and isohalines in these deep waters indicates a positive shear (increasing upwards) in the geostrophic currents.

Near the surface, south of 64°S, the mixed layer deepens towards the south. This deepening also occurs in temperature and salinity (not shown) and at these depths indicates a negative shear to the geostrophic currents. At 64.8°S there is very sharp front in the oxygen contours separating the oxygen-poor waters to the north and the oxygen-rich waters to the south. The same feature is also present in temperature, salinity and other tracers. This front occurs approximately half way up the continental slope between the 1000 and 2000 m isobaths. On this leg the oxygen content is higher offshore reaching $240\,\mu\,\mathrm{mol/kg^{-1}}$ compared with the lower oxygen concentration at the bottom in shallower waters near 64.5°S.

This leg is approximately halfway between the start and finish of the experiment. Further to the west the Antarctic Divergence is further offshore while to the east the Antarctic Divergence tends to become progressively closer to the continent. The Antarctic Slope Front tends to occur at approximately the same depth range over the continental slope and thus the distribution of the major water-masses are closer together for the most easterly sections.

In addition this section shows a very significant anomaly of high oxygen ($255\,\mu\,\mathrm{mol/kg^{-1}}$ between 1000 and 1500 m) at 64.7°S. The CTD casts were very close over this part of the shelf and this anomaly was well resolved. The temperature was cold (-0.2°C), fresher and had higher CFCs than the water above and below. This lens of anomalous water appears to have broken off from the oxygen-rich, (cold, fresh and CFC rich) continental slope front a short distance to the south. This plume may not have separated in the plane of the section, but must have come

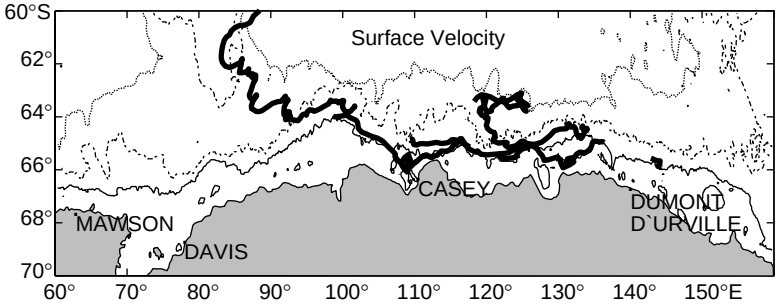

Figure 4. The drifter tracks for the six buoys deployed during the MARGINEX experiment. The tracks are plotted over bathymetry. Only the 0, 800 and 3000 m contours are shown.

from the shelf close by. The sections to the west and east (legs 4 and 6) show the shelf front to be further up the slope and with waters more like Circumpolar Deep Water (CDW) in the depth range of the plume. This plume is important because it gives insight into how the intermediate depth water masses along the continental slope are refreshed and modified.

Property-property plots from leg 6 are shown in Fig. 3. Although the RSBW has a distinctive salinity signal on leg 8, this signal is totally mixed away by leg 6 (Fig. 3a). Here the temperature-salinity correlation for waters <0°C forms a straight line that is noise free. The shelf waters have a temperature near the surface freezing temperature (-1.85°C) and a salinity less than 34.5 psu. For this leg there is no simple two point mixing scheme between these summer shelf waters, and the bottom waters. By contrast the CFC-temperature plot shows a different relationship between the shelf and bottom waters. The shelf waters at (-1.85°C) and the bottom waters (0°C) lie along a single straight line. This suggests that in the source region the shelf waters are mixing with cold slope waters to form bottom water approximately consistent with a two point mixing scheme. The atmospheric CFC-11 concentration increased rapidly up to the 1990s when it levelled out. The approximate consistency of the bottom waters with a two point mixing scheme suggests that these waters are relatively "young". Such a mixing scheme implies that the shelf salinity during formation of the bottom waters must have been as high as 34.63 psu possibly from sea-ice formation or on shelf mixing of CDW.

While CFC-11 is a passive tracer, oxygen can be reduced by biological consumption, in addition to mixing and surface boundary processes. Assuming surface mixing processes are very similar for both CFC-11 and oxygen there is some evidence for consumption of oxygen that can be seen in the oxygen-temperature plot (Fig. 3c). Here the bottom waters (<0°) form a straight line but unlike the CFC-temperature correlation this line projects onto a point below the concentration of the shelf waters ($330\,\mu mol/kg^{-1}$, -1.85°C). This difference suggests a total oxygen consumption of $16\,\mu mol/kg^{-1}$ since these waters left the continental shelf.

South of the Antarctic Divergence the density stratification is quite weak and the vertical shear of the density field is positive, this makes the appropriate choice of reference level ambiguous for estimating thermal wind transports, which is particularly important over the continental shelf and slope regions. The drogued buoy tracks are shown in Fig. 4. All of the buoys drifted west, with their paths following the bathymetry.

Most of the buoys crossed the north-south CTD sections and made possible a comparison of the eastward component of the buoy's velocity with the surface speeds estimated from the CTD data (assuming a deepest common-depth reference level). The velocity of the buoys is significantly more westward for all ocean depths up to 3.5 km than that estimated from the CTD data by 0.05 to $0.1\,m\,s^{-1}$. Although this comparison is incomplete (since it does not allow for the effect of the winds) it does suggest that bottom waters should have a significant westward component of flow broadly consistent with the distribution of CFC-11 concentrations (Fig. 1, page 21) and the other tracers (not shown).

Discussion

There is now enough data to resolve most of the bottom water distribution and to define the source region. The results point to the need to sample the water masses on and off the shelf during all seasons, and particularly in winter. There are two possible mechanisms by which the shelf salinity can be increased to allow bottom water formation between 140° and 150°E. These are through the formation of sea-ice or through the on-shelf mixing of the relatively warm and salty slope waters. The relative importance of these two mechanisms is still unclear. Future work will address the full three-dimensional circulation, and estimate the rate of formation of bottom and intermediate depth waters in this region.

Acknowledgements

We thank the crew of the RV Aurora Australis and support staff for their professionalism during the course of this 72 day voyage. Mark Rosenberg, Steven Bray and Steve Covey are thanked for their tireless work in processing the CTD, nutrient and CFC data.

References

Foster, T.D., 1995: Abyssal water formation off the eastern Wilkes Land coast of Antarctica. Deep-Sea Res., 42, 501–522.

Gordon, A.L., and P. Tchernia, 1972: Waters of the continental margin off Adelie coast, Antarctica. In Antarctic Oceanolgy II: The Australian–New Zealand Sector, Vol. 19 of Antarctic Research Series, edited by D.E. Hayes, pp. 59–69. American Geophysical Union.

Rintoul, S.R., 1997: On the origin and influence of the Antarctic Bottom Water of the Southeast Indian Ocean, in Oceanology of the Antarctic Continental Margin of the Antarctic Research Series, edited by S.S. Jacobs. American Geophysical Union (submitted).

Comparison of Bottom-Tracking and Profiling LADCP Data in a Section Across the ACC at Drake Passage

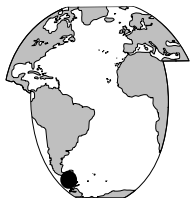

Stuart A. Cunningham, Michael J. Griffiths, Brian A. King, Southampton Oceanography Centre, Southampton; and Mark Brandon, British Antarctic Survey, Cambridge.
s.cunningham@soc.soton.ac.uk

Between 15 and 20 November 1996, the Drake Passage repeat hydrography section SR1 was occupied on RRS James Clark Ross with CTD stations at 35 km spacing. This was the third such occupation of the section by the UK, following those in November 1993 and 1994. As before, the hydrography was piggy-backed onto a cruise whose main purpose was Antarctic Base relief west of the Peninsula (King and Alderson, 1994). In addition, the cruise afforded an opportunity for the Proudman Oceanographic Laboratory to service their Bottom Pressure Recorder array.

New to this section was the deployment of a 150 kHz BroadBand ADCP on the lowered package, providing direct measurements of the ACC in Drake Passage with unprecedented horizontal and vertical resolution. The purpose of this article is to report on the use of bottom tracking in this lowered (L)ADCP.

As a result of previous cruises, we suspected the presence of strong currents throughout the water column. In 1993, for example, Vessel-Mounted ADCP (VMADCP) data revealed near-surface currents of 50 cm/s in an eddy or retroflection at a latitude of 60°S. Since the geostrophic calculations suggested shear of no more than 25 cm/s down to the seabed, there appeared to be a barotropic component of 25 cm/s at the bottom of the water column. This difference between geostrophic and observed speeds was more than could be accounted for by the acceleration terms due to curvature of the flow.

With this particular interest in near-bottom flows, it was decided to configure the LADCP in Bottom-Tracking (BT) mode. Perhaps surprisingly, there seem to be rather few reports of experiments using BT on LADCPs. BT data were acquired on 29 of the 30 stations occupied, and enabled absolute water velocities to be calculated relative to BT when the instrument was within 350 m of the seabed. Water track data were acquired in the usual way and processed to absolute velocities independent of BT using the University of Hawaii software, kindly made available by Eric Firing.

For each station, we therefore have three different datasets. The VMADCP, averaged during the occupation of the station, the LADCP velocities computed by integrating the shear from top to bottom, and the BT data. The VMADCP and LADCP are distinct measurements from different instruments, but employ the same ship navigation file for processing. The BT data contain the same shear information as the LADCP, but are navigated relative to the bottom rather than relative to the ship. In the present report, we discuss only averages taken throughout the station duration. Thus the LADCP profile is from the mean of up and down cast data, and VMADCP is for the entire duration of the station.

Offsets near the surface between the VMADCP and LADCP data have been determined for each station. Also near the seabed between LADCP and BT. For these comparisons, a single offset has been determined by averaging over several hundred metres. These offsets were in the range 0.1 to 17.2 cm/s, with an rms of 5.9 cm/s. It had been anticipated that offsets at the surface would, to some degree, match those at the bottom. This would have indicated an error in the estimation of the barotropic component of velocity. However, surface and bottom offsets were uncorrelated. We deduce that in our dataset, errors in the absolute LADCP profiles are dominated by errors in the vertically integrated shear, and that such errors are of the order of 5 cm/s. This is therefore an estimate of the uncertainty of the LADCP velocities following the 'standard' University of Hawaii software, without including either BT or VMADCP data. Note that in our dataset, the difference in top-to-bottom shear between upcast-only and downcast-only data was typically 5 cm/s. However, our error estimate may be more pessimistic than is needed for some other datasets.

The pay-off for employing bottom tracking is to acquire fewer Water Track (WT) pings. In this experiment, the configuration was 2-second ensembles, with one WT and one BT per ensemble. The profiler was able to avoid wasting battery power by omitting BT pings when it was out of range of the bottom, but still only achieved one WT ping per two seconds. Configured in WT only mode, twice as many WT pings (one per second) can be achieved, presumably leading to improved estimates of the shear and smaller errors in the baroclinic velocity profile. Unfortunately the small number of stations and compressed time scale of the cruise meant there was little scope to experiment with different configurations.

The result of the BT experiment can be seen in Fig. 1 (page 24). The LADCP profiles have been gridded and the cross-track component plotted as a section. Each profile has had a single offset applied so that it agrees with the BT data. The near-bottom velocities are displayed in the lowest part of the figure. Speeds up to 30 cm/s are observed, including the strong barotropic eddy or recirculation at 60°S. This rather persistent feature has been observed in the CTD and VMADCP data in all our realisations of the section. The upper panel shows the VMADCP data for comparison and is a completely independent dataset.

At this stage it is still rather difficult to know how best to use the BT data. One rather appealing possibility is to adjust the shear profile from the LADCP data so that it agrees with the VMADCP and BT data, perhaps using

linear interpolation of the top and bottom offsets through the water column. However, an informed decision must await a detailed analysis of the error budgets of all of the three different measurements.

Reference

B.A. King and S. Alderson, 1994: SR1 Repeat Hydrography/ ADCP, Drake Passage, Nobember 1993. International WOCE Newsletter, 15, 13–15.

Recent Speeding Up of the Pacific Subarctic Circulation

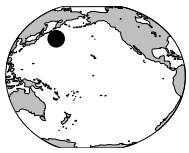

Costa Rogachov, Pacific Oceanological Institute, Vladivostok, Russia. toi@stv.iasnet.ru

Density of the upper layer in the western subarctic is lower than density of intermediate and deep layer due to low salinity of the surface water. Because of this there is no deep convection in the northern North Pacific in winter (Reid, 1973). Another important factor, preventing convection is the presence of the warm intermediate layer. The shallow Bering Strait blocks transport of this warm water northward to the Arctic. Thus, stratification in the North Pacific Ocean is maintained not only by excess of precipitation but also by the Bering Strait trapping warm, dense intermediate water in the Pacific. The Alaska current brings this water to the western subarctic. The Oyashio and Kamchatka currents comprise the subarctic western boundary currents which transport this water to the Sea of Okhotsk. Another example of fresh water control of subarctic circulation is the Great Salinity Anomaly (Dickson *et al.*, 1988). By contrast, Heath *et al.*, (1991) described the transport of high salinity water to the Northern Sea in January 1990. Such high salinities (perhaps the highest this century) had not been observed since 1908. 1990 was confirmed as an anomalous year by Quadfasel *et al.*, (1991), who observed a significant temperature anomaly in the Arctic.

Here, I report measurements of temperature and salinity in the Oyashio and its large fresh-core eddies during a 7-year programme. This includes one year of observations of the WOCE section, and shows significant interannual changes very similar to the decadal-scale regime shift described by Francis and Hare, (1994). The recent changes in water properties in the western subarctic boundary currents link these variations to the speeding up of the Pacific subarctic circulation.

The measurements

The initial hydrographic programme was part of a joint research effort between the Canadian Institute of Ocean Sciences (IOS) and the Pacific Oceanological Institute (POI) in the western subarctic (Fig. 1). The programme included four cruises in the Oyashio area during 1990–1992 (two in spring and two in fall-August/September), by the RV Academician Vinogradov and Academician Lavrentyev. These cruises occupied a high resolution station grid, which allows detailed description of the Oyashio fresh-core eddies, as the principal oceanographic phenomena of the area (Fig. 1). Each eddy was crossed by two perpendicular sections, so as to locate the eddy centre. These were followed by Russian/Canadian WOCE CTD measurements in the Oyashio in early September 1993. Detailed CTD measurements in the Oyashio region were again made in August 1994 by the RV Academician Lavrentyev and again by RV Professor Gagarinskiy in June 1996. These measurements make a 7-year time-series of the Boussole Eddy which shows dramatic changes in the subarctic circulation.

Some results

Fig. 1 presents dynamic topography of the 200 db surface relative to 1000 db in Autumn of 1991. It shows the Oyashio as a chain of eddies. These eddies move slowly along the Kuril-Kamchatka trench at about 1 cm/s (Rogachov and Goryachov, 1991, Rogachov *et al.*, 1996a).

The observations of eddies off the Boussole Strait during 1990–1996 show two features: first the large size of the 1990 eddy and its higher dynamic topography; second is a change in the position of the main Oyashio Branch. In 1990 the main branch of the Oyashio (determined by the maximum volume transport) was offshore, while in 1996 it was the coastal Oyashio. Fig. 2 presents a time-series of geostrophic transport by these two branches. The definition

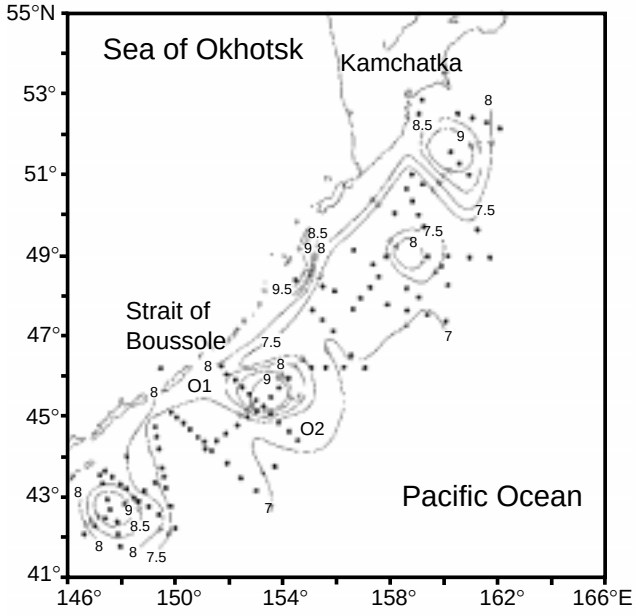

Figure 1. 200/1000 dbar geopotential anomaly (J/kg) for September 1991. O1 and O2 mark the position of the coastal and offshore Oyashio. These terms are strictly determined on the section across the centre of the Boussole Eddy.

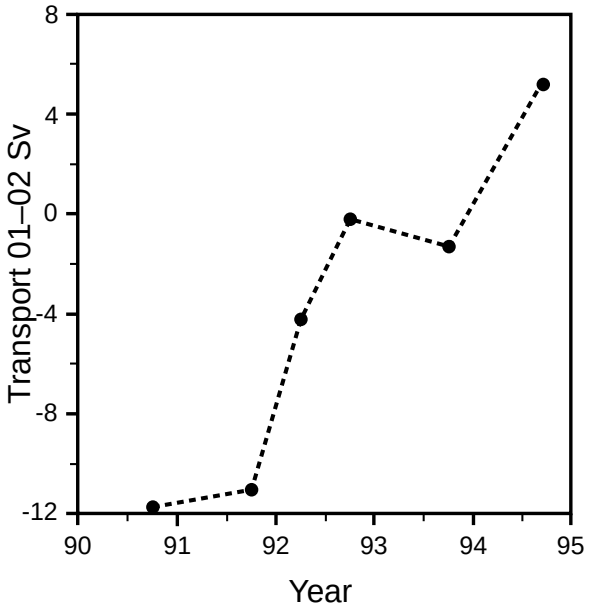

Figure 2. The difference between Coastal (O1) and Offshore Oyashio (O2) volume transport (Sv) for 1990–1994.

for the coastal (offshore) Oyashio is: the southward flowing current to the west (east) of the Boussole eddy centre. The difference between the volume transport by these two branches varied significantly (Fig. 2). Maximum geostrophic velocity of the coastal Oyashio also increased (Fig. 3). It appears that low transport of the coastal Oyashio in 1990–1991 is in agreement with observations of Stabeno and Reed (1992) of an unusual southern position of the Alaska Current and the absence of large inflow to the Bering Sea through the Aleutian Straits (compare weak coastal Oyashio and strong offshore). Recently, Reed and Stabeno (1993) reported the return of the Alaska Current to

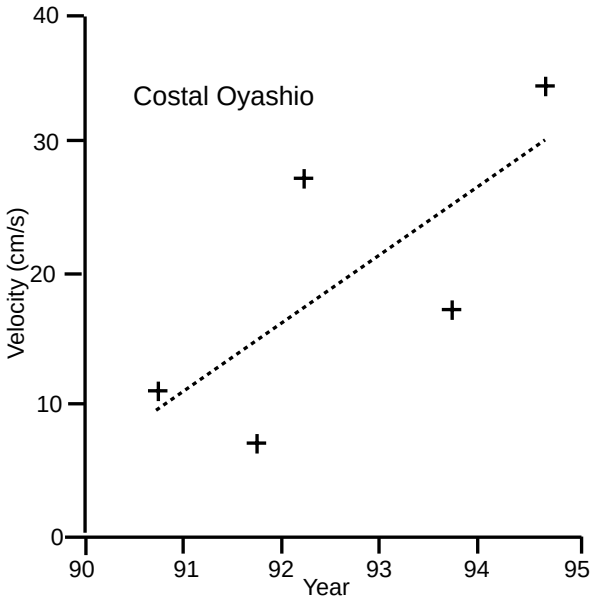

Figure 3. Maximum geostrophic velocity in the coastal Oyashio (relative to 1000 dbar). The WOCE section was made in 1993.

the Near Strait and stronger transport to the Bering Sea (compare strong coastal Oyashio).

There were property changes of the warm subarctic intermediate layer and vertical salinity distribution associated with variations of the Oyashio volume transport. Analysis of the salinity sections across the Boussole Strait eddies shows a large water mass transformation in their fresh-cores. The 1990 eddy had a thick 840 m core with low vertical density gradient, while it became about 300 m in 1996 (Fig. 4). The 1990 eddy, or so-called WCR86B (Rogachov *et al*., 1996a, b), had the greatest salinity of the upper layer. Fig. 4 demonstrates sigma-t vertical gradient time-series at the Boussole eddies central stations. Specific density time-series during 1990–1996 prove that there is significant increase of stratification at depth between 250–700 m, associated with the speeding up of the Coastal Oyashio (Figs. 2–3). As the result of large change in thermohaline structure, the dynamic height in the centre of the eddy dropped about 16 cm. Since the dynamic height difference which maintains the Oyashio transport is about 25 cm (see Fig. 1), we suggest that this change in sea level can be responsible for variations of the transport by western subarctic boundary currents.

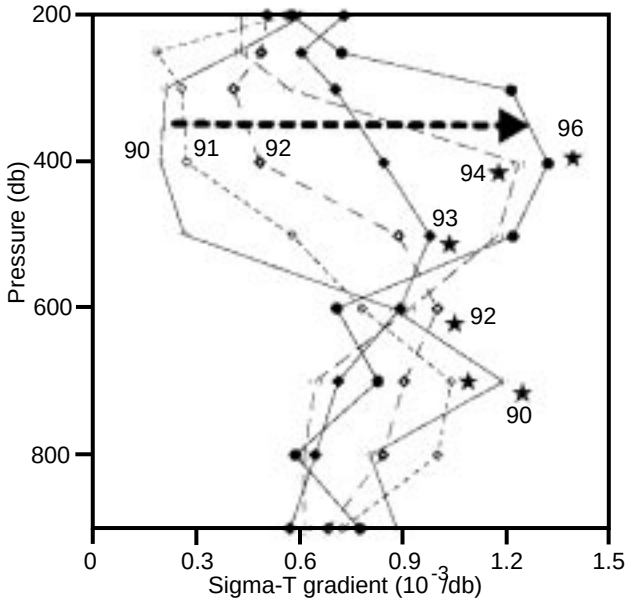

Figure 4. Time series of σ_t vertical gradient for stations inside the centre of the Boussole eddies (1990–1996). Note sharp increase in stratification in 1996. Position of the maximum stratification in each year is marked by star.

1990 was an extreme year in our hydrographic observations. Several authors also note unusual features of this year (*e.g.* Jacobs *et al.*, 1994). Quadfasel *et al.* (1991) describe a significant temperature anomaly (about a degree higher) in the Arctic, observed from the Russian icebreaker Yamal in 1990. Roach *et al.* (1995) conducted direct measurements of volume transport through the Bering Strait during 1990–1994 and found significant interannual differences in salinity. It can be suggested that a possible salinity anomaly source was again weakening Alaska coastal

current in 1990. Such hypothesis agrees with the observations under the transport of Alaska current (Stabeno and Reid, 1992; Reed and Stabeno, 1993).

Plans for extending such hydrographic programme should be developed, since these data are really necessary for climate research.

Acknowledgements

We deeply appreciate the efforts of all science personnel on the RV Academician M.A. Lavrentyev, RV Academician A. Vinogradov and Professor Gagarinskiy. Eddy Carmack and Robert Lake from IOS supported the implementation of the INPOC project and calibration of the Guildline instruments. Fig. 1 was created with the help of Rick Pearson from IOS.

References

Dickson, R.R., H.H. Lamb, S.A. Malberg, and A.J. Lee, 1988: The great salinity anomaly in the North Atlantic, 1968–1982. Progr. Oceanogr., Vol. 20, 102–151.

Francis, R.C., and S.R. Hare, 1994: Decadal-scale regime shifts in the large marine ecosystems of the North-East Pacific: a case for historical science. Fish. Oceanogr., 3:4, 279–291.

Heath, M.R., E.W. Henderson, and G. Slesser, 1991: High salinity in the North Sea. Nature, 1991, Vol. 352, No. 6331, 116.

Jacobs, G.A., H.E. Hurlburt, J.C. Kindle, E.J. Metzger, J.L. Mitchell, W.J. Teague and A.J. Wallcraft, 1994: Decadal-scale trans-Pacific propagation and warming effects of an El Niño anomaly. Nature, Vol. 370, No. 6488, 360–363.

Quadfasel, D., A. Sy, D. Wells, and A. Tunik, 1991: Warming in the Arctic. Nature, Vol. 350, 385.

Reid, J.L., 1973: Northwest Pacific Ocean Waters in winter. The John Hopkins University Press, Baltimore, 96 pp.

Reed, R.K., and P.J. Stabeno, 1993: The recent return of the Alaskan Stream to Near Strait. J. Mar. Res., 51, 515–527.

Roach, A.T., K. Aagaard, C.H. Pease, S.A. Salo, T. Weingartner, V. Pavlov, and M. Kulakov, 1995: Direct measurements of transport and water properties through the Bering Strait. J. Geophys. Res., Vol. 100, (C9), 18443–18458.

Rogachov, K.A., and V.A. Goryachev, 1991: Mixing in warm-core rings of the Kuroshio. J. Geophys. Res., Vol. 96, 8773–8777.

Rogachov, K.A., A.S. Salomatin, and E.C. Carmack, 1996a: Concentration of pelagic organisms at mesoscale fronts in the western subarctic Pacific: small fish on long waves. Fish. Oceanogr. 5, 153–162.

Rogachov, K.A., P.Ya. Tishchenko, G.Yu. Pavlova, A.S. Bychkov, E.C. Carmack, C.S. Wong, and G. Yurasov, 1996b: The influence of fresh-core rings on chemical concentrations (CO_2, PO_4, O_2 and pH) in the western subarctic Pacific Ocean. J. Geophys. Res., 101, 999–1010.

Stabeno, P.J., and R.K. Reed, 1992: A major circulation anomaly in the western Bering Sea. Geophys. Res. Lett., Vol. 19, No. 16, 1671–1674.

The Ashtech GG24 as an Alternative to P-Code GPS

Brian A. King, Michael J. Griffiths, Southampton Oceanography Centre; and Paul Woodroffe, British Antarctic Survey. b.king@soc.soton.ac.uk

A new Ashtech GG24 was fitted to RRS James Clark Ross in September 1996, and tried for the first time during the occupation of SR1 later in the year. The GG24 is a combined GPS/GLONASS receiver with a single antenna, and has 12 channels for tracking each constellation of satellites. It can be configured to compute positions from either system separately, or in a mixed mode whereby a position is determined from all satellites in view, typically 15 or more. Results from the latter mode are reported here.

The big advantage of the GG24 above GPS-only receivers is that while GPS suffers from Selective Availability, which introduces errors of several tens of metres, GLONASS does not. Thus the GG24 is able to deliver accuracy equivalent to a single-frequency GPS P-code receiver, mainly from the GLONASS satellites.

Installation and performance

The GG24 on James Clark Ross came in the form of a card with two serial ports. To this was added low-voltage power supply and antenna. The user supplies their own PC for configuration of the receiver. Data logging was of NMEA messages via one of the serial ports. The static performance of the receiver has been judged from data acquired while the ship was moored at two locations in the south-west Atlantic. Positions were logged at 1-sec intervals. At Stanley, Falkland Islands, the rms variation was 5 metres from 12 hours data, and at Rothera it was 8 metres from 5 hours data. Although coverage is essentially continuous, there were some unexplained gaps in the dataset acquired. On a couple of occasions the receiver hung, requiring user intervention before position messages were restored. Data were lost until the situation was noticed by watchkeepers. In the time available, we were unable to determine the causes of these faults, which may have originated in the receiver or may have been caused by communications problems with the PC datalogger. Data logging has now been integrated with the main shipboard computer system so that an alarm sounds if the data supply is interrupted.

Conclusion

For the majority of research ship users who are unable to gain access to a GPS P-Code receiver, the Ashtech GG24 seems to offer an attractive alternative, which may be just as good for many purposes. Supplied as a card without a fancy housing and front panel, the price is below that of most other GPS receivers and should be within range of all research ship operators. Anyone interested in purchasing one is recommended to obtain a price quote direct from the manufacturer, but is also welcome to contact the authors. Subject to the continued availability of the GLONASS system without Selective Availability, this looks set to become the standard position tool for users without GPS P-Code or real-time DGPS.

OCEAN DATA SYMPOSIUM

15–18 October 1997
Dublin Castle, Dublin, Ireland

Objectives

To assess the data management requirements of ocean scientists and to investigate the application of technological advances in order to increase the efficiency and effectiveness of present data management methods.

Themes

(a) The data and metadata requirements of scientists in order to support ocean research.
(b) The benefits modern technology offers to scientists and the facilities available for the analysis and exchange of ocean data.
(c) Developing the use of advanced technology for data collection, analysis and exchange; also the implication of these developments on ocean studies world-wide.
(d) Advances in the development of information and data management tools for policy and decision makers.

Symposium Format

1. paper presentation sessions
2. panel discussions (with provocateurs)
3. poster displays
4. exhibitions/demonstrations by service and technology suppliers

Exhibition by service and technology suppliers

The exhibition of services, hardware and software and related products will from an integral part of the symposium, with hands-on demonstrations of products. Both scientists and commercial operators are invited to present – these will include packages designed to assist both scientists and data managers with the quality control, manipulation, visualisation and management of ocean data, as well as telecommunications and data exchange systems. If you wish to demonstrate IT packages you are invited to submit a short description of your proposed demonstration.

Send abstracts of papers and posters before 30 May to:

OD Conference Desk
Irish Marine Data Centre
80 Harcourt Street
Dublin 2
Ireland
e-mail: data.centre@marine.ie
Tel: +353 1 475 7100
Fax: +353 1 475 7104

Further details/on-line registration available at
http://www.marine.ie/oceansym/

"MONITORING THE OCEANS IN THE 2000s: AN INTEGRATED APPROACH"

International Symposium
15–17 October 1997
Biarritz, France

Following on from research programmes such as WOCE, TOGA, JGOFS and associated space missions (GEOSAT, ERS, TOPEX/POSEIDON, ADEOS etc.) there are new global programmes starting (CLIVAR, GOOS, GCOS). These programmes, preparing forthcoming operational systems, will rely on future satellite missions, *in situ* networks and development of numerical models. In the long run, observations, measurements, models, analysis and forecasts are required for an integrated approach which will alone result in a real-time operational system for both the marine environment and climate-related purposes. This is a new challenge for the third millennium.

Organisation

The symposium is open to all those interested in the subject. It will be organised on the basis of half-days, each including one plenary and one poster session. Guest speakers will present their papers during the plenary sessions, whereas all other submitted papers will be presented as posters.

Organising Committee

Chairperson: Agnes Letraublon, CNES, Toulouse, France
Members: Yves Menard, CNES, Toulouse, France
Clotaire Pancrate, CNES, Paris, France
Cordula Riedel, Biarritz Tourisme, Biarritz, France
Corinne Saint-Paul, CTA, Toulouse, France

For further information

http://www.cnes.fr/actualities/OCEAN97
murielle.richard@cnes.fr
Corinne Saint-Paul
Capitole Tourisme Affaires,
31700 Blagnac-France
Tel. +33 5 61715571
Fax +33 5 61714437

Note on Copyright

WOCE is a component of the World Climate Research Programme (WCRP), which was established by WMO and ICSU, and is carried out in association with IOC and SCOR. The scientific planning and development of WOCE is under the guidance of the Scientific Steering Group for WOCE, assisted by the WOCE International Project Office.

The International WOCE Newsletter is edited at the WOCE IPO at the Southampton Oceanography Centre, Empress Dock, Southampton, SO14 3ZH, UK, Tel: 44-1703-596789, Fax: 44-1703-596204, e-mail: woceipo@soc.soton.ac.uk,
http://www.soc.soton.ac.uk/OTHERS/woceipo/ipo.html

We hope that colleagues will see this Newsletter as a means of reporting work in progress related to the Goals of WOCE as described in the Scientific Plan.

The editor will be pleased to send copies of the Newsletter to institutes and research scientists with an interest in WOCE or related research.

Printed by the Design and Print Centre of the University of Southampton